CBM PROGRESS REPORT 2007

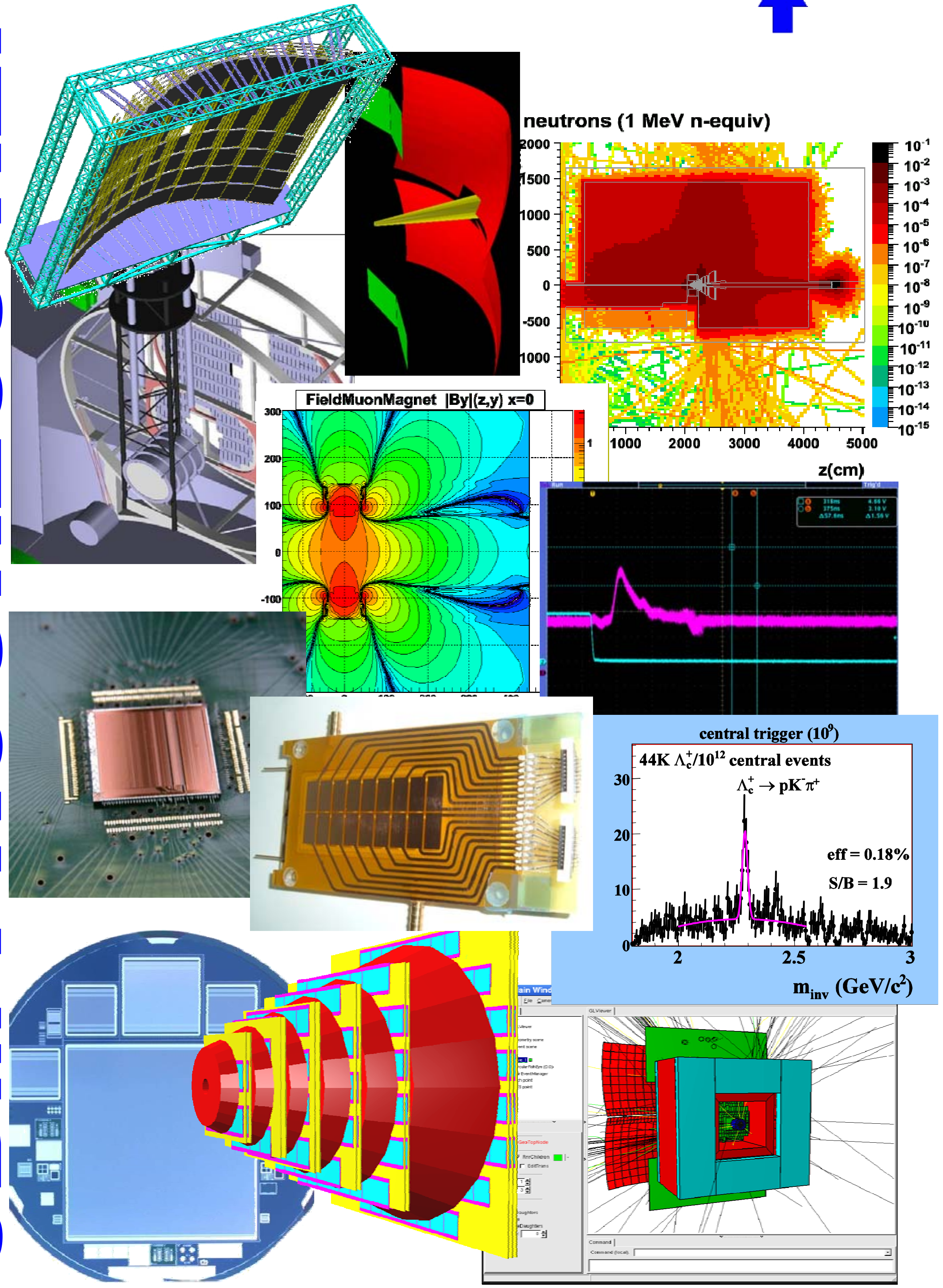

This work is supported by the EU Integrated Infrastructure Initiative Hadron-Physics Project (I3HP) under Contract number RII3-CT-2004-506078, by INTAS Ref. № 06-1000012-8729, -8778, -8781, -8810, -8914, and by the German Federal Ministry for Education and Research.

10th CBM collaboration meeting, Dresden, September 2007

ISSN: 0171-4546
ISBN: 978-3-9811298-5-4

Preface

This report documents the activities within the CBM project in 2007. Significant progress has been made in the optimization of the simulation software, the layout and development of detectors, the design of front-end electronics, and the concepts for data acquisition.

The simulation and analysis routines have been completely integrated into the software framework (FAIRroot and CBMroot), and can be used now easily by users outside GSI. A breakthrough has been achieved in the development of fast algorithms for track and vertex reconstruction which have been improved in speed by a factor of 10^5. These fast routines permit to perform high-statistics simulations for detailed detector layout optimization. Full event reconstruction based on realistic detector properties and particle multiplicities as given by microscopic transport models are routinely used in the feasibility studies.

A version of the Silicon Tracking System is now implemented in the simulation software comprising 8 detector layers based on microstrip technology only, including the readout cables, and the mechanical detector structure. The studies of open charm detection have been extended to D_s^+ and Λ_c, taking into account a realistic layout of the Silicon Pixel Microvertex detector. The identification of electrons has been optimized by improved ring recognition algorithms and transition radiation simulations. The Ring Imaging Cherenkov (RICH) detector has been redesigned, resulting in a reduction by a factor of two in mirror size and number of readout channels without reducing the pion rejection capability. The muon detection system has been optimized with respect to the number of detector layers. The muon simulations take into account detector inefficiencies and a segmentation of the muon chambers into pads according to a nominal occupancy of 5% for central Au+Au collisions. Studies for a dimuon trigger show promising results. Radiation dose simulations using the FLUKA transport code have been started.

A new generation of pixel sensors for the Microvertex detector (MVD) with fast read-out architecture has been tested with pion beams at CERN. The tolerance of the sensors to non-ionizing radiation has been improved, and the construction of a MVD demonstrator has been started. The first double-sided microstrip sensors have been built and will be tested. Prototype MWPCs for the measurement of transition radiation have been tested and optimized for high rate capability. Prototype straw-tube tracker modules haven been built and tested. The n-XYTER readout ASIC was characterized in various test benches and is now ready for deployment in detector and beam tests in 2008. The design work on the CBM-XYTER, a radiation-hard second-generation readout ASIC for Silicon and fast gas detectors, has started in 2007. The FEE development for the RPC-TOF system saw two major milestones in 2007: the preamplifier-discriminator chip PADI was successfully tested, and the preparatory studies of several time-to-digital converter buildings blocks were concluded with the design choices for the first full system chip to be developed in 2008. Within the development of a future data acquisition system, the scalability of high-throughput event building was demonstrated on a 110 node cluster. A very important milestone will be the proton beam test of Silicon microstrip and gas detectors read out by n-XYTER ASICs at GSI end of September 2008.

In 2007 seven institutions joined the CBM collaboration: University of Split (Croatia), Aligarh Muslim University (India), Rajasthan University (India), Jammu University (India), Srinagar University (India), Kolkata University (India), and the Academy of Mining and Metallurgies Krakow (Poland). An important decision has been taken concerning the participation of GSI groups in FAIR. The GSI efforts in FAIR will concentrate on five experiments, and one of them is CBM. The CBM Physics Book is almost finished and will be submitted for publication in 2008.

Many thanks to all the colleagues who have contributed to this report.

February 2008 Peter Senger

Contents

Status of the FAIR Project

FAIR Joint Core Team
GSI, Darmstadt, Germany

The year 2007 saw tremendous progress in the realisation of the FAIR facility. During the year, the FAIR member states have been joined by Austria and Slovenia. The Republic of Georgia has been granted observer status.

Although not all necessary funding for the entire project could be achieved to that date, the FAIR project was officially started at 7th November 2007 (see Fig. 1). With more than 1,400 people attending, delegates of the member states signed a communiqué reaffirming their commitment to build FAIR.

The celebration was followed-up by a symposium which gave a concise overview of the physics at FAIR and its significance in the international research environment. It was attended by more than 500 physicists.

FAIR is unique in its attempt to build an entire facility, accelerators and experiments, in a distributed fashion. It is planned that sub-systems will be built within the various member countries and provided to FAIR as so-called in-kind contributions. This concept relies on the capabilities and willingness of the laboratories of the member states. In autumn 2007 this was put to test. In a first round of enquiries, 22 laboratories from 9 member states expressed the interest into particular in-kind contributions. The response exceeded all expectations, already covering the majority of the work packages that have to be executed. The needed consolidation and organisation of these work packages will be addressed during 2008.

The 14 experiment collaborations with more than 2,500 scientists have consolidated their attempts to acquire their necessary funding. In parallel, significant progress in research and development of the various detectors has been achieved.

The first technical design reports are expected for 2008. They are needed to start the construction of the particular sub-detectors, e.g. the PANDA electro-magnetic calorimeter.

The creation of the FAIR GmbH and its first year of operation will be supported by a FP7 grant of the European Commission.

Figure 1: More than 1,400 people attended the start of the FAIR project on 7th November 2007

The CBM experiment at FAIR

V. Friese[1], W. F. J. Müller[1], P. Senger[1], and the CBM Collaboration
[1]Gesellschaft für Schwerionenforschung, Darmstadt

Compressed Baryonic Matter: Physics case and detector setup

The mission of the Compressed Baryonic Matter (CBM) experiment at FAIR is to explore the QCD phase diagram in the region of high baryon densities. The physics of dense baryonic matter and the relevant observables in nucleus-nucleus collisions have been worked out in detail in the CBM Physics Book which will appear in 2008. The detailed understanding of the evolution of the partonic/hadronic fireball requires new measurements which have not yet been performed at FAIR energies. The most promising observables are rare probes which carry information on the matter properties, such as particles containing charm quarks (D mesons and charmonia), low-mass vector mesons decaying into dilepton pairs (ρ, ω and ϕ mesons), or Ω hyperons (consisting of 3 strange quarks). The measurement of event-by-event fluctuations, correlations, and of the collective flow of hadrons (including the flow of rare probes) will provide important information on the dynamics of the fireball.

The goal of the CBM research programme is to determine the equation-of-state of strongly interacting matter, to discover the phase transition from hadronic to partonic matter and the QCD critical endpoint, and to investigate the in-medium properties of hadrons as a signature for the onset of chiral symmetry restoration. This programme requires the systematic and comprehensive investigation of the above mentioned observables as function of beam energy, system size and collision centrality.

The experimental task is to identify hadrons and leptons in collisions with up to 1000 charged particles at event rates of up to 10 MHz. These measurements require fast self-triggered read-out electronics, a high-speed data acquisition (DAQ) architecture, and an appropriate high-level event-selection concept. A particular experimental challenge is the measurement of D mesons which is based on the real-time selection of displaced vertices with an accuracy of about 50 μm.

The core of the CBM detector concept is the Silicon Tracking System (STS) located in a large-aperture dipole magnet. It is made up of several layers of silicon microstrip detectors and has to provide track reconstruction and momentum determination. The STS is supplemented with the Micro-Vertex Detector (MVD), consisting of two layers of silicon pixel sensors, for high-precision determination of primary and secondary vertices. Electrons from the decay of low-mass vector mesons or charmonia will be identified by the combination of a Ring Imaging Cherenkov Detector (RICH) and a system of Transition Radiation Detectors (TRD). A wall of timing RPC detectors (TOF) serves hadron identification by time-of-flight measurement. The setup is completed by an electro-magnetic calorimeter (ECAL) used for the identification of photons. A schematic view of the CBM setup for electron and hadron measurements is shown in Fig. 1.

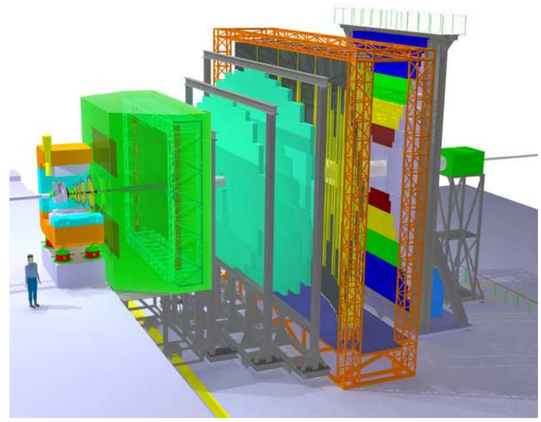

Figure 1: The Compressed Baryonic Matter (CBM) experiment planned at FAIR. The setup consists of a high-resolution Silicon Tracking System (STS), a Ring Imaging Cherenkov detector (RICH), three stations of Transition Radiation Detectors (TRD) with 3-4 radiator/detector layers each, a time-of-flight (TOF) system made of Resistive Plate Chambers (RPC), and an Electromagnetic Calorimeter (ECAL) based on lead/scintillator "Shashlik" technology.

For the complementary measurement of low-mass vector mesons and charmonia through their decay into muon pairs, the RICH detector will be replaced by a muon detection system consisting of several iron absorbers interlayed with large-area tracking detectors. In this setup, the TRD will serve as a pure tracking detector. The TOF detector will be used for background suppression during muon measurements or, with the absorbers removed, for hadron identifcation as in the case of the electron setup.

In the following, we briefly review the status of the feasibility studies and the detector R&D for CBM. The simulations have been performed within the FAIRroot software framework (see M. Al-Turany et al., this report). The routines for track and vertex reconstruction have been improved in speed by a factor of 1000 which allows to perform sophisticated high-statistics simulations for detector layout optimization (see I. Kisel et al., this report).

The Silicon Tracking System

In order to reduce the number of detector technologies (hybrid pixel and micro-strips), a detector system consisting of 8 double-sided micro-strip sensor layers only was designed. This tracking system has been optimized with respect to track reconstruction efficiency, momentum resolution and redundancy (see R. Karabowicz et al., this report). In addition, details of the detector including a realistic sensor layout, micro-cables and support structures have been implemented in the simulation software. First prototype double-sided micro-strip sensors with different sizes have been produced and tested. The next step is to produce a demonstrator consisting of a double-sided sensor connected to a self-triggered read-out chip (n-XYTER), and to perform test measurements with proton beams at GSI (see J. Heuser et al. and C. Schmidt et al., this report).

D meson identification and vertex detector

The Micro-Vertex Detector (MVD) - which is close to the target and has limitations in radiation hardness and read-out speed - will be installed only for open charm measurements which requires high-precision vertexing. The MVD consists of two layers of Monolithic Active Pixel Sensors (MAPS) which can be made very thin in order to reduce multiple scattering. Feasibility studies demonstrate that particles with open charm ($D^0, D^\pm, D_s$, and Λ_c) can be measured with good efficiency and excellent signal-to-background ratio using a detector setup consisting of 2 MAPS and 6 double-sided micro-strip stations (see I. Vassiliev et al., this report). The R&D on the MVD concentrates on the improvement of radiation hardness and readout speed of the MAPS, and on the development of a demonstrator (see S. Amar-Youcef et al., this report).

Hadron identification by Time-of-Flight

The study of event-by-event fluctuations and particle correlations is based on the measurement of pions, kaons and protons. Hadron identification in CBM requires track reconstruction using the STS and the TRD, and TOF determination with the timing RPC wall. The total reconstruction efficiency for hadrons (STS-TRD-RPC) is well above 80 %. This result is based on realistic detector layouts and performances. The R&D on prototype timing RPCs concentrates on high rate capability, low-resistivity material, long-term stability, and the realization of large arrays with overall excellent timing performance.

Electron identification with RICH and TRD

The simulations on electron identification are based on reconstructed tracks in STS and TRD, on ring recognition in the RICH photon detector, on ring-track matching, and on the statistical analysis of the energy loss signal in the TRD (see C. Höhne et al., this report). The combined information from RICH and TRD is sufficient to suppress the pion contamination in the electron sample. Low-mass vector mesons can be identified using elaborated background rejection strategies (see T. Galatyuk et al., this report). The J/ψ meson yield is well visible above the combinatorial background (see A. Maevskaya et al., this report). The TRD-R&D activities are focused on the development of highly granular and fast gaseous detectors which can stand the high-rate environment of CBM. Prototype gas detectors based on MWPC and GEM technology have been built and tested with particle rates of up to 200 kHz/cm^2 without deterioration of performance (see M. Klein-Bösing et al. and D. González-Diaz et al., this report). Moreover, test measurements of RICH mirror and photon detector performances have started.

Muon measurements with hadron absorbers

The CBM muon detection system consists of active hadron absorbers located just behind the Silicon Tracking System. The idea is to continuously track all charged particles through the complete absorber, starting with the tracks measured by the Silicon tracker (which defines the momentum). This concept requires highly granulated and fast tracking detectors which are located in each gap between the absorber layers. The muon detection system is schematically shown in Fig. 2.

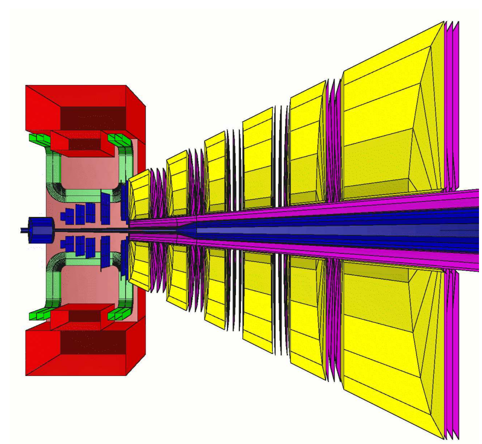

Figure 2: Sketch of the CBM muon detection system consisting of alternating layers of iron hadron absorbers and detectors

The simulations are based on track reconstruction algorithms taking into account a realistic pad layout of the muon chambers according to an occupancy of 5%. The studies demonstrate that both low-mass vector mesons and charmonia can be identified above the combinatorial background which is dominated by muons from weak pion decays (see A. Kiseleva et al., this report). The challenge for the muon chambers and for the track reconstruction algorithms is the huge particle density of up to 1 hit/cm^2 per event in the first detector layers. Therefore, the current detector R&D concentrates on the design of fast and highly granulated gaseous detectors based on GEM technology.

Cave and infrastructure for CBM

W. Niebur[1]
[1]Gesellschaft für Schwerionenforschung, Darmstadt

The experimental cave for the CBM experiment will be located south of the SIS100/300 synchroton rings, near the production target for the Super-FRS. The cave provides an area of 38 m x 21 m; its height is about 17 m. It wil be built underground and covered with compacted earth for radiation protection. Access to the cave will be granted by a 10 m x 6 m breakthrough in the front part of the ceiling which can be reached by heavy loads through the access road. Here, experimental equipment can be lowered to the experimental area by an external crane.

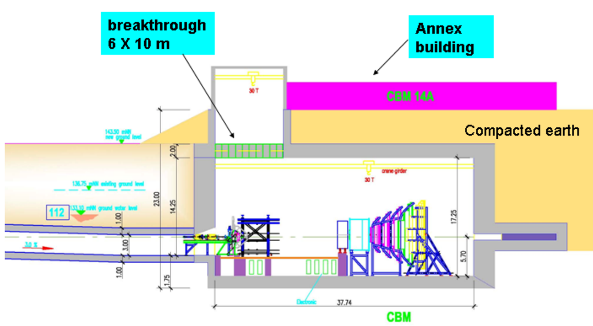

Figure 1: Side view of the CBM cave

Inside the cave, an internal crane will be used to place equipment. The capacity of the crane will be about 30 t. A side view and a top view of the planned cave are shown in Figs. 1 and 2, repectively.

Unlike previous designes, the cave floor on one level only. An intermediate ceiling at about 3 - 4 m above floor level will provide acces to the beam line and the target region. The beam line is at about 5.70 m from floor level. Below the inserted ceiling, electronics and supplies will be located which are shielded from the interaction zone by the concrete support of the dipole magnet.

The HADES experiment will be placed in front of the CBM setup. To avoid additional focusing magnets between HADES and CBM, the distance of the two is to be minimised. Currently, the CBM target position is foreseen at about 12 m from the cave wall.

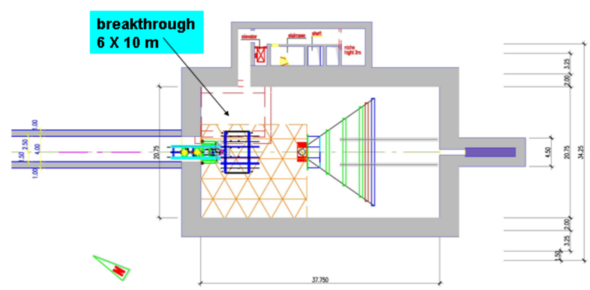

Figure 2: Top view of the CBM cave

The CBM infrastructure is complemented with an Annex building hosting the control room, the computing farm, various laboratory rooms including a clean room, a montage room and a meeting room. The cave can be accessed from the Annex by an elevator as well as by a stair case.

Dipole magnet study for the CBM experiment

P. Akishin, V. Ivanov, and E. Litvinenko
LIT JINR, Dubna, Russia

In order to estimate the possibility of using the dipole magnet of the HERMES set-up at DESY for the CBM experiment, we created a model of this magnet on the basis of the available information – a one-page technical drawing and some basic parameters of the magnet [1]. The field map, calculated with TOSCA, and magnet geometry were converted to be compatible with the cbmroot framework: the field map ”Hermes” corresponds to the nominal current 1500 A.

As the opening angle of the HERMES magnet was not sufficient for CBM experiment needs, a modified model of this magnet was developed and studied (Fig. 1). Since the field value in the center of the magnet was significantly reduced after this modification (Fig. 3, left plot), the modified geometry did not provide enough bending power (field map ”HermesEn”, 1500 A current), even if the electrical current in the coils is increased up to the maximum value (map ”HermesE”, 1650 A current).

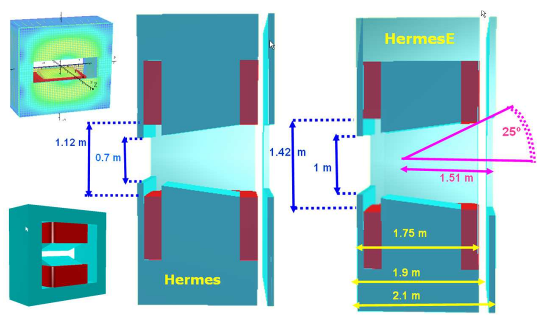

Figure 1: Geometry of HERMES magnet models in TOSCA and cbmroot. Differences between original and modified models are shown

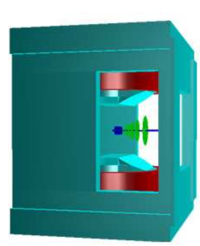

Figure 2: HERA magnet model as represented in cbmroot

Previously, similar studies have been conducted with the magnet (Fig. 2) used at DESY in the experiment Hera [2].

Motivated by increased requirements for the apperture, additional calculations have been carried out for the magnet model “MuonMagnet” (Fig. 4), reported in September 2006 [3]. To achieve this, the magnet model was redesigned and the field map was recalculated on a new grid.

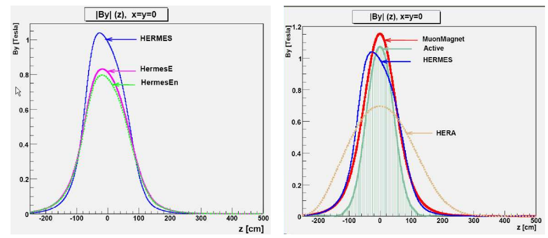

Figure 3: Left plot: B_y field components for ”Hermes” magnet and its modified version. Right plot: comparison of B_y components for different dipole magnet models. Here “Active” is the former “standard” magnet model for CBM simulations

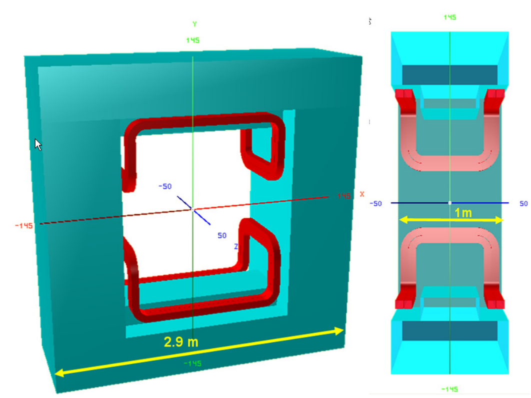

Figure 4: Muon magnet model as represented in cbmroot

For all above mentioned magnet models the field maps were calculated using TOSCA (Fig. 3, right plot) and converted into a cbmroot compatible format. The geometry files are also provided, so that these magnet models can be used in GEANT simulations and analysis in the cbmroot framework. The magnet model “MuonMagnet” is selected now as a new “standard” model for CBM simulations. Presently, a further design study of this magnet for the CBM experiment is conducted.

References

[1] http://www.gsi.de/documents/DOC-2007-Oct-110-1.pdf
[2] http://www.gsi.de/documents/DOC-2007-Mar-51-1.pdf.
[3] http://www.gsi.de/documents/DOC-2007-May-1-1.pdf.

Superconducting Dipole Magnet for CBM

E.A.Matyushevskiy, P.G. Akishin, A.V. Alfeev, V.S. Alfeev, V.V. Ivanov, A.I. Malakhov
JINR, Dubna, Russia

One of the major components of the CBM setup is the superconducting dipole magnet which is located closely to RICH detector. The magnet should provide a field integral along the beam axis of about 1.5-2 Tm. The maximal value of the magnetic field in the magnet gap should amount to 2 T. The working gap acceptance should be within 50º in height (1.4 m) and 60º in width (1.6 m).

The conceptual design of the SC dipole magnet with a magnetic steel yoke and a SC excitation winding is presented at Fig.1.

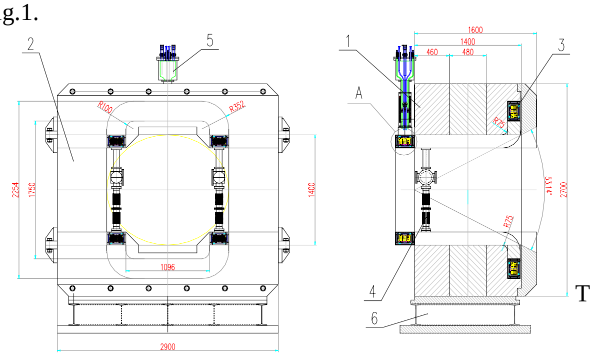

Fig. 1. Superconducting dipole magnet.
1.Beam; 2.Rack; 3.Winding; 4. Connector;
5. Fill in device; 6. Support basic.

The magnet's yoke consists of top and bottom beams and lateral racks made of magnetic steel with low carbon content (Steel 10). The set of three pairs of top and bottom beams forms the magnet's poles. The cryostats for the excitation windings are fixed on the magnet's yoke, which receives the magnetic forces acting on the coil. The windings are made of superconducting cable with a cross-section of 7*4.5 mm². The cable consists of superconducting wires with niobium-titanic strings put in a copper matrix. The cross-section ratio of superconductor area to copper matrix is 1/3; the ratio of the superconducting wires to the aluminum matrix is 1/12.

The winding (Fig. 2) consists of two coils (pancakes) in rectangular form with a rounding at the corners. The parts of the coils in the magnet's outlet are turned up and down ('Duck nose' form), that makes the working aperture wider. In the magnet's outlet the winding is covered by a magnetic screen to reduce a field in the RICH area.

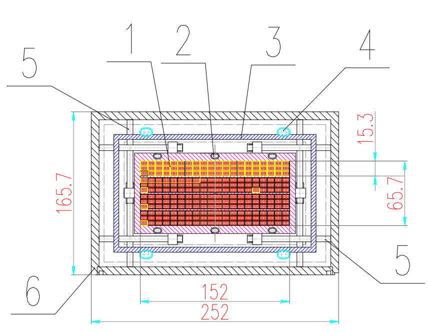

Fig. 2. SC winding with cryostat.

The excitation winding cryostat (Fig. 2) consists of the helium vessel (1), nitric screen (3) and vacuum casing (6). The nitric screen and helium vessel are the supporting elements of the construction. They transfer the forces from the windings to the vacuum casing. The cooling of the helium vessel is made by tubes (2) with circulating liquid helium. The external vessel's surfaces are polished and covered by Al foil to reduce heat flow from radiation. The heat flow from radiation is 0.22 watt. The helium vessel rests upon the nitric screen through Kevlar bases. The heat flow through the bases is 1.8 watt. The copper nitric screen with copper tubes (4), soldered to it, rests upon the vacuum casing of the stainless steel cryostat. The cover and hatches on the casing provide an access to the equipment inside of it. Thickness of the external wall of the vacuum casing, that must be less than 4 mm, is defined according to operating stability and admissible sag. The casing is equipped with tubes to connect vacuum pumps and install sensors for vacuum monitoring.

The inner surface of the vacuum casing is polished. A multilayer shield-vacuum isolation is placed between the vacuum casing and nitric screen. The top and bottom intercryostat connection is realized by two vacuum-cryostats adapters which allow jointing them to the winding. This permits to place here the elements of the helium and nitric circulation monitoring. The top cryostat is equipped with the lead-in device with two current leads designed for 5 kA, the inputs for liquid helium and nitrogen supply, sensors, control and monitoring devices and others. The pipes and other communications coming to the helium vessel create a heat flow to this vessel at a level of 5 watt.

The calculations with the program "RADIO" give a field in the gap of 1.5 T and in the RICH area of below 250 Gauss for an excitation current of 4 kA. The picture of magnetic field distribution along the Z and X axis is presented at Fig. 3.

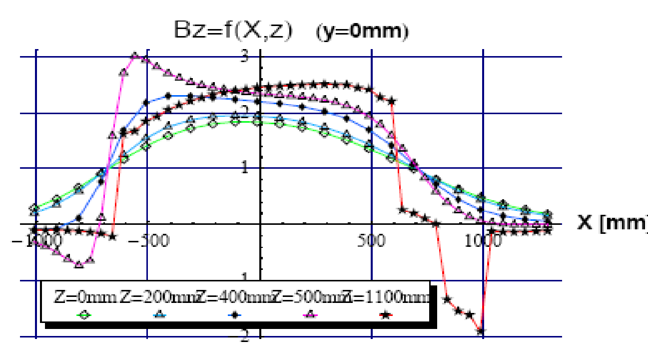

Fig. 3. Field distribution along the X-axis of the magnet for different height levels.

Radiation environment in the CBM experiment

R. Karabowicz and D. Bertini
GSI, Darmstadt, Germany

The CBM experiment focuses on the investigation of matter under extreme conditions as produced in heavy ion collisions by observing rare probes such as light vector mesons or charmonium particles [1]. The achievement of this goal depends crucially on the collection of high-statistics data, which requires running of the experiment at high collision rates. At present, we expect the collision rates to reach 10^7 minimum bias Au+Au collisions per second on a 1% interaction target. Such running conditions produce a high radiation environment, which has to be studied to identify both hot spots and regions in the experimental cave with low radiation levels, where infrastructure can be located.

Radiation simulations were performed with the FLUKA package [2]. 50 UrQMD minimum bias Au+Au collisions at 25 AGeV were injected into FLUKA which transported the produced particles in a simplified geometry of the CBM experimental cave. The result is shown in the left part of Fig. 1 as a scatter plot of the particle fluence converted to 1 MeV neutron equivalent units in a y-z projection of the CBM cave. We obtain a rather uniform distribution of the radiation level in the CBM cave except of the regions close to the target and in the beam dump, where the radiation level is much higher.

To estimate the radiation background induced by beam particles not interacting in the target, single gold ions were studied in a separate simulation. The results are displayed in the right part of Fig. 1, demonstrating that the back scattering of the beam in the beam dump produces a cone of heavy radiation comparable to the background from target interactions.

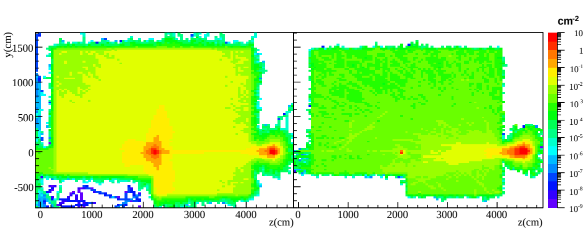

Figure 1: y-z scatter plot of particle fluence in the CBM cave for gold nuclei colliding with the gold target at 25 AGeV (left) and for gold nuclei interacting in the beam dump (right) normalized to one minimum bias interaction in the target

In the course of performing the FLUKA simulations, it appeared necessary to compare the results obtained with this transport code with the default transport code of the CBM experiment, GEANT3 [3]. We have chosen the charged particle energy loss in the silicon stations as a benchmark to compare the two engines. The energy loss predicted by GEANT was found to be about 20 % higher than that produced by FLUKA. The results proved to be relatively stable against changing GEANT or FLUKA settings. The only significant difference was observed when adjusting the number of tracking steps in the silion material; this dependence is currently under study.

The above comparison resulted in the possibility of performing radiation studies in the demanding environment of the STS. Assuming a CBM experiment lifetime of about $3 \cdot 10^{14}$ minimum bias Au + Au interactions at 25 AGeV (which corresponds to about 6 years of running), the estimated integrated dose in the silicon detector reaches 20 Mrad (see Fig. 2).

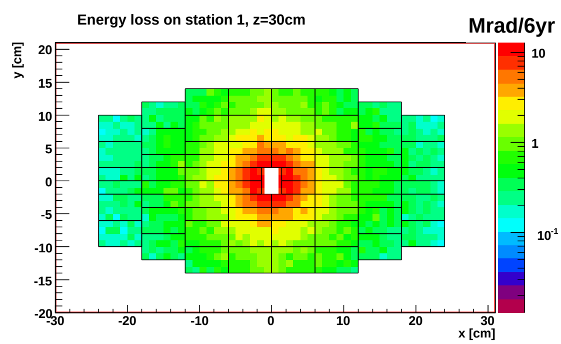

Figure 2: Radiation dose on the first STS station in 6 years of running

The preliminary studies of the radiation environment in the CBM experiment performed in the last year underline the challenging aspects of the detector setup and running conditions. Rough estimates predict radiation doses on levels comparable to that expected for the LHC experiments. It appears that the present construction of the beam dump is far too simplistic; its design is crucial for a minimization of the radiation doses in the CBM cave. Thus, future efforts will focus on optimizing the cave geometry with respect to the radiation environment, and on performing radiation tolerance tests of the most exposed detectors.

References

[1] P. Senger, *The CBM experiment at FAIR*, this report

[2] A. Fassó et al., *FLUKA, a multi-particle transport code*, CERN-2005-10, INFN/TC_05/11, SLAC-R-773

[3] M. Goossens, *GEANT: Detector description and simulation tool*, CERN W5013 (1993)

Status of the FairRoot Simulation and Analysis Framework

M. Al-Turany[1], D. Bertini[1], and F. Uhlig[1]
[1]GSI, Darmstadt, Germany

The FairRoot framework is used for simulation and analysis by the CBM and Panda collaborations at the GSI. Among the new developments in 2007 are a generic event display, an interface to external decayers and an interface for user-defined simple phase space decay. Moreover, a new mode of the main application has been introduced providing an easy way for the calculation of the radiation length in the different detector materials.

Event display

The event display in FairRoot is based on the Eve (Event Visualization Environment) package of ROOT [1]. Combined with trajectory visualization in FairRoot [2], it can be used directly from the macro to display TGeoTracks (MC Tracks) and all sub-classes of CbmPoint and CbmHit, together with the detector geometry (see Figs. 1 and 2). The FairEventManager implemented in FairRoot provides an easy way of applying cuts on energy, transverse momentum and particle type in the user events.

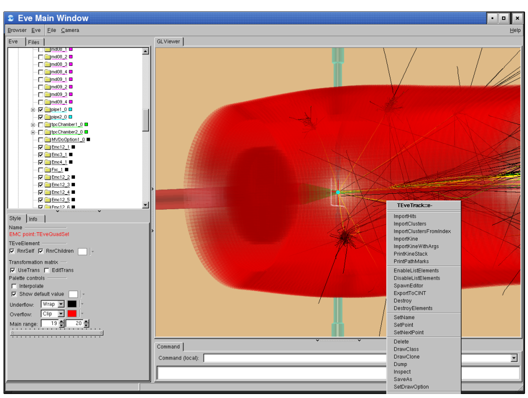

Figure 1: MC tracks and points in the PANDA-EMC detector

External decayer

An external decayer (TPythia6Decayer) can be used in place of the Monte Carlo native decay mechanisms for decays defined by the user in a configuration macro. The user can also force certain decay channels to be used instead of decaying according to the tabulated branching ratios (default in Pythia). The design allows the simutaneous use of different decayers for different particles.

Phase space 2 and 3 body decay

The GSDK routine of GEANT3 [3] was interfaced to enable the user to define custom 2 or 3 body decays for certain particles or fragments. This new interface was also communicated to the developers of ROOT and GEANT4-VMC [4]. In case of GEANT3-VMC, it is simply a wrapper of the GSDK routine. In GEANT4-VMC, more work had to be invested from the FairRoot and the VMC side in order to make the interface transparent for users and to enable the use of this facility without changing of the physics list.

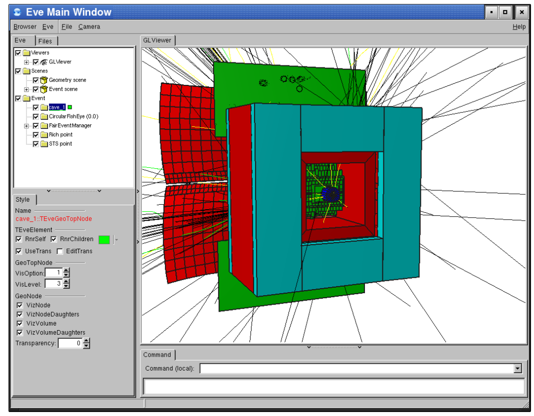

Figure 2: MC tracks and RICH points in the CBM detector

Radiation length manager

In a new mode of the framework application, the entrance and exit points of the particle trajectories in all volumes, sensitive and passive, are registered. This mode enables the user to calculate the effective material in units of radiation length for each trajectory.

Outlook

The development of the FairRoot framework is ongoing in close cooperation with the users, in particular the CBM and Panda collaborations, and the ROOT and VMC teams at CERN.

References

[1] http://root.cern.ch

[2] M. Al-Turany, D. Bertini, and I. König, *CBM Simulation and Analyis Framework*, GSI Scientific Report 2004 (FAIR-EXP-07), Darmstadt 2005, p. 13

[3] R. Brun et al., CERN DD/EE/84-1, Geneva 1987

[4] http://root.cern.ch/root/vmc

3D B-spline approximation of magnetic fields in inclined dipole magnets

P. G. Akishin, V. V. Ivanov, and E. I. Litvinenko
LIT JINR, Dubna, Russia

We consider the numerical problem of a three-dimensional (3D) magnetic field approximation. This is a typical problem not only for the CBM experiment, but for many experiments in high-energy physics where one deals with the task of track fitting. It arises in solving the equation of motion of charged particles in the magnetic field.

In practice, we deal with a non-homogeneous field known from field measurements or from mathematical calculations at some set of space points. The problem of approximation and continuation of the field is usually solved by applying piece-wise linear node functions. However, such field approximations provide neither the availability of high-order derivatives of the field nor even the existence of first derivatives.

The presence of high-order derivatives is very important when we apply high-accuracy numerical methods for solving the equation of motion. Such methods may provide a good convergence of numerical solutions to continuous ones only in the case of availability of corresponding derivatives of the field.

The best approach for continuation of the differentiable field is a spline approximation method [1]. For the first time we discussed the application of the B-spline approximation to 3D-rectangular magnetic field regions for the CBM experiment in [2]. However, this approach can not be directly applied to magnets with a non-rectangular working region as is the case for magnets which were considered as possible variants of the dipole magnet for the CBM experiment (Figs. 1-3). In this context, we adopted the approach presented in [2] for such cases using special variables for the field description [3].

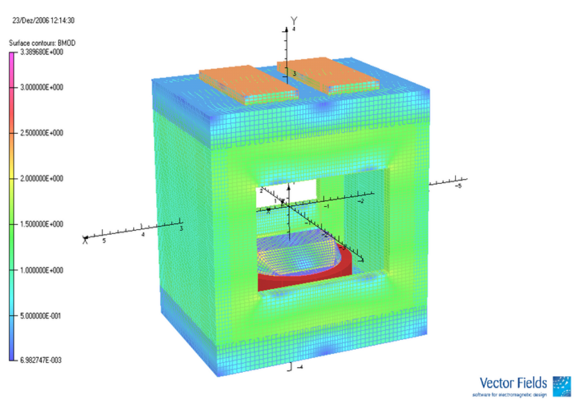

Figure 1: 3D model of the HERA dipole magnet

The main idea of the new approach was to transform the working region of the dipole magnet into a 3D-rectangular region. After such a transformation, the method described in [2] could be directly applied. The developed scheme can be used for the construction of a differentiable 3D B-spline approximation of the magnetic field for different types of dipole magnets for the CBM experiment.

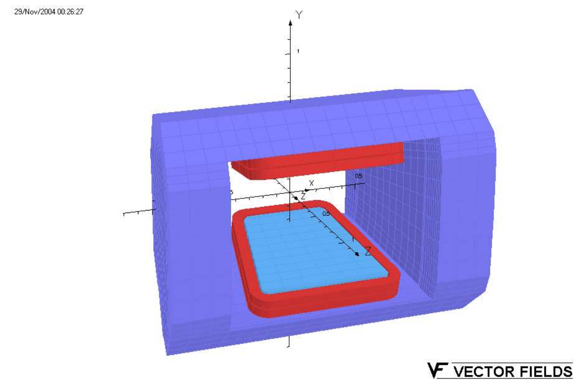

Figure 2: 3D model of the inclined version of the CBM dipole magnet (Alligator)

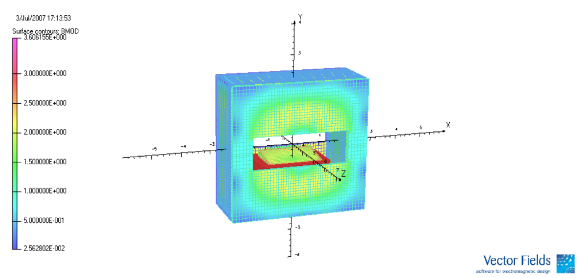

Figure 3: 3D model of the HERMES dipole magnet

References

[1] J. C. Zavialov, B. I. Kvasov, and B. L. Miroshnichenko, *Spline-function methods*. Nauka, Moscow 1980

[2] V. Ivanov, *LIT contribution to CBM*, 7^{th} CBM Collaboration Meeting, Darmstadt 2006, `http://www.gsi.de/documents/DOC-2006-Feb-176-1.pdf`

[3] P. G. Akishin, V. V. Ivanov, and E. I. Litvinenko: *3D-spline approximation of the dipole magnetic field in the CBM experiment*, in: *Proc. of the XXI International Symposium on Nuclear Electronics & Computing* (NEC2007) (Varna, Bulgaria, September 10-17, 2007), JINR, Dubna 2007 (in press)

Fast SIMDized Kalman filter based track fit

I. Kisel*[1,2], S. Gorbunov[2], U. Kebschull[2], V. Lindenstruth[2], and W.F.J. Müller[1]
[1]GSI, Darmstadt, Germany; [2]KIP, University of Heidelberg, Germany

The core of data reconstruction in high energy physics is the Kalman filter. Therefore, the development of fast, Kalman filter based reconstruction algorithms, making maximal use of the available processor power, is of utmost importance. A powerful feature supported by almost all up-to-date PC processors is a SIMD instruction set, which allows to pack several data items in one register and operate on all of them in one go, thus achieving more operations per clock cycle. A novel Cell processor extends the parallelization further by combining a general-purpose PowerPC processor core with 8 streamlined co-processing elements (SPEs) which greatly accelerate vector-processing applications.

In our investigation, after a significant memory optimization and a comprehensive numerical analysis, the Kalman filter based track fitting algorithm of the CBM experiment has been vectorized using inline operator overloading [1]. The algorithm thus continues to be flexible with respect to any CPU family used for data reconstruction.

Stage	Time/track	Speedup
Initial scalar version	12 ms	—
Approximation of the field	240 μs	50
Optimization of the algorithm	7.2 μs	35
Vectorization	1.6 μs	4.5
Porting to SPE	1.1 μs	1.5
Parallelization on 2 Cells	0.1 μs	10
Final simdized version	0.1 μs	120000

Table 1: Summarized stages of the porting procedure

Table 1 summarizes all stages of the investigation. The elimination of the magnetic field map and, as a result, the possibility to avoid access to the main memory increases the speed of the algorithm by up to 50 times. Optimization of the algorithm results in a 35 times faster performance. The vectorization stage, requiring both software and hardware changes, gives a speedup by a factor of 4.5. Porting to SPE resulted in an 1.5 increase of the speed with respect to a Pentium 4 processor used at the previous stages, probably because of the increased number of registers. The last stage is another hardware improvement that makes use of all 16 SPEs of the Cell Blade computer and, because of such simple parallelization as in the case of track fitting, gives another 10 times speedup. In total, the speed of the algorithm has been increased by a factor of 120,000.

We have compared the timing performance of the simdized version of the Kalman filter based track fitting

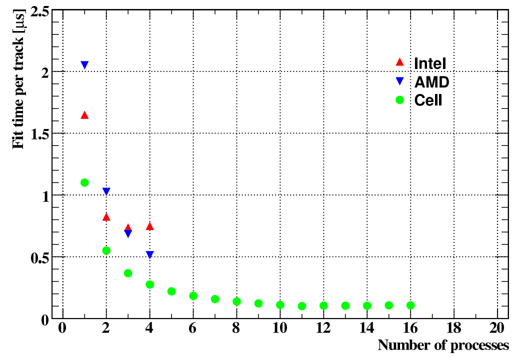

Figure 1: Fit time per track for the Intel, AMD and Cell based computers running different number of processes in parallel

routine running on three different CPU architectures: Intel[1], AMD[2] and Cell[3]. Both the Intel and the AMD based personal computers are treated by the operating system as having 4 processors each. Figure 1 shows that the hyperthreading of the Intel Xeon processor does not improve the performance in this particular case of the fitting procedure. In contrast, the dual core technology of the AMD Opteron processor shows stability of the timing performance due to its NUMA architecture. In the Cell Blade computer, all 16 SPEs work completely independently and in parallel. They show a constant speed of the algorithm per processing unit up to 11 processes. For more processes, the speed is slightly reduced, presumably due to the large data flow through the element interconnect bus. In general, despite of having significant differences in architecture and clock rate, all computers have shown a similar speed of the algorithm per processing unit.

The SIMDized Kalman filter based fitting routines have been also included into the cellular automaton track finder of the CBM experiment, resulting in an increase of the reconstruction speed by a factor of 1,000 with respect to the initial scalar version running on the same Pentium 4 based computer.

References

[1] S. Gorbunov, U. Kebschull, I. Kisel, V. Lindenstruth and W. F. J. Müller, *Fast SIMDized Kalman filter based track fit*. Comp. Phys. Commun., 2008, in press

* I.Kisel@gsi.de

[1] `lxg1411` (2 Intel Xeon with HT, 2.66 GHz) at GSI.
[2] `eh102` (2 Dual Core AMD Opteron 265, 1.8 GHz) at KIP.
[3] `blade11bc4` (2 Cell Broadband Engines, 2.4 GHz) at the IBM Laboratory Böblingen.

Implementation of a Hough Tracker for CBM

C. Steinle[1], A. Kugel[1], and R. Männer[1]

[1]University of Mannheim, Department of Computer Engineering V, 68131 Mannheim, Germany

The Hough transform is a global method for track finding, which in CBM is used for track reconstruction in the main tracking system (STS). All STS detector hits have to be transformed into a histogrammed parameter space according to the components of the track momentum $p(\theta, -\frac{q}{p_{xz}}, \gamma)$. This leads to our 3D Hough transform [1].

The hardware algorithm structure and the block diagram of the data path in front of the histogram was described previously [2]. The strategy for the usage of the histogram can be found in [1]. The implementation of the final parts is not yet developed in hardware. All investigated concepts are at first suitable for a single-chip FPGA implementation; however, due to the limited resources of such a chip and the huge algorithm resource requirements, we adapted the algorithm to be also suitable for a multi-chip system as depicted in figure 1. Within this concept, it is now possible to balance the hardware resources with regard to the necessary system speed which is defined by the data input and the number of parallelly used tracking systems. In addition, we can exploit the flexibility of the Hough tracking algorithm by implementing the different units on different platforms like FPGA or CELL BEs, since different parallelism levels can be used.

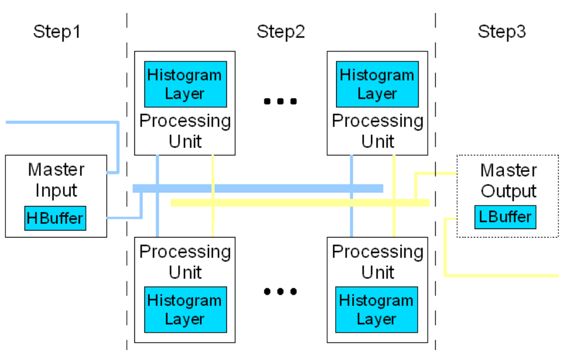

Figure 1: System design

In such a multi-chip system, the single-FPGA strategies can be used on different chips connected by a networking system. A common CELL BE has, except for the final LBuffer, resources for all mentioned units on a single chip. Furthermore, with the usage of a CELL BE it is easy to develop and proof the networking concept. A cheap and fast prototyping system is the Playstation3 system. Obviously, the possible parallelism level on such a system is different compared to the FPGA. Here, the major used parallelism is given by the fact that the histogram entry for one transformed hit is a plane in consecutive layers. Thus, having 128 bits ALU width, a plane can be inserted in up to 16 consecutive layers in parallel. Our next steps hence aim at the implementation and validation of the developed concepts on a Playstation3 system. In additon, the final stage of the algorithm has to be developed and implemented in a HDL for a FPGA.

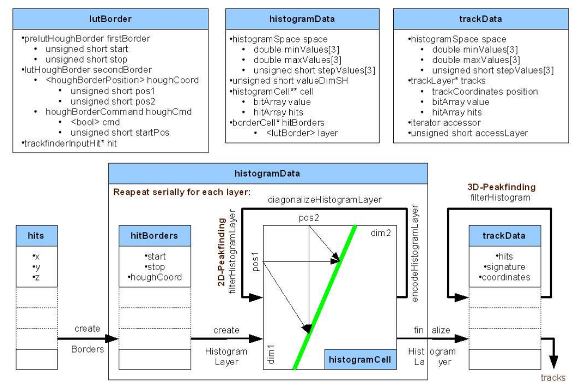

Figure 2: Software design

The software simulation of the Hough tracking algorithm was set up and is ready to be used in the CBMROOT framework. Figure 2 depicts the software design of the algorithm. The CBMROOT module 'htrack' contains the Hough tracking algorithm and many analyses to help adopting the parameters of the algorithm. Further on, there are internal analyses to check and verify each step of processing. A summary of all implemented analyses will be made available in the manual of the module which is by now in a reviewing state. In addition, the external interfaces are described in a separate 'how-to' which is also currently being reviewed. The next step in software development is the introduction of an automatised analysis in order to arrive at an optimal peak finding geometry. Furthermore, the two transformation formulas should be exchangeable such that the 4^{th} order Runge-Kutta method can be used for improving the track model as mentioned in [2].

References

[1] J. Gläss, C. Steinle and R. Männer, *Tracking in the Silicon Tracker System of the CBM Experiment using Hough Transform*, RT2005, June 2005, Stockholm, `http://www.gsi.de/documents/DOC-2007-Jul-9.html`

[2] C. Steinle, A. Kugel and R. Männer, *Implementation of a Hough Tracker for CBM*, CBM Progress Report 2006, Darmstadt 2007, `http://www.gsi.de/documents/DOC-2007-Mar-137.html`

D^0 detection in the CBM experiment

I. Vassiliev[1], S. Gorbunov[2], and I. Kisel[1,2]
[1]GSI, Darmstadt, Germany; [2]KIP, Ruprecht-Karls-Universität Heidelberg, Heidelberg, Germany

One of the major experimental challenges of the CBM experiment is to trigger on the displaced vertex of the D mesons in the high-multiplicity environment of a heavy-ion collision. This task requires fast and efficient track reconstruction algorithms and high-precision secondary vertex determination. Particular difficulties in recognizing the displaced vertex of the rare D meson decays are the very low multiplicities, low branching ratios, and multiple scattering in the beam pipe and detectors. In addition, weak decays of K^0_S, Λ and Σ taking place several cm behind the target result in a huge background of off-vertex tracks. In this report, we study the feasibility of the D^0 measurement via its decay modes $D^0 \to K^-\pi^+$ and $D^0 \to K^-\pi^+\pi^+\pi^-$. The simultaneous measurement of two decay channels of the same particle will provide an unique opportunity to reduce systematic uncertainties.

The study is based on about 10^4 central Au+Au events simulated in the CBM detector setup. D^0 decays were embedded into the background events in order to study the signal in the environment of background hadrons. A STS geometry with 2 MAPS and 6 double-sided strip detector stations was used. The first MAPS detector is located at 10 cm downstream of the target in order to reduce radiation damage. Track reconstruction was performed using the L1 reconstruction algorithms. The primary vertex was reconstructed with high accuracy (5.7 μm along and 1.0 μm perpendicular to the beam) from about 450 tracks fitted in the STS inside a non-homogeneous magnetic field by the Kalman filter procedure as described in [1].

A novel algorithm has been developed to reconstruct the D^0 life time and its decay length together with the corresponding errors. D^0 decay vertices are reconstructed from two or four daughter track candidates, respectively, assuming the previously found primary vertex as D^0 production point. Because of originating from a displaced vertex, the daughter tracks have a non-vanishing impact parameter in the target plane. Thus, a significant part of the background ($\approx$ 99 %) can be rejected on the single-track level by a cut on the distance of the track to the primary vertex. Further suppression of the combinatorial background is achieved by geometrical and topological quality cuts on the decay vertex. The resulting invariant-mass spectra, corresponding to 10^9 central events, are displayed in Fig. 1. The shape of the background in the signal mass region was estimated using the event-mix technique.

Table 1 presents the performances obtained for the two- and four-particle decay channels, respectively. In case of the 4-particle decay, the geometrical acceptance is lower by a factor of about three since all four daughter tracks are required to be accepted simultaneously. The vertex resolution

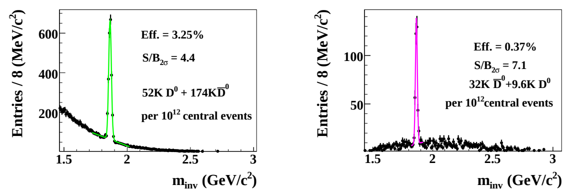

Figure 1: Invariant-mass spectra for $D^0 \to K^-\pi^+$ and charge conjugated (left) and $D^0 \to K^-\pi^+\pi^+\pi^-$ (right) corresponding to 10^9 central Au+Au events at 25 AGeV

is reduced due to the increased effect of multiple scattering on the daughter tracks which have, on average, lower momenta. This reflects in a lower signal efficiency of the vertex cut. On the other hand, the restriction imposed by the requirement of a good 4-particle vertex reduces the background very efficiently as visible in Fig. 1. All in all, the signal-to-background ratio expected in the 4-particle decay channel turns out to be even better than that obtained in the 2-particle channel.

	$D^0+\overline{D}^0$	D^0
decay channel	$K^-\pi^+$	$K^-\pi^+\pi^+\pi^-$
multiplicity	$1.5\cdot10^{-4}$	$4.0\cdot10^{-5}$
branching ratio	3.8%	7.7%
geom. acceptance	55.7%	19.3%
reconstr. efficiency	98%	97.7%
z-resolution	54 μm	82 μm
total efficiency	3.25%	0.37%
$\sigma_m[MeV/c^2]$	11.0	12.0
$S/B_{2\sigma}$ ratio	4.4	7.1
yield D^0	52 K	10 K
yield $\overline{D}^0$	174 K	32 K

Table 1: Acceptances and efficiencies, mass resolution, and signal-to-background ratio (S/B) in a $2\sigma_m$ region around the peak for D^0 reconstruction in central Au+Au collisions at 25 AGeV beam momentum. The total efficiency is calculated from the product of geometrical acceptance, reconstruction and cut efficiency. Reconstructed yields are given per 10^{12} central events.

References

[1] S. Gorbunov, I. Kisel and I. Vassiliev, *Analysis of D^0 Meson Detection in Au+Au Collisions at 25 AGeV*, CBM-PHYS-note-2005-001, [http://www.gsi.de/documents/DOC-2005-Jun-181.html]

D^+, D_s^+ and Λ_c^+ decay feasibility study in the CBM experiment

I. Vassiliev[1], S. Gorbunov[2], I. Kisel[1,2], S. Seddiki[1,3], and I. Sevastiuk[4]

[1]GSI, Darmstadt, Germany; [2]KIP, Ruprecht-Karls-Universität Heidelberg, Heidelberg, Germany; [3]Institut Pluridisciplinaire Hubert Curien, Strasbourg, France; [4]National Taras Shevchenko University, Kiev, Ukraine

Charged D mesons and Λ_c constitute a significant contribution to the open charm production at FAIR energies. Moreover, model predictions of their multiplicities differ noticeably, enabling the experiment to discriminate charm production scenarios. Therefore, the feasibility studies of open charm detection in the CBM experiment have been extended to the decay channels $D^+ \to K^-\pi^+\pi^+$, $D_s^+ \to K^-K^+\pi^+$ and $\Lambda_c^+ \to pK^-\pi^+$, with the corresponding life times of 312 μm, 150 μm and 59 μm, respectively. A high-precision measurement of the displaced decay vertex is mandatory in particular for the Λ_c^+ in order to suppress the overwhelming background of prompt charged hadrons. Vertexing in CBM is performed by the Micro-Vertex Detector (MVD), here assumed to be composed of two stations of 150 μm equivalent Si thickness each, positioned at 10 and 20 cm from the target.

The study is performed analogously to that for the D^0 mesons [1]. Time-of-flight information is used to reject (or select in case of Λ_c^+) proton tracks. A set of mainly topological cuts is imposed on single tracks as well as on reconstructed vertices. As an example, Fig. 1 demonstrates the background suppression by a cut on the secondary vertex position in the case of the D^+ meson. Single-track cuts mainly rely on the back-extrapolation to the primary vertex requiring the tracks to miss it. The reconstructed mother tracks, on the other hand, are required to point to the event vertex, a restriction which allows to strongly reduce random combinations.

The resulting invariant-mass spectra for the three decay channels under investigation are shown in Fig. 2 for central Au+Au collisions at 25 AGeV. Table 1 summarises acceptances, efficiencies and signal-to-background ratios.

	D^+	D_s^+	Λ_c^+
decay channel	$K^-\pi^+\pi^+$	$K^-K^+\pi^+$	$pK^-\pi^+$
multiplicity HSD	$4.2 \cdot 10^{-5}$	$5.4 \cdot 10^{-6}$	-
multiplicity SM	$8.4 \cdot 10^{-5}$	$1.4 \cdot 10^{-4}$	$4.9 \cdot 10^{-4}$
branching ratio	9.5%	5.3%	5.0%
geom. acceptance	39.6%	29.6%	53.0%
reconst. efficiency	97.5%	97.5%	97.6%
z-resolution	60 μm	67 μm	70 μm
total eff.	4.2%	1.0%	0.5%
$\sigma_m [MeV/c^2]$	11.0	12.0	12.0
$S/B_{2\sigma}$ ratio	9.0	0.3	0.25
yield (10^{12} events)	162K	72(2.9)K	107K

Table 1: Acceptance and efficienciy, mass resolution, and signal-to-background ratio (S/B) in a $2\sigma_m$ region around the peak for open charm reconstruction in central Au+Au collisions at 25 AGeV beam energy. The total efficiency is calculated from the product of geometrical acceptance, reconstruction and cut efficiencies. Multiplicities are taken from HSD [2] and the Statistical Model [3].

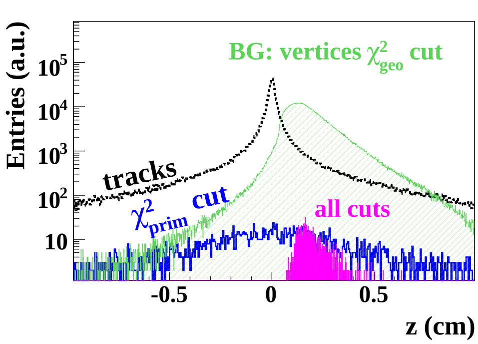

Figure 1: Distribution of single tracks and secondary vertices along the beam line for $D^+ \to K^-\pi^+\pi^+$ reconstruction. All primary tracks are shown by the black line, those selected as secondaries by the χ^2_{prim} cut as blue line. Secondary vertices after the geometrical cuts are shown in green, after the more stringent topological cut in magenta.

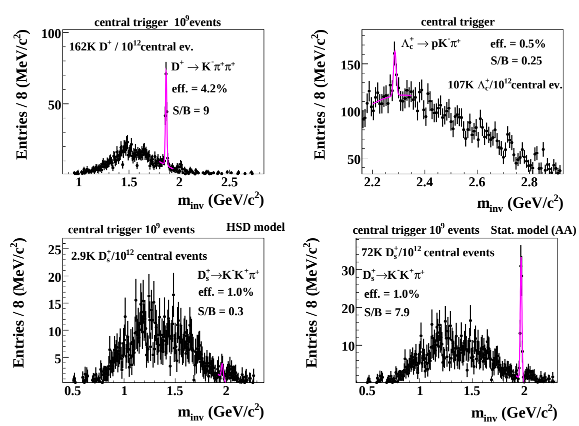

Figure 2: Reconstructed charmed hadrons in 10^9 central Au+Au collisions at 25 AGeV. $D^+ \to K^-\pi^+\pi^+$ (upper left), $\Lambda_c^+ \to pK^-\pi^+$ (upper right), $D_s^+ \to K^-K^+\pi^+$ with prediction from HSD (lower left) and from the Statistical model (lower right)

References

[1] I. Vassiliev et al., D^0 *detection in the CBM experiment*, this report

[2] W. Cassing, E. Bratkovskaya, and A. Sibirtsev, Nucl. Phys. A **691** (2001) 751

[3] A. Andronic et al., Phys. Lett. B **659** (2008) 159

Open charm trigger feasibility study in the CBM experiment

I. Vassiliev[1] and I. Kisel[1,2]
[1]GSI, Darmstadt, Germany; [2]KIP, Ruprecht-Karls-Universität Heidelberg, Heidelberg, Germany

One of the most important experimental tasks of the CBM experiment is to identify D mesons and Λ_c baryons at extreme interaction rates. Online event selection based on an open charm trigger signature is therefore mandatory in order to reduce the data volume to the recordable rate. This study investigates the possibility of a common trigger for the decay channels $D^0(\overline{D}^0) \to K^\mp\pi^\pm$, $D^\pm \to K^\mp\pi^\pm\pi^\pm$, $D_s^\pm \to K^\mp K^\pm\pi^\pm$ and $\Lambda_c \to pK^-\pi^+$. As the lifetimes of the charmed hadrons range from 60 μm to 312 μm, their most prominent characteristic is a decay vertex located from several 100 μm to several mm downstream of the target. Another common feature is the presence of an off-vertex kaon. For the feasibility study of the open charm trigger, 10^4 central and minimum bias Au+Au events at 25 AGeV have been simulated in the CBM setup. An STS geometry with 2 MAPS and 6 double-sided strip detector stations was assumed.

First, a trigger based on the secondary kaon was investigated. This requires kaon identifcation by TOF and thus combined STS and TOF information, and global tracking. However, central Au+Au events at 25 AGeV contain on average about 40 K^+ and 13 K^-, some of which having large normalised impact parameters χ^2_{prim} in the target plane due to multiple scattering in the target and the STS detectors. Even the relatively strong cut $\chi^2_{prim} > 3\,\sigma$ rejects only 32 % of central events (rejection factor 1.47).

In order to achieve higher rejection factors, the topology of the displaced decay vertex has to be exploited. This has the advantage of using local STS information only, but involves computationally expensive combinatorics. The flow chart of the Detached Vertex Trigger (DVT) is illustrated in Fig. 1. First, local reconstruction in the STS is performed by track finding, track fitting and primary vertex finding. Candidates for tracks from open charm decay are then selected based on the normalised impact parameter at the event vertex χ^2_{prim}. Pairs of oppositely charged track candidates are combined to look for decay vertex candidates. The pair vertex is required to satisfy the geometrical quality criterion $\chi^2_{2,geo} < 3\,\sigma$ and to be located between 250 μm and 1 cm along the beam axis. Events without a decay vertex candidate satisfying these criteria are rejected. The analysis of the selected tracks at this stage reveals that they are predominantly primary tracks having suffered multiple scattering, or secondary tracks from K^0_S and Λ decays as demonstrated in Fig. 2.

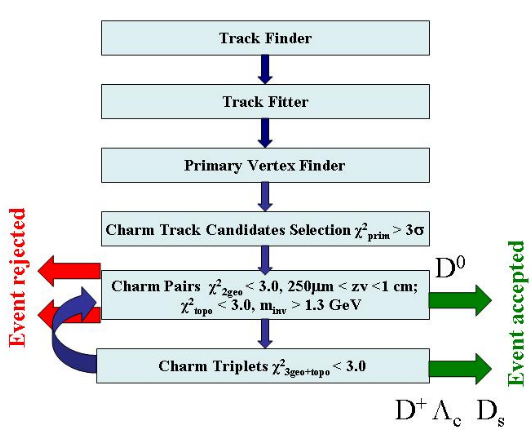

Figure 1: Flow chart of the Detached Vertex Trigger

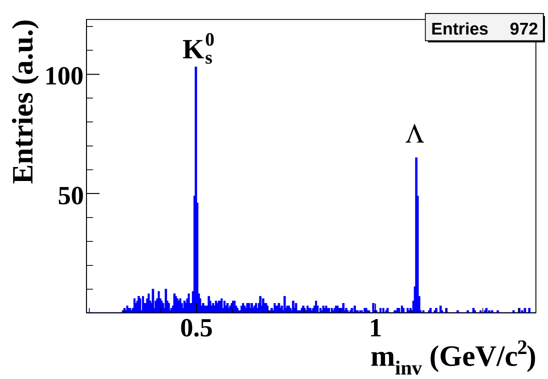

Figure 2: Invariant mass of the pair vertices selected at the first stage of the trigger algorithm. K^0_S and Λ decays are the main sources of the background.

In the last stage of the algorithm, 3-particle vertices are looked for by combining pair vertices with single candidate tracks. The triplet vertex has to fulfill the combined geometrical (closest approach of the track triplet) and topological (triplet momentum pointing to the event vertex) constraint $\chi^2_{3geo+topo} < 3\,\sigma$. Events containing such a 3-particle vertex are accepted as candidate for D^+, D_s^+, Λ_c and the 4-particle decay of D^0. For the other events, the 2-particle vertex is checked for the topological criterion $\chi^2_{topo} < 3\,\sigma$ and an invariant mass above 1.3 GeV/c^2, assuming kaon and pion mass for the daughter tracks, respectively. The event is accepted if these two conditions are fulfilled, signalling a candidate for a 2-particle decay of the D^0.

In the current STS setup, the DVT gives a rejection factor of 5.2 for central and about 40 for minimum bias Au+Au events at 25 AGeV.

Track reconstruction in the TRD and MuCh detectors

A. Lebedev*[1,2] and G. Ososkov[2]
[1]GSI, Darmstadt, Germany; [2]JINR LIT, Dubna, Russia

The successful application of the TRD tracking algorithms [1] lead to the idea to generalize and optimize those algorithms in a flexible way in order to make them applicable for other, similar detectors. In this contribution, we present how this idea was realized and applied for the TRD layout optimization and for track finding in the MuCh detector.

Since both tracking detector setups (TRD and MuCh) are analogous in many details, the same approach can be used for tracking in these detectors. Therefore, a generalized algorithm of track finding in the CBM tracking detectors has been developed. It is based on the Kalman Filter and track following methods where the next track point is searched in an area surrounding a predicted point. The main idea is to apply a general algorithm of track finding to different detectors and only adopt it to a specific one by changing the tracking routine parameters. This helps to decrease code duplication, thus significantly easing the software support.

In our implementation, tracking is accomplished in an iterative way. In each iteration, tracking parameters have to be specified, and hits belonging to tracks found in the current iteration are deleted from the hit array. In order to use the tracking routine, one has to specify the number of tracking iterations, the maximum number of allowed missing hits in a detector station, start and end station for the tracking, the sigma coefficient determining the searching region, and other parameters of the tracking. The searching region can be determined in two different ways: (1) using the covariance matrix of the predicted track parameters and position errors of the hits; (2) calculating the maximal deviation between the predicted position and a hit on the basis of a look-up table obtained from a simulation with large statistics.

For the TRD, two different approaches have been used: a standalone TRD track finder (using only TRD information), and an algorithm based on the information from tracks found in preceding detectors (STS-based or MuCh-based). For the MuCh detector, which consists of a sequence of several absorber and detector layers, vertex tracks reconstructed in the STS have been used as seeds for track reconstruction.

The software was embedded into the CbmRoot framework and tested on central Au+Au collisions at 25 AGeV beam energy from UrQMD.

Using the TRD track finder, a detector layout study has been performed in order to optimize the detector setup while keeping high reconstruction efficiency. The aim of this study is to minimize the costs of the detector. The standard detector setup for the TRD consists of 3 stations and 4 layers in each station (4-4-4), 12 layers in total. To minimize the number of stations, several TRD geometries with 3 layers in each station (25% savings) and with 2 layers in each station (50% savings) have been studied. For the standalone TRD track finder, two additional geometries have been studied, with 4 layers in the first station and 2 or 3 layers in the others (4-3-3 and 4-2-2). The tracking performance for the different TRD layouts looks surprisingly similar. An efficiency of 95-96% for the STS-track based TRD track finder and of 89% for the standalone TRD track finder has been achieved. However, this conclusion on the layout relates to tracking performance only without considering the task of electron-pion separation and should be completed by that consideration. The STS-track based TRD track finding efficiency for the standard TRD geometry (4-4-4) is shown in Figure 1 as function of momentum.

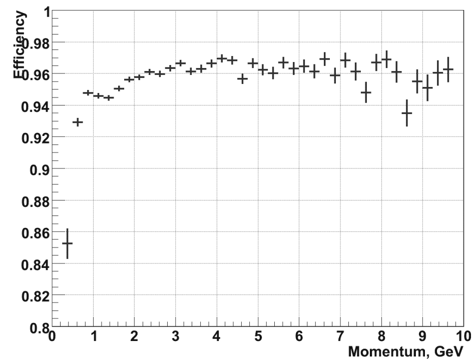

Figure 1: TRD tracking efficiency as function of momentum for tracks found in the STS

Similar to the scheme introduced above, track finding routines for the so called "compact" MuCh geometry [2] have been developed and tested. Decay muons from the omega meson were embedded into UrQMD events in order to simulate interesting track candidates. First results are rather promising. An efficiency at the level of 1.9-2.6% for signal pairs was achieved. This efficiency includes acceptance and full track reconstruction. The performance depends on the tracking parameters; typically, an increase of the signal finding efficiency also increases the background.

References

[1] A. Lebedev, G. Ososkov, *TRD and Global tracking*, X. CBM collaboration meeting, Dresden, 27 September 2007, [http://www.gsi.de/documents/DOC-2007-Oct-97.html]

[2] A. Kiseleva et al., *The muon detection system for the CBM experiment*, this report

* andrey.lebedev@gsi.de

Ring reconstruction in the CBM RICH detector

S. Lebedev*[1,2] and G. Ososkov[2]
[1]GSI, Darmstadt, Germany; [2]JINR LIT, Dubna, Russia

In this contribution we will present innovations and improvements which have been developed for ring reconstruction in the CBM RICH detector.

The RICH ring recognition algorithm based on the Hough Transform (HT) [1, 2] was rewritten improving the speed and the ring finding efficiency. It is now optimized for the Hamamatsu PMT H8500-03 (22 hits per electron ring), which did not result in an efficiency drop in comparison to the PMT proposal from Protvino (40 hits per electron ring).

In systematic studies for both the standard and the compact RICH layout [3], the following parameters were varied: type of photo-multiplier (Hamamatsu or Protvino), beam energy, number of noise hits in the PMT plane, and the magnetic field (active shielding magnet and dipole magnet with larger stray field in RICH). In dependence on those conditions, ring finding and ring-track matching efficiencies and fake ring rejection were investigated as function of momentum, radial position and hit density. It was found that due to an increasing hit density, the ring finding efficiency drops slightly with increasing beam energy, while the fake ring rate and ring-track mismatches increase at the same time. As long as less then 1% of the PMTs have noise hits in one event, the ring finding efficiency is not affected. The integrated ring finding and ring-track matching efficiencies for the two magnetic fields are the same.

As the rings in the photodetector plane have a slightly elliptic shape, an ellipse fitting method was developed in order to have a more precise determination of the ring parameters and, thus, an improved ring-track matching. It will be investigated whether these parameters can be used in order to separate primary and secondary electrons as many of the latter cross the RICH detector at large angles, hence showing different ring distortions in the photodetector plane.

The algorithm for handling ellipse-like rings was implemented into the CBM software framework. We use Kepler's ellipse definition to build the fitting functional, which is minimized using MINUIT. This algorithm was tested on simulated data and has shown good and interesting results. We observed that in the current CBM-RICH setup, the mean eccentricity of the rings is 0.43. For electrons from the main vertex, the ellipse rotation angle shows a clear dependence on the azimuthal angle of the electrons.

The sizes of the major and minor axes of the ellipses are strongly dependent on the position on the PMT plane. The mean value of the major half axis varies from 5.8 cm in the outer part of the PMT to 6.6 cm in the inner part; the half minor axis shows a variation from 5.2 cm to 5.9 cm. Therefore, a radius (axes) correction algorithm was introduced for an improved radius resolution and thus pion suppression. Our algorithm is based on a radius correction map obtained from a large-statistics simulation. The correction improves the resolution by a factor of two.

The existing fake ring rejection algorithm was improved after studying the distributions of 10 parameters related to the fitted ellipses, like major half axis, minor half axis, rotation angle etc. These parameters are used as input to a trained artificial neural network (ANN), which suppresses strongly the contribution of fake rings.

The current performance of the RICH ring reconstruction after all improvements is presented in Figure 1. The results were obtained for electrons embedded into central Au+Au collisions at 25 AGeV. The integrated ring finding efficiency for primary electrons is 93.6 % with an average number of fake rings of 4.0 per event. After applying the fake rejection routine based on the ANN, the number of fake rings was reduced to 0.29 per event at an efficiency of 90.9 %. The quoted effiencies do not include ring-track matching.

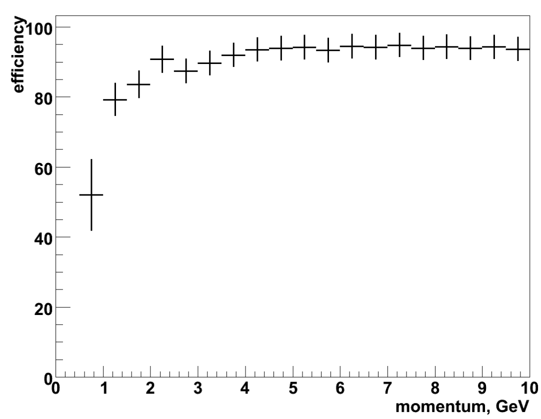

Figure 1: Ring finding efficiency of the HT ring finder for electrons from the main vertex as function of momentum, after fake ring rejection by use of the neural net

References

[1] P. V. C. Hough, *Method and Means for Recognizing Complex Patterns*, U.S. Patent 3,069,654 (1962)

[2] S. Lebedev, G. Ososkov and C. Höhne, *Ring recognition in the CBM RICH detector*, CBM-RICH-note-2008-001, Darmstadt, 2008 [http://www.gsi.de/documents/DOC-2008-Jan-29.html]; JINR Communication E10-2007-88, Dubna, 2007

[3] C. Höhne, *CBM-RICH layout optimization*, this report

* s.lebedev@gsi.de

CBM-RICH layout optimization

C. Höhne[1]
[1]GSI, Darmstadt, Germany

The RICH detector in CBM shall provide electron identification together with the TRD detectors for the measurement of low-mass vector mesons and charmonium in the di-electron decay channel. Both observables are considered key probes for the study of compressed baryonic matter in heavy ion collisions. A RICH design based on first general considerations has been developed and applied in detector simulations and feasibility studies [1, 2]. These studies include full event reconstruction and electron identification in the proposed CBM setup. Current results clearly demonstrate the feasibility of these measurements [2]. Combining RICH, TRD and TOF information, a pion suppression of 10^{-4} at an electron identification efficiency of 80% is reached for 2 GeV/c $< p <$ 8 GeV/c. Efficiencies and signal-to-background ratios for reconstructed low-mass vector mesons and charmonium are very promising [3, 4]. However, the layout of the RICH detector was only implemented based on a first, educated guess. An optimization of the RICH in particular with respect to minimizing its dimensions is awaiting. This process has been started and first results will be presented in this report.

In order to keep the number of detected photoelectrons per electron ring when reducing the overall length of the detector, a radiator gas with larger refractive index has to be chosen to compensate the lower yield of Cherenkov photons. We investigated CO_2 instead of N_2, see table 1. The larger refractive index of CO_2 slightly lowers the threshold of Cherenkov light production for pions; otherwise both gases have similar, convenient properties. With mirrors of

	large RICH	compact RICH
radiator gas	N_2	CO_2
γ_{th}	41	33.3
p^{π}_{th} [GeV/c]	5.6	4.65
λ_{th} [nm]	< 160	~ 175
radiator length	2.5 m	1.76 m
full length	2.9 m	2.1 m
mirror radius	4.5 m	3 m
mirror size	$2(5.7 \cdot 2)$ m^2 $\sim$ 22.8 m^2	$2(4.2 \cdot 1.4)$ m^2 $\sim$ 11.8 m^2
photodetector size	$2(3.2 \cdot 1.4)$ m^2 $\sim$ 9 m^2	$2(2.4 \cdot 0.78)$ m^2 $\sim$ 3.7 m^2
No. of channels	$\sim$ 200k	$\sim$ 85k

Table 1: Comparison of layout parameters for the large and compact RICH detector. The size of the photodetector can be further reduced on account of the acceptance; the mirror would be reduced accordingly.

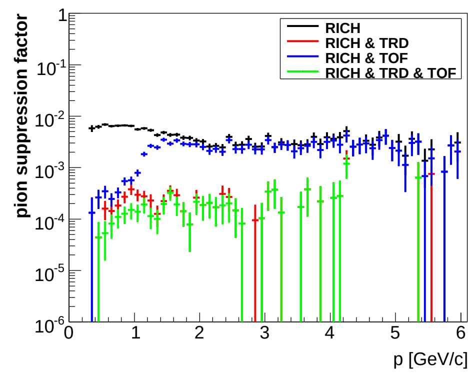

Figure 1: Pion suppression factor for central Au+Au collisions at 25 AGeV with the small RICH layout

3 m radius, this allows to reduce the detector length by 30% resulting in an overall reduction of the RICH dimensions by a factor 2-3 (table 1, compact RICH) while keeping the same geometrical acceptance. The number of channels in the photodetector plane has been calculated based on the H8500 MAPMT from Hamamatsu. Considering the fact that the RICH acceptance so far has been kept rather large and has not yet been optimized with respect to the physics analysis, a total number of 64k channels corresponding to 1000 MAPMTs is realistic. A first design of a compact RICH detector based on the parameters given in table 1 was implemented in the CBM simulation framework in order to study its characteristics. The layout is not yet optimized as rings still show strong distortions in the photodetector plane. Currently, this reduces the efficiency of ring reconstruction from 90% to 75% and increases the ring radius resolution from 2% to 6%. With an optimized position of the photodetector plane, we expect to reach the same performance as before. However, even with this reduced RICH performance, a pion suppression factor of nearly 10^{-4} is again reached in combination with TRD and TOF information. Based on this first promising results we will continue developing an optimized, reduced RICH layout for CBM.

References

[1] C. Höhne et al., Nucl. Instr. Meth. A 553 (2005) 91

[2] C. Höhne et al., Proceedings of 6$^{\text{th}}$ international workshop on RICH counters 2007, to be published in Nucl. Instr. Meth. A

[3] T. Galatyuk et al., *Di-electron spectroscopy in CBM*, GSI Scientific Report 2007 and CBM Progress Report 2007

[4] A. Maevskaya et al., *Charmonium reconstruction in CBM*, CBM Progress Report 2007

TRD layout studies and energy loss simulations

F. Uhlig[1]
[1]GSI, Darmstadt, Germany

The tasks of the Transition Radiation Detector [1] in the CBM experiment are electron identification and tracking between STS and TOF. The TRD has to be operated at count rates up to 100 kHz/cm^2. Prototypes of single TRD layers which could fulfill the experimental requirements were developed by several groups [2, 3, 4].

Geometries

The geometries of two of these prototypes, a single gap MWPC with a gas layer of 6 mm and a double-sided MWPC with two gas layers of 6 mm each [5] were implemented in the simulation of the CBM experiment. In order to study general properties of the TRD like energy loss, electron identification or tracking performance, idealized versions of the geometries are employed which are sensitive in the entire detector plane. These idealized geometries are also used to compare the simulation with the beam test data.

A more realistic detector performance is studied by a TRD built up from single detector chambers. The layout is optimized such that the complete detector with several layers can be built with only three different detector modules.

Energy Loss

For a realistic estimate of the electron identification capabilities provided by the TRD, it is essential to correctly describe the energy loss of charged particles in the detector gas. Since transport engines do not provide a reliable description of the transition radiation induced by electrons in the radiators, the TR is modeled by hand according to experimental data. For the ionzing energy loss, a correct description of measured data was achieved within GEANT3 by choosing the proper physics model as shown in Fig. 1. A similar tuning of the transport engine will be done for GEANT4 in the near future.

Electron identification

Electron identification is based on the energy loss information in all twelve layers of the TRD. Three different algorithms have been developed and implemented in the CBM software framework. The first is based on a maximum-likelihood method making use of the normalised energy loss spectra of electrons and pions as obtained from simulations. From these spectra, the probabilities $P(E|e)$ and $P(E|\pi)$ of an electron or a pion, respectively, depositing the energy E in a detector layer are derived. Adding the

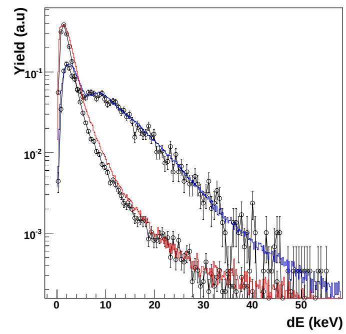

Figure 1: Measured energy losses for pions and electrons (black) compared to simulations for pions (red) and electrons (blue)

information of all twelve layers and assuming that the layers are identical, the likelihood to be an electron is defined as

$$L_e = \frac{P_e(E)}{P_e(E) + P_\pi(E)}. \tag{1}$$

The value of L_e ranges between 0 and 1 and is used to discriminate electrons from pions.

The second method is also a probabilistic approach which is described in detail in [6]. The third method uses a neural network which was trained with a pure electron (signal) and a pure pion (background) sample [7].

References

[1] B. Dolgoshein, *Transition radiation detectors*, Nucl. Instrum. Meth. A **326** (1993) 434

[2] M. Klein-Bösing et al. *Position resolution of a high efficiency transition radiation detector for high counting rate environments*, Nucl. Instrum. Meth. A **585** (2008) 83

[3] M. Petris et al., *High counting rate transition radiation detector*, Nucl. Instrum. Meth. A **581** (2007) 406

[4] A. Andronic et al., *Electron/pion identification with fast TRD prototypes*, CBM Progress Report 2006, Darmstadt 2007, p.35 [`http://www.gsi.de/documents/DOC-2007-Mar-137.html`]

[5] M. Klein-Bösing et al., *High efficiency TRD for CBM in test beam and simulation*, this report

[6] V. V. Ivanov and P. V. Zrelov, Int. J. Comput. & Math. with Appl., vol. 34, No. 7/8, (1997) 703

[7] E. P. Akishina et al., *Electron/Pion Identification in the CBM TRD Using a Multilayer Perceptron*, JINR Communication E10-2007-17, Dubna 2007

Electron Identification in the Compressed Baryonic Matter (CBM) experiment

S. Das[1] and C. Höhne[1]
[1]Gesellschaft für Schwerionenforschung mbH (GSI), Darmstadt, Germany

One of the key physics programs of CBM is the spectroscopy of both low and high mass vector mesons (namely ρ, ω, ϕ, J/ψ, ψ') through their di-electron decay channels. The first step towards this is the identification of electrons. In the current CBM setup, electron identification involves the Ring Imaging CHerenkov counter (RICH), the Transition Radiation Detector (TRD) and the Time Of Flight (TOF) detector. The informations from RICH and TRD are used to identify the electrons, and those from TOF help to suppress the pions in the identified electron sample. A software package has been developed to perform these tasks. The methods and performance of electron identification after full event reconstruction will be presented in this report.

In the event reconstruction, particles are first tracked by the tracking detectors placed inside a dipole magnetic field, providing the momentum of the tracks. The information from RICH, TRD and TOF is then associated to these tracks to form a global track.

RICH rings are found using ring reconstruction algorithms [1]. Next, the tracks are extrapolated from the last STS plane to the photodetector plane. Rings are associated to tracks choosing pairs with closest distance between track and ring centre. Rings with ring-track distance more than 1 cm are rejected as wrong matches. A set of ring quality cuts is also applied in order to reject fake rings. Finally, the electrons are identified choosing a range of radii of $\langle R\rangle \pm 3\sigma$, with $\langle R\rangle$ = 6.17 cm and σ = 0.14 cm. Pion rings leak into this band and are identified as electrons only for momenta larger than 8 GeV/c.

While passing through the TRD planes, pions suffer only from the specific energy loss dE/dx whereas electrons are subject to additional energy loss by emission of transition radiation. The CBM electron identification framework provides three different methods to discriminate electrons from pions based on the total energy loss, namely the Likelihood, the Ω_n^k [2] and the Artificial Neural Network methods.

In addition to RICH and TRD, the information from TOF is also used to separate hadrons from electrons. The squared mass of charged particles m^2 is calculated from the length traversed by the particle and the time of flight. A momentum dependent cut on m^2 is used to reject hadrons from the identified electron sample.

After the electron identification, each of the identified tracks is associated to its available Monte Carlo information for the quality assessment of the electron identification. The relevant quantities are defined as

$$\text{efficiency} = \frac{\text{identified true electrons}}{\text{electrons in RICH acceptance}}$$

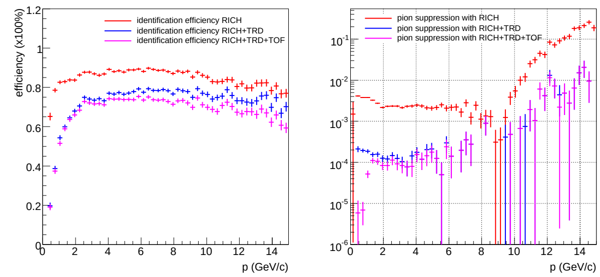

Figure 1: Efficiency of electron identification (left) and pion suppression factor (right) as function of momentum for central Au+Au collisions at 25 AGeV beam energy

and

$$\text{pion suppression} = \frac{\text{pions identified as electrons}}{\text{pions in RICH acceptance}}$$

The performance of the detectors as well as the electron identification software were studied for central Au+Au collisions at 25 AGeV beam energy, generated by UrQMD [3]. These events were tracked through the CBM detector system using GEANT3 [4] and reconstructed afterwards. The electron identification efficiency as well as the π-suppression factor as function of momentum are shown in Fig. 1. With the combined information from all detectors, we achieve an efficiency of 70% for momenta larger than 2 GeV/c. The drop in efficiency towards low momentum results from tracking, ring finding efficiencies and TRD and TOF acceptance losses compared to RICH. Using the RICH alone, a π-suppression factor of 500 is achieved whereas after combining information from TRD and TOF, the π-suppression factor reaches up to $\sim 10^{-5}$ for low momentum. Evidently, the use of TRD information significantly improves the electron-pion separation; TOF suppresses pions by about an order of magnitude for momenta below 1 GeV/c.

The set of cuts for different detectors are being optimized to obtain the best values for electron efficiency and pion suppression. The electron identification is expected to be further improved by an optimized combination of various detector information.

References

[1] S. Lebedev et al., *Ring reconstruction in the CBM RICH detector*, this report

[2] P. Zrelov and V. Ivanov, Nucl. Instr. Meth. A **310** (1991) 623

[3] S. A. Bass et al., Prog. Part. Nucl. Phys. **41** (1998) 255

[4] `http://wwwasd.web.cern.ch/wwwasd/geant`

On the distribution of energy losses in the CBM-TRD

E. P. Akishina, T. P. Akishina, O. Yu. Denisova, and V. V. Ivanov
LIT JINR, Dubna, Russia

We analyze the energy loss of electrons and pions at p = 1.5 GeV/c in the TRD detector, using both measurements with a single-layer TRD prototype obtained in a beam test at GSI in February 2006, and simulations of the TRD with n layers with GEANT3 in the framework of CbmRoot.

Fig. 1 shows the measured energy loss distribution of pions in the TRD protoype. It can well be approximated by a log-normal function [1]

$$f_1(x) = \frac{A}{\sqrt{2\pi}\sigma x} \exp^{-\frac{1}{2\sigma^2}(\ln x - \mu)^2},$$

where μ is the mean value, σ the dispersion, and A a normalization constant.

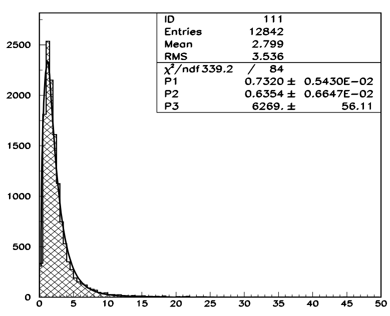

Figure 1: Distribution of the energy loss of pions in the TRD prototype

In addition to ionization, electrons suffer energy loss due to the production of transition radiation. Their energy loss distribution (see Fig. 2) can be approximated with high accuracy by the weighted sum of two log-normal functions

$$f_2(x) = B\left(\frac{a}{\sqrt{2\pi}\sigma_1 x}\exp^{-\frac{1}{2\sigma_1^2}(\ln x-\mu_1)^2} + \right.$$
$$\left. + \frac{1-a}{\sqrt{2\pi}\sigma_2 x}\exp^{-\frac{1}{2\sigma_2^2}(\ln x-\mu_2)^2}\right).$$

Here, μ_1 and μ_2 are the mean values, σ_1 and σ_2 the dispersions, a and $1-a$ the contributions of the first and second log-normal distribution, respectively, and B is a normalization constant.

The energy loss distributions of pions and electrons obtained from the GEANT3 simulations are also well described by log-normal distributions. Table 1 compares mean values and RMS of the distributions from the prototype measurements and from simulation. Deviations in the values are below 10 %.

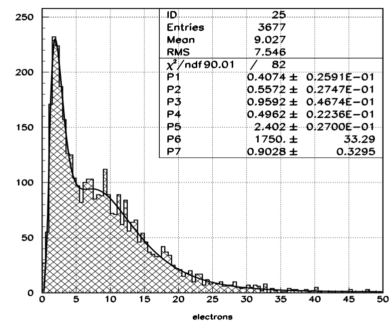

Figure 2: Distribution of the energy loss of electrons in the TRD prototype

distribution	m.v. (π)	RMS (π)	m.v. (e)	RMS (e)
prototype	2.8	3.5	9.0	7.5
GEANT	3.0	3.8	9.6	7.7

Table 1: Mean values (m.v.) and RMS of the energy loss distributions of pions and electrons from prototype measurements and simulations

In order to study the pion suppression capabilities in the TRD consisting of n layers, random values were generated for each layer from the distributions of Figs. 1 and 2. Three approaches for electron identificaton were applied [2]: the Likelihood Functions Ratio (LFR) method, the mean value (MV) method, and the ω_n^k test. The pion suppression factors obtained with these methods at 90 % electron efficiency in a TRD with $n = 12$ layers are presented in Table 2, showing that the moderate deviations of the simulated energy loss distributions from the prototype measurements result in a significantly reduced pion suppression capability. The reasons for these deviations are under study.

data	LFR	ω_n^k (only)	MV	MV + ω_n^k
prototype	108	83	73	781
GEANT	41	55	17	262

Table 2: Pion suppression for different methods in case of prototype measurements and simulations

References

[1] E. P. Akishina et al., *Distribution of energy losses for electrons and pions in the CBM TRD*, JINR Communications E10-2007-158, Dubna 2007

[2] E. P. Akishina et al., *Comparative study of statistical criteria for e/π separation in the TRD*. this report

Comparative study of statistical criteria for e/π separation in the TRD

E. P. Akishina, T. P. Akishina, O. Yu. Denisova, and V. V. Ivanov
LIT JINR, Dubna, Russia

We compare different approaches for the e/π separation using the Transition Radiation Detector (TRD) in the CBM experiment. The methods are based on the energy loss measurements for π and e at p = 1.5 GeV/c in a single-layer TRD prototype as obtained in the beam test of February 2006 at GSI. The distributions of these measurements have been used for the simulation of energy losses of e and π in the TRD consisting of n identical layers.

In the first approach, the method of Likelihood Functions Ratio (LFR) is used for particle identification. The value

$$L = \frac{P_e}{P_e + P_\pi}, P_e = \prod_{i=1}^{n} p_e(\Delta E_i), P_\pi = \prod_{i=1}^{n} p_\pi(\Delta E_i)$$

is calculated for each set of energy losses, where $p_{\pi,e}(\Delta E)$ denotes the probability density function for the energy loss ΔE in a single layer for pions and electrons, respectively. The approximation of the probability density functions, which with good accuracy reproduces the measured energy loss distributions, is described in [1]. Fig. 1 shows the distributions of L for pions (top left) and electrons (top right) and the sum of both (bottom) in 12 layers. Electrons are identified by a custom cut in this variable.

The second approach is based on the successive application of two statistical criteria: the Mean Value (MV) method and the ω_n^k-test [2]. In the mean value method, the mean energy loss $\overline{\Delta E}$ of a track in all TRD layers is calculated. Its distributions for pions and electrons are shown in Fig. 2. Again, electrons are selected by an appropriate cut.

Fig. 3 shows the distributions of the ω_n^8 measure [2] for pions and electrons. Here, $n = 12$ is the number of TRD layers. Pions, peaking strongly at small values of ω_n^8, can well be separated from electrons.

Table 1 presents the comparison of the discussed methods. Here, α is the fraction of rejected electrons (electron efficiency = 1 - α) and β the fraction of misidentified pions (pion suppression = 1 / β). The successive application of the mean value method and the ω_n^k test provides the best results with a pion suppression of about 800 at an electron efficiency of 90 %.

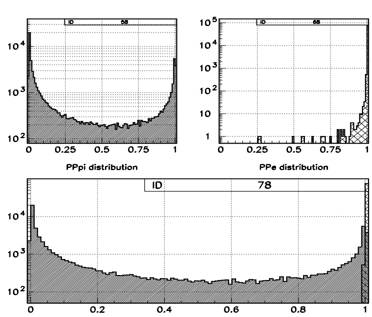

Figure 1: Distributions of L for pions (top left), electrons (top right) and the sum of both (bottom) in a TRD with 12 layers

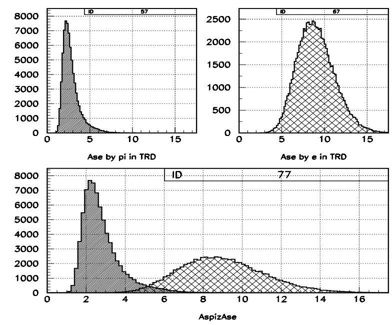

Figure 2: Distributions of $\overline{\Delta E}$ for pions (top left), electrons (top right) and the sum of both (bottom)

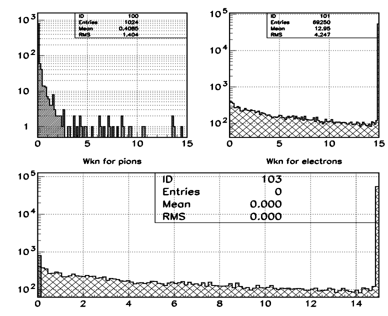

Figure 3: Distributions of ω_n^k for pions (top left), electrons (top right) and the sum of both (bottom)

method	α [%]	β [%]	pion suppression
LFR	10	0.925	108
ω_n^k	10	1.152	87
MV	7.7	1.365	73
MV + ω_n^k	10	0.128	781

Table 1: Comparison of the identification methods (see text)

References

[1] E. P. Akishina et al., *On the distribution of energy losses in the CBM-TRD*, this report

[2] P. V. Zrelov and V. V. Ivanov, Nucl. Instr. Meth. A **310** (1991) 623

Di-electron spectroscopy in CBM

T. Galatyuk[1], S. Das[1], and C. Höhne[1]
[1]GSI, Darmstadt, Germany

The emission of lepton pairs out of the hot and dense collision zone of heavy ion reactions is a promising probe to study the electromagnetic structure of hadrons under extreme conditions. The reconstruction of low-mass vector mesons (ρ^0, ω, ϕ) is one of the prime tasks of the CBM experiment. In this report, we present the status of simulations of the electron pair measurement in CBM and compare the expected performance to that of previous or existing dilepton experiments.

The general challenge of di-electron measurements in heavy-ion collisions is to cope with the large background of electrons originating from other than the desired sources. This is in particular difficult in the CBM spectrometer since electron identification is not provided in front of the magnetic field required for tracking. This leads to a considerable material budget in front of the RICH detector.

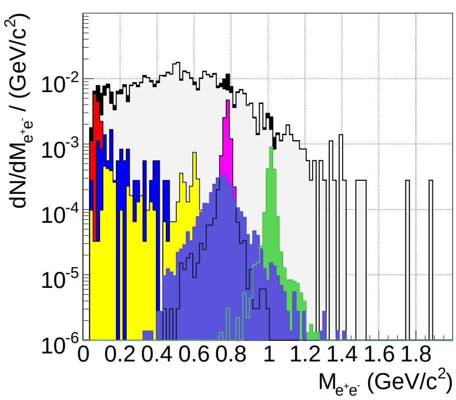

Figure 1: Di-electron invariant mass spectra for central $Au + Au$ collisions at a beam energy of 25 AGeV. Black area: unlikesign combinations of e^+ and e^-, grey: combinatorial background. Red: π^0, dark blue: η, yellow: ω-Dalitz, magenta: ω, green: ϕ, violet: ρ^0. The simulated data sample (200 k events) corresponds to 10 seconds of beam time.

An important requirement for efficient background rejection is electron identification with high efficiency and purity. In CBM, the RICH detector in combination with TRD and TOF provides a π-suppression factor of 10^4 at 50 % electron efficiency for momenta below 2 GeV [1]. With such high a purity of the identified electron sample, the dominant background sources are random combinations of e^- and e^+ from π^0-Dalitz decay and γ conversion, the latter mostly in the target. Several topological cuts have been developed to reduce the background [2]. The invariant mass spectrum of dielectron pairs including full event reconstruction and electron identification after applying all cuts is shown in Figure 1. The signal-to-background (S/B) ratio in a $\pm 2\ \sigma_m$ range around the ω pole mass is 0.3 at a signal efficiency of 6.7%. For the invariant mass region above 200 MeV/c^2 a S/B ratio of 1/16 is obtained.

A strong excess of di-lepton pairs over the yield expected from neutral meson decays was observed by hitherto existing dilepton experiments [3, 4, 5]. From a parametrisation of the published enhancement factors as function of $\sqrt{s}$ and dN_{ch}/dη, we expect this factor to be not smaller than 6 in central Au+Au collisions at 25 AGeV. For CBM, we thus deduce a S/B ratio of $6 \times 1/16$ for $m_{inv} > 200\,\mathrm{MeV}/c^2$. As Figure 2 demonstrates, this performance is well competitive with previous experiments measuring di-leptons in heavy-ion collisions at similar charged track densities.

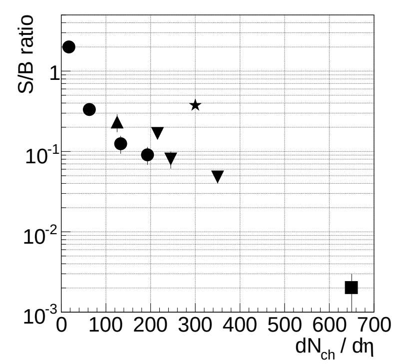

Figure 2: Signal-to-background ratio for m_{inv} larger than 200 MeV$/c^2$ as function of dN_{ch}/dη. Circle: NA60 data; triangle: CERES data, square: PHENIX data; star: CBM assuming an enhancement factor of 6.

References

[1] S. Das et al., *Electron identification with RICH and TRD in CBM*, this report

[2] T. Galatyuk et al., *Strategies for electron pair reconstruction in CBM*, GSI Scientific Report 2005/FAIR-QCD-CBM-06

[3] D. Adamova et al. (CERES collaboration), *Enhanced Production of Low-Mass Electron-Positron Pairs in 40-AGeV Pb-Au Collisions at the CERN SPS*, Phys. Rev. 91 (2003) 042301

[4] S. Damjanovic for the NA60 collaboration., *First measurement of the ρ spectral function in nuclear collisions*, arXiv:nucl-ex/0609026 v1, 16 Sep 2006

[5] S. Afanasiev et al., (PHENIX collaboration), *Enhancement of the dielectron continuum in Au+Au collisions at $\sqrt{s_{NN}}$=200 GeV*, atXiv:0706.3034v1[nucl-ex], 20 Jun 2007

Systematic investigations on the di-electron setup of CBM

K. Antipin[1], H. Appelhäuser[1], and C. Höhne[2]
[1]IKF, University of Frankfurt, Frankfurt, Germany; [2]GSI, Darmstadt, Germany

In this report, we present a systematic investigation on an optimization of the di-electron setup of CBM for the measurement of low-mass vector mesons, and establish a limit on the pion misidentification. The main challenge in the di-electron spectroscopy is the efficient reduction of background electrons which dominantly stem from π^0 Dalitz decay and γ conversion in the target. This study is fully based on MC information.

In the currently applied background suppression strategy [1], first a cut of $M_{inv} < 0.025$ GeV is placed in order to reject reconstructed pairs from γ-conversion. Afterwards, a topological cut on the distance of identified tracks to the closest hit of not accepted tracks in the first tracking station (MAPS, 10 cm behind the target) is applied.

In order to increase the power of this cut, we consider a reduction of the magnetic field between target and first MVD station and the possibility of electron identification in the first MVD. Fig. 1 shows the distance of electron tracks identified after the STS to the nearest hit of not accepted tracks for different sources of lepton tracks. Two cases are presented: No magnetic field in the first 10 cm (solid lines), and e-ID in the 1^{st} MVD with 70% of the nominal CBM field (0.07 Tm field integral, dashed lines). As the mean distances of electrons from π^0 or γ conversion differ from those stemming from ρ mesons, a cut can be placed to reject background.

Cut values were established for field integrals varying from 0 % to 100 % of 0.07 Tm. Fig. 2 shows the resulting fraction of rejected electrons from π^0 and γ conversion. Electrons from ρ mesons are rejected on a constant 20% level for the configuration with e-ID in the first MAPS detector and with a larger and further increasing fraction

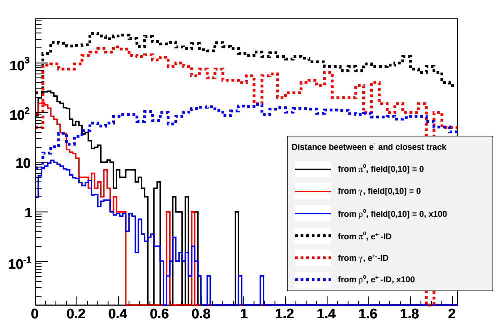

Figure 1: Distance of electrons in the first MVD station to hits from the closest not accepted track without magnetic field in the first 10 cm (solid lines) and with e-ID and 70 % nominal field (dashed lines)

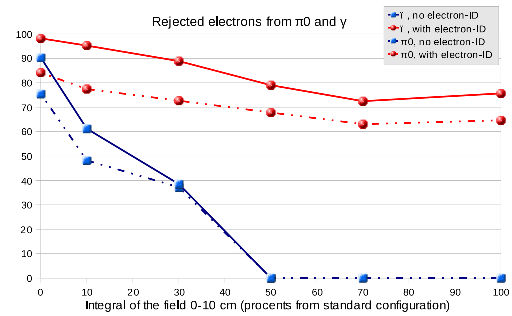

Figure 2: Rejection of electrons from π^0 and γ conversion with and without e-ID versus a given field integral in the first 10 cm (100% correspond to 0.07 Tm)

without. However, the signal-to-background ratio in the di-electron invariant-mass range 0.2 - 0.9 GeV is increased only by a factor of two under these conditions, i. e. with e-ID and field integral less then 0.02 Tm, and remains nearly unaffected without e-ID but reduced field.

In a second study, the influence of pion misidentfcation was investigated by adding a certain amount of pions accepted by the RICH detector, corresponding to pion suppression levels of 100, 1000, 5000 and 10000, to the sample of identified electrons. The combinatorial background was calculated applying all cuts established in [1]. The contribution of the misidentified pions to the combinatorial background is 85 %, 37 %, 11.2 %, and 6.8 %, respectively. We thus find that a pion suppression of 5000 or better is required for the combinatorial background to be dominated by physical sources.

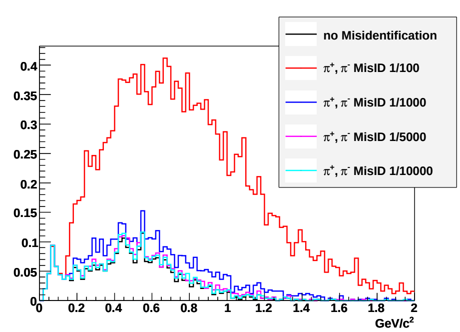

Figure 3: Combinatorial background assuming different levels of pion misidentification

References

[1] T. Galatyuk et al., GSI Scientific Report 2005, Darmstadt 2006, p. 62

J/ψ and ψ' detection in the di-electron decay channel in CBM

A. Maevskaya[2], A. Kurepin[2], and C. Höhne[1]
[1]INR RAS, Moscow, Russia; [2]GSI, Darmstadt, Germany

The study of the energy dependence of charmonium production in heavy-ion collisions recently received renewed interest due to new measurements at RHIC showing that the anomalous J/ψ suppression for central events is about the same as for NA50 at much lower energies [1]. So far this effect is difficult to explain in theoretical models. New results of the NA50 experiment [2] show that the anomalous suppression of ψ' is much stronger than that of J/ψ, and is similar for S+U and Pb+Pb. The measurement of both charmonium states at CBM energies (15 - 35 AGeV) would provide crucial information for the understanding of charm production in heavy-ion collisions. In this report, we present a study on the feasibility of J/ψ and, for the first time, ψ' reconstruction in the CBM experiment.

The simulations were perfomed with an implementation of the standard CBM detector layout [3]. Decay electrons from J/ψ and ψ' (simulated by PLUTO) were embedded into central Au+Au collisions generated by UrQMD. Due to the very low J/ψ and ψ' rates, the event mixing technique was used for the background simulations of electron-positron pairs [4]. In order to minize γ conversion in the gold target, shown to be the most prominent contribution to the electron background, the target thickness was reduced to 25 μm. The STS detector was implemented using silicon strip detectors only. Full event reconstruction in CBM was performed using the currently available semi-realistic detector response descriptions. All reconstructed tracks from the main vertex crossing at least 4 STS stations and being identified as electrons in RICH and TRD were used for the analysis.

The procedure of electron identification in CBM is described in detail in [5]. Here, we use the elliptic ring fit in RICH and apply ring quality cuts based on the neural network. A maximal distance of 1 cm was allowed for ring-track matching. Tracks were identified as electrons if the reconstructed ring radius was between 5.3 and 7 cm. For the electron identification in the TRD, we employed three different statistical analysis methods: neural network, likelihood and goodness-to-fit criterion [6]. For all three methods, cuts were tuned to provide an electron efficiency of 90 %. Electrons were selected if they were identified by all three methods. The combined RICH and TRD identification suppressed pions to a level of 10^{-4} for momenta from 1 to 13 AGeV/c.

In order to suppress the physical electron background, a transverse momentum cut at 1.2 GeV/c was applied for each track identified as electron as described above. The identification and p_t cuts do not introduce a limitation in phase space for both J/ψ and ψ'. Figure 1 shows the resulting invariant-mass spectrum in the charmonium mass region. The spectrum corresponds to $4 \cdot 10^{10}$ central Au+Au collisions at 25 AGeV, or roughly one hour of beam time at full CBM interaction rate. Signal-to-background ratios, total reconstruction efficiencies and mass resolutions are summarised in Table 1.

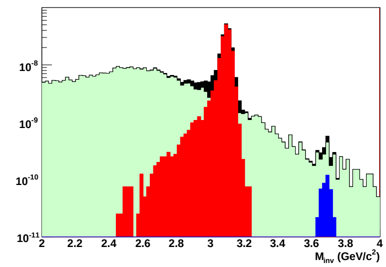

Figure 1: Invariant mass spectra for J/ψ and ψ' mesons after a lower p_t cut of 1.2 GeV/c and an upper momentum cut of 13 GeV/c on the electrons (central Au+Au at 25 AGeV)

We conclude that the feasibility of J/ψ and even ψ' measurements in central collisions of heavy-ions with CBM looks promising provided a very thin target will be used. The study will be continued with the investigation of a charmonium trigger.

	mult.	branch. ratio	S/B	eff	σ_m
J/ψ	$1.92 \cdot 10^{-5}$	0.06	13	0.14	27 MeV
Ψ'	$2.56 \cdot 10^{-7}$	0.0088	0.3	0.19	29 MeV

Table 1: Multiplicity, branching ratio, signal-to-background ratio, reocnstruction efficiency and mass resolution for $J\psi$ and ψ' in central Au+Au collisions at 25 AGeV. The multiplicities of J/ψ and ψ' were taken from the HSD model [7]

References

[1] A. Adare et al., Phys. Rev. Lett. 98 (2007) 232301

[2] B. Alessandro et al., Eur. Phys. J. C 49 (2007) 559

[3] P. Senger et al., *Compressed Baryonic Matter: physics case and detector setup*, this report

[4] A. B. Kurepin et al., *Charmonium detection in the CBM experiment*, CBM-PHYS-note-2007-001

[5] S. Das et al., *Electron identification in the CBM experiment*, this report

[6] E. Akishina et al., *Comparative study of statistical criteria for electron identification in the TRD*, this report

[7] W. Cassing, E. I. Bratkovskaya, and S. Juchem, Nucl. Phys. 674 (2000) 249

Standalone TRD event selection using Cellular Automaton based tracking

M. Krauze[1], W. Zipper[1], and A. Bubak[1]
[1]University of Silesia, Katowice

Charmonium measurements in CBM will be performed with the highest available interaction rates and thus rely on an efficient and fast online event selection scheme. For the online event selection, the usage of local information, i. e. from one detector system only, is highly desirable. We hence consider the feasibility of filtering events with respect to $J/\psi \rightarrow e^+e^-$ signatures in CBM using TRD information only.

A TRD setup with 12 detector layers was investigated. For track finding, we employ the Cellular Automaton algorithm [1] as developed for standalone TRD tracking [2], which results in a track finding efficiency of 93 % for tracks with momenta above 1 GeV/c in central Au+Au events at 25 AGeV. The mean processing time is about 0.6 s per event on a P4 3 GHz machine.

As the TRD is located outside of the magnetic field, the momentum determination is performed iteratively. First, the found track is fitted by a straight line using the Kalman Filter [3] and extrapolated backwards towards the point where the magnetic field vanishes [4]. At this stage, multiple scattering in the detector material is taken into account by assuming a momentum of 1 GeV/c. A first momentum estimate is then obtained by backwards extrapolation through the magnetic field to the target region. This momentum estimate is used for a more accurate determination of the multiple scattering. The procedure is iterated three times. The relative momentum resolution after the last iteration is 13.8 % as shown in Fig. 1. The mass resolution for the J/ψ is about 16 %.

The TRD serves not only tracking but also electron identification by the measurement of transition radiation. For this study, we assume a hadron suppression of 100 obtained using TRD information only.

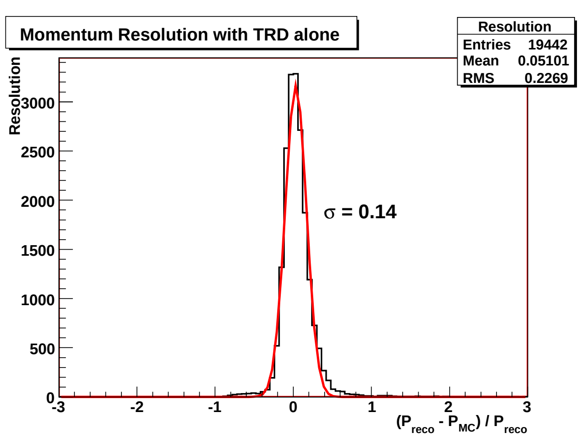

Figure 1: Residuals of momentum magnitude obtained from TRD information only

The event selection algorithm consists of the following steps:

- Tracks in the TRD are reconstructed using the Cellular Automaton algorithm.
- 99 % of the tracks are randomly rejected according to a hadron suppression factor of 100.
- The remaining tracks are fitted and extrapolated to the target region. The momentum is determined iteratively in three steps. Tracks without a valid extrapolation to the target are rejected.
- A transverse momentum cut $p_t > 1$ GeV/c is applied on the fitted tracks.
- The invariant mass of pairs of surviving, oppositely charged tracks is calculated assuming the electron mass for both. A pair is considered a J/ψ candidate ($m_{J/\psi} = 3.096$ GeV/c^2) if its invariant mass is between 2.5 and 3.5 GeV/c^2.
- Events containing at least one J/ψ candidate are accepted; all others are considered background and are rejected.

To test the event selection algorithm, signal events were constructed by embedding $J/\psi \rightarrow e^+e^-$ decays into minimum bias Au+Au UrQMD events at 25 AGeV. For the background, pure UrQMD events were taken. Both were transported through the CBM setup.

The algorithm rejects 98 % of the background events while keeping 52 % of events with a J/ψ signal. Thus, when being used in a Level-1 event selection scheme, the data volume can be reduced by a factor of 50 before more precise and time-consuming reconstruction and event selection are performed on a higher level.

References

[1] M. Gardner, Scientific American **223** (1970) 120

[2] A. Bubak, M. Krauze and W. Zipper, *Standalone TRD tracking using the Cellular Automaton algorithm*, CBM Progress Report 2006, Darmstadt 2007, p. 9, http://www.gsi.de/documents/DOC-2007-Mar-137.html

[3] S. Gorbunov and I. Kisel, CBM-SOFT-note-2005-001, Darmstadt 2005, http://www.gsi.de/documents/DOC-2005-Mar-212.html

[4] CBM Experiment - Technical Status Report, Darmstadt 2005, http://www.gsi.de/documents/DOC-2005-Feb-447.html

The muon detection system for the CBM experiment

A. Kiseleva[1], S. Gorbunov[2], I. Kisel[1, 2], E. Kryshen[3], V. Nikulin[3], M. Ryzhinskiy[4], and P. Senger[1]

[1]GSI, Darmstadt, Germany; [2]University, Heidelberg, Germany; [3]PNPI, Gatchina, Russia; [4]SPbSPU, St.Petersburg, Russia

The layout of the CBM muon detection system has been improved and optimized in 2007 with respect to background suppression and a more realistic detector response. The modifications include:

- compact absorber system in order to reduce the number of muons from pion and kaon decays;
- realistic detector segmentation according to an occupancy of 5%, including digitization of the muon detectors with charge sharing and hit finding;
- additional shielding in order to reduce the background of secondary electrons produced in the beam pipe;
- additional ToF detector to suppress the background due to punch-through kaons and protons.

The present design of the muon detection system consists of several iron absorber layers of varying thickness and 15-18 tracking detectors based on GEM technology. For the measurement of muons from low mass vector mesons (ρ, ω, ϕ), the total iron absorber thickness is 125 cm (7.5 λ_I), whereas for muons from charmonia, 1 m of iron is added (total thickness of 13.4 λ_I). For Au+Au collisions at 25 AGeV, on average about 0.3 background tracks per event are reconstructed. These background tracks consist of muons (60 %), kaons (25 %), pions (7 %), protons (3 %), and ghosts (5 %). About 80 % of the muons originate from weak meson decays inside the absorber system, the rest from decays in front of the absorbers. These numbers refer to the iron absorber of 125 cm thickness.

The vector meson decays were simulated with the PLUTO generator assuming an isotropic thermal source with a temperature of 130 MeV. The multiplicities for central Au+Au collisions at 25 AGeV beam energy were taken from the HSD transport code [2]. The background was calculated with the UrQMD event generator. Both signal and background are transported through the detector setup using the transport code GEANT3 within the cbmroot simulation framework. The L1 tracking procedure has been used for track finding in the STS and the muon system, and for momentum reconstruction in the STS.

The resulting invariant mass spectra are shown in Figure 1 for the low-mass vector meson region (left) and the charmonium mass region (right). The efficiencies for vector meson detection and the signal-to-background ratios, calculated in a $\pm 2\,\sigma$ window around the signal peaks, are presented in Table 1. A lower transverse momentum cutoff at 1 GeV/c was applied for tracks in the charmonium region.

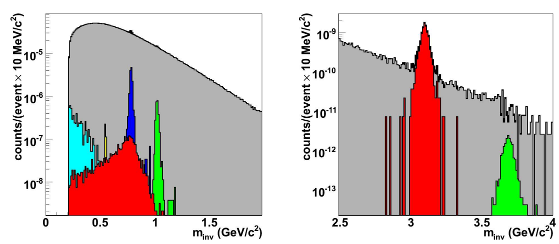

Figure 1: Muon pair invariant mass spectra. Left: low-mass region with η_{Dalitz} (1), η (2), ω (3), ϕ (4), ρ (5), and combinatorial background (grey area). Right: charmonium mass region with J/ψ (1), ψ‘ (2), and combinatorial background (grey area) for muons with $p_t > 1$ GeV/c.

	ρ	ω	ϕ	J/ψ	ψ‘
S/B ratio	0.002	0.11	0.06	7	0.09
efficiency (%)	2.8	4	7	7.7	8.2
mass resolution (MeV/c^2)		10	12	22	31

Table 1: Reconstruction efficiencies, signal-to-background ratios and mass resolutions for vector mesons in central Au+Au collisions at 25 AGeV

In the ongoing simulations, we have started to take into account detector inefficiencies and clustering of pads. Moreover, we have removed one out of three detector station after each absorber layer, and reduced thus the total number of tracking detectors from 15 to 10. It turned out that a detector efficiency of 95% can be tolerated without losses of track reconstruction efficiency which is very similar for the setup with 15 and 10 detector stations. In order to further optimize the muon detection system, we will improve the track propagation algorithm for thick absorbers. Moreover, we will investigate the possibility to generate a hardware dimuon trigger both for charmonium and low-mass vector mesons.

References

[1] E. Kryshen, V. Nikulin and M. Ryzhinskiy, *Digitization and hit finding in the CBM muon detector*, this report

[2] W. Cassing, E. L. Bratkovskaya and A. Sibirtsev, Nucl. Phys. A 691 (2001) 753

Digitization and hit finding in the CBM muon detector

E. Kryshen[1], V. Nikulin[1], and M. Ryzhinskiy[2]
[1]PNPI, Gatchina, Russia; [2]SPbSPU, St-Petersburg, Russia

Detector Granularity

The tracking chambers of the CBM muon detector (MUCH) will work under conditions of high hit density (up to 1 hit per cm^2) and high event rates (10^7 events/s). Modern gas pad detectors like GEM and micromegas are expected to meet these requirements. Taking into account the large variation of hit density with distance from beam, each chamber is subdivided into ring-like regions with appropriate pad sizes. The radii of the rings are chosen such that the mean hit density is doubled from ring to ring, while the pad area varies inversely with the hit density. Each region is mapped onto rectangular sectors, a sector being a group of 128 channels connected to a front-end electronics chip. The identical sector sizes within a ring simplify the design of the printed circuit boards for the detector read-out. Another constraint is the spatial resolution which should match the tracking requirements: ~ 0.4 mm for the central area, decreasing towards the periphery. The required resolution defines the maximal pad size.

Detector Response Simulations

The GEANT package is not well suited for the simulations of the ionization energy loss in very thin layers. On the other hand, HEED [1] — a reliable microscopic tool for such kind of analyses — can not be effectively integrated into GEANT. We adopt a compromise solution: the distribution of the number of primary electrons in an appropriate gas gap has been simulated with HEED and fitted to a Landau function. The thus obtained parameterizations of expectation value and variance as functions of logarithm of kinetic energy of the ionizing particle are used for the simulation of the number of primary electrons in the MUCH digitizer. The primary electrons are then distributed according to the Poisson law along the direction of the incident track.

The gas gain for each primary electron fluctuates according to an exponential distribution with a mean value of 10,000. The transversal diffusion of the avalanche (spot size) is assumed to be constant; its value (0.3 mm for micromegas and 1.5 mm for GEM) has been chosen to reproduce the existing experimental data.

The avalanche spot for each primary electron is projected to the pad plane, and the sum of charges at each pad is calculated. With the currently foreseen pad design, typically 2.5 pads are fired by a vertex track, while highly inclined secondary particles cover much larger clusters of pads (up to several tens).

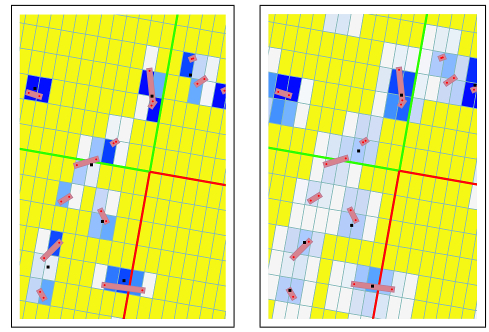

Figure 1: Example of micromegas (left image) and GEM (right image) responses to the same track sample. Red rectangles correspond to MC track projections, black dots represent reconstructed hit positions.

Hit Finder

The next important step of detector simulations involves the analysis of charge distributions and the production of hits. First, clusters of neighbouring fired pads are found, and the hit finding procedure is applied on a cluster level. On average, 1.2 Monte-Carlo tracks contribute to one cluster. For the time being, a simple cluster unfolding algorithm has been developed. It is based on the search for local maxima in the cluster charge distribution and the splitting of large clusters into secondary ones. Hits are attributed by calculating the center of gravity for each secondary cluster. However, the efficiency of this algorithm can still be optimized for complicated clusters. Figure 1 shows a visualization of the detector response simulation and the hit finding for micromega and GEM detectors.

Outlook

In the proposed approach, some effects are not taken into account, namely the cluster nature of primary electron production, the microscopical estimation of the transverse avalanche component (essentially detector dependent), the response of the front-end electronics, and threshold and digitization effects. The cluster deconvolution algorithms need being optimized with respect to the muon reconstruction efficiency. Besides, the developed model should be tuned according to beam test results.

References

[1] I. Smirnov, NIM A 554 (2005) 474
http://ismirnov.web.cern.ch/ismirnov/heed.html

Acceptance study for HADES@SIS100

A. Kugler[1], J. Garzon[2], M. Golubeva[3], D. Gonzales-Diaz[4], F. Guber[3], R. Holzmann[4], and P. Tlusty[1]
[1]NPI, AS CR, 25068 Rez, Czech.Republic; [2]DFP, University of Santiago de Compostela, 15706 Santiago de Compostela, Spain; [3]INR, Russian AS, Moscow, 117259 Moscow, Russia; [4]GSI, 64220 Darmstadt, Germany

While the CBM experiment at FAIR is designed to study heavy-ion collisions at beam energies from 10 to 45 AGeV, the energy range from 2 to 10 AGeV, accessible also with the future accelerator facility, can be covered by an upgrade of the existing HADES di-lepton spectrometer [1]. Therefore, we carried out simulations of dilepton production in heavy-ion collisions at bombarding energies of about 8 AGeV as seen by the HADES detector.

Results of the simulations of the full di-lepton cocktail from Au+Au at 8 AGeV were published in [2, 3], and demonstrated that, in principle, HADES in its current configuration and after replacement of the inner TOF wall by a high granularity RPC detector system is able to measure dileptons using beams up to that energy.

We continued our study, concentrating on the changes of the acceptance for both hadrons and di-leptons with increasing beam energy from 2 AGeV (HADES optimum acceptance) up to 8 AGeV. In order to study the response of the HADES spectrometer, first, events generated by UrQMD were used to investigate the acceptance for hadrons. For simplicity, at this stage of simulations we used the HADES acceptance matrices instead of propagating the track throughout the HADES detection system using GEANT. These matrices were obtained for hadrons as a function of momentum, polar angle and azimuthal angle by propagating the particles from a white source through the HADES detector using the HGeant package. Note that HADES is designed to study symmetric systems with bombarding energy around 2 AGeV, for which the acceptance of light particles is symmetric around mid-rapidity ($y_{CM} \approx 0.9$). At 8 AGeV beam energy, the rapidity distribution is shifted to higher values ($y_{CM} \approx 1.5$), but still the HADES acceptance for pions safely covers the maximum, ranging in rapidity up to 2. The ratio of accepted particles to those emitted to the full solid angle is shown in Table 1.

The HADES acceptance for di-leptons was studied in a similar way as described above. As an example of a dilepton source of physical interest, we generated di-leptons from the direct electron-positron decay of the ω meson using the Monte-Carlo generator PLUTO. For the ω source,

particle	2 AGeV	8 AGeV
π^+	0.63	0.50
π^-	0.64	0.52
p	0.40	0.15

Table 1: Acceptance of hadrons emitted from ^{12}C+^{12}C at 2 and 8 AGeV

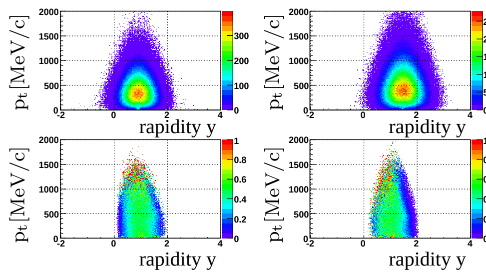

Figure 1: Phase space distributions of di-electrons from the direct decay of the ω meson from a thermal source at 2 AGeV (left) and 8 AGeV (right). The upper row shows all generated di-electrons, the lower row those accepted in the HADES spectrometer.

we used a thermal model of an expanding fireball, with inverse slope parameters of 89 MeV at 2 AGeV and 105 MeV at 8 AGeV as motivated by UrQMD model predictions and comparison with experimental data. The individual leptons were then propagated through the HADES acceptance filter in the same way as described for hadrons. Pairs of accepted leptons with opening angle above 9 degrees were considered.

The results of the calculations are shown in Fig. 1. At 2 AGeV, the overall acceptance for di-lepton pairs from ω decay decreases moderately from 33 % at 2 AGeV to 21 % at 8 AGeV. From the distributions shown in Fig. 1 it is also visible that the acceptance of the HADES detector, without change of its geometrical configuration, still covers the mid-rapidity region at 8 AGeV. Taking into account the presumably much higher yields of vector mesons at the higher energy, we can expect a significantly higher observable rate in the corresponding region of invariant mass spectra at 8 AGeV as compared to 2 AGeV.

References

[1] P. Salabura et al. (HADES collaboration), Prog. Part. Nucl. Phys. **53** (2004) 49
P. Salabura et al. (HADES collaboration), Nucl. Phys. A **749** (2005) 150

[2] A. Kugler et al., *CBM progress report 2006*, Darmstadt 2007, p.25, `http://www.gsi.de/documents/DOC-2007-Mar-137.html`

[3] A. Kugler et al., Proceedings of XLIV International Winter Meeting on Nuclear Physics, Bormio 2006, vol. 125, p. 282

Timing Properties of CVD-Diamond Detectors at RelativisticVelocities

E. Berdermann, M. Ciobanu, M. Kiš, W. Koenig, M. Pomorski and M. Träger
GSI, Darmstadt, Germany

Heavy-Ion Induced Transient Currents (TC)

In order to investigate the behaviour of Single-Crystal CVD-Diamond Detectors (SC-DD) at relativistic ion velocities, we measured original TC Signals (TCS) induced by ^{132}Xe ions of 215AMeV in a SC-DD of a thickness d_D =400µm and a capacitance C_D=0.9pF. At a rate of 1.6kHz, a charge Q_G^{Xe}=1.2*10^8 e-h pairs/ion was generated in the diamond bulk. We present a data discussion according to the theory of Space-Charge Limited Current transients (SCLC) [1], expected for $Q_G > Q_{BI,}$ with $Q_{BI} = C_D*V_D$ the bias-induced charge at the electrodes of the sensor.

The ^{132}Xe pulses were recorded with a 1GHz DSO of 10GS/s resolution, connected to the diamond via a high-frequency transmission line of 30m lengths. We compare the shapes of the ^{132}Xe transients with α-signals measured in the laboratory using a broadband amplifier and a 3GHz DSO. Each α-particle generates a charge of $Q_G^{\alpha} = 4.2*10^5$ e-h pairs within the α-range of 12µm, and represents the 'small-signal case' at 'single-carrier drift'.

Figure 1 shows average ^{132}Xe transients obtained in the bias range 10V≤ $|V_D|$ ≤ 800V (solid and dotted lines) and an average α-signal (dashed line) measured at V_D=800V. Note, the α-amplitude is magnified by an arbitrary factor.

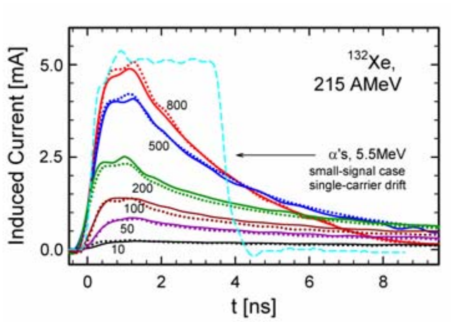

Figure 1: Original TCS obtained in the bias range 10V ≤ $|V_D|$ ≤ 800V from ^{132}Xe ions of 215AMeV (solid and dotted lines). A ^{241}Am-α-transient (dashed line) represents the 'small-signal case' at 'single-carrier drift'. (see text)

The RC_D time constant of the circuit was as short as 45ps at 50Ω impedance. In addition, the bias resistor of 10kΩ ensured a constant voltage on the electrodes at all times, and the measurements were performed in the so-called 'current mode'. The flat top of the α-signal demonstrates the homogeneity of the internal drift field and the absence of trapping and recombination. The right 'kink' indicates the arrival of the leading hole to the backward, grounded electrode and the top width defines the transition time t_{Tr}. In contrary to the prompt signal decay in the 'small-signal case', ^{132}Xe-generated TCS show much longer relaxation time (≈7ns), given by the time needed to expel all space charge from the crystal. Charge expulsion is supported by free carriers present in the neutral detector at thermal equilibrium. Hence, it is faster for low-quality diamond detectors, e.g. for polycrystalline sensors.

The rising slope dI/dt of the ^{132}Xe TCS was maintained at t_{rt} ≤ 200ps. The area of pulses recorded at $|V_D|$ ≥ 25V were equal to the theoretically predicted charge of Q_G = 19.22pC, indicating a charge-collection efficiency near to unit. The transition time t_{Tr} decreased from t_{Tr}=3ns for the 'small-signal' case to t_{SCLC} = 650ps for the ^{132}Xe transients. This effect was expected, however not only because of the 'dual-carrier drift'. According to the standard SCLC theory, the transit time drops also at 'single-carrier drift' to a constant value $t_{SCLC} = 0.78*t_{Tr}$ in the transition from the 'small-signal' case to the SCLC case. In our experiment, t_{Tr} saturates for $|V_D|$ ≥ 50V, and that is evident to the onset of SCLC for Q_G^{Xe} ≥ 45pC (i.e., two ions in a time in the counter). The almost same level of both 'kinks', confirms equal mobility of electrons and holes and the absence of bulk trapping.

Time Resolution for Relativistic Protons

We tested the time resolution of SC-DD using 3.5GeV protons and a new low-capacitance broadband amplifier designed for the diamond start detectors of the HADES spectrometer. Two SC-DD of a thickness d=300µm, equipped with 3mm circular electrodes segmented in four quadrants, were mounted each on an amplifier pcb in order to minimize stray capacitances. Figure 2 shows the time spectrum obtained with two opposite diamond segments aligned in the proton beam. The intrinsic resolution σ ≈ 107ps achieved, is a significant milestone towards the difficult goal of a σ_{MIP}< 100ps. The tail is due to boarder events of longer drift time - an unavoidable experimental drawback in measurements where relativistic particles are used to test sensors smaller than the beam spots.

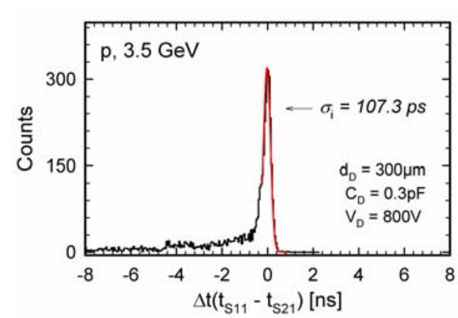

Figure 2: Time resolution of SC-DD for 3.5GeV protons measured with a low-capacitance broadband amplifier.

References

[1] G. Juška *et al.,* Phil. Mag. **B 69** (1994) 277

Achievements of CMOS Pixel Sensors for the CBM Micro-Vertex Detector

A.Besson[1], G.Claus[1], M.Deveaux[1,2], A.Dorokhov[1], G.Dozière[1], W.Dulinski[1], Ch.Hu-Guo[1], A.Himmi[1], K.Jaaskelainen[1], F.Morel[1], I.Valin[1], and M.Winter[1]

[1]IPHC and Université L.Pasteur, Strasbourg; [2]J.W.Goethe Universität, Frankfurt

CMOS pixel sensors are being developed for the CBM Micro-Vertex Detector (MVD). They provide the high resolution required to reconstruct efficiently decay vertices of short-lived particles, such as charmed mesons. The present R&D is mainly driven by the severe running conditions expected in the vicinity of the experimental target. The most significant outcome obtained in 2007 is summarised hereafter. Prominent results include performances of a fast sensor architecture with discriminated outputs, the tolerance to non-ionising radiation, the design of a zero-suppression micro-circuit and industrial thinning. The report also gives an overview of the R&D plans for 2008.

Fast read-out architecture

The fast read-out architecture developped for the MVD was already presented in previous reports [1]. The most recent sensor featuring this architecture (called MIMOSA-16) is composed of 32 columns of pixels read out in parallel. Each pixel includes correlated double sampling micro-circuits. 24 columns are ended with a discriminator (the remaining 8 columns have analog outputs for test purposes).

The sensor was mounted on a Si-strip telescope and its detection performances were assessed as a function of the discriminator threshold with a 180 GeV π^- beam at the CERN-SPS. A detection efficiency of $\sim$ 99.9 % was observed for fake hit rates in the order of a few 10^{-5}. The single point resolution was found to be $\lesssim 5\ \mu m$, i.e. substantially better than the binary resolution ($\sim 7.2\ \mu m$) reflecting the pixel pitch (25 μm). This value satisfies the MVD requirements, aleviating the need for ADCs.

The MIMOSA-16 architecture is foreseen to evolve towards a sensor incorporating integrated zero-suppression micro-circuits. A prototype zero-suppression chip (called SUZE-01) was designed and fabricated in 2007. It features a 2-step logic encoding the compactified address of pixels delivering a charge above the discriminator threshold, and is equipped with output memories. Preliminary test results indicate that the zero-suppression logic performs according to the specifications.

The next major objectives consist in fabricating 2 full scale sensors: a first one, without integrated zero-suppression, for the STAR Heavy Flavour Tracker, and a second one for the beam telescope of the FP-6 project EUDET, which incorporates zero-suppression. To bridge the gap with these final sensors, a medium size prototype (MIMOSA-22) was designed in 2007 and submitted to fabrication in Octobre. It features 128 columns of 576 pixels (18.4 μm pitch), each ended with a discriminator. It adds to the MIMOSA-16 design integrated JTAG steering micro-circuits and improved testability. The chip characterisation should start in February 2008.

Radiation tolerance

The tolerance of the sensors to non-ionising radiation, already studied in previous years, was assessed with a sensor expected to withstand higher fluencies than chips tested previously. The sensor (called MIMOSA-18) is composed of 4 matrices of 256$\times$256 pixels. The pixel pitch amounts to only 10 μm, a value which reinforces the charge collection efficiency. Several chips were exposed to low energy neutrons at the Llubjana irradiation facility. The highest integrated doses amounted to $\sim 6{\cdot}10^{12}$ and 10^{13} n_{eq}/cm^2. In the latter case, the photon gas accompanying the neutrons and irradiating the sensor translated into a integrated ionising dose of 100–200 kRad. Irradiated sensors were subsequently mounted on a Si-strip telescope and exposed to a 120 GeV π^- beam at the CERN-SPS. The detection performances observed for a coolant temperature of -20°C and a read-out time of 3 ms are summarised in the table below. The latter displays the sensor noise, the cluster charge, the signal-to-noise ratio and the detection efficiency for the two values of the fluence and before irradiation.

Fluence (n_{eq}/cm^2)	**0**	**$6{\cdot}10^{12}$**	**$1{\cdot}10^{13}$**
Noise ($e^- ENC$)	10.8±0.3	12.2±0.3	14.3±0.3
Q_{clust} (e^-)	1026	680	560
S/N (MPV)	28.5±0.2	20.4±0.2	14.7±0.2
Det. Eff. (%)	99.93±0.03	99.85±0.05	99.5±0.1

The major outcome of the study is that MIMOSA sensors can tolerate fluences of O(10^{13} n_{eq}/cm^2), provided the pixel design is adapted to this issue. The R&D next steps aim to adapt the design to the other MVD specifications.

Thinning

Several different MIMOSA sensors were thinned individually to $\sim 50\ \mu m$ in industry. Thinned MIMOSA-18 sensors (5.5$\times$7.5 mm^2 large) were mounted on their interface board and consecutively characterised at the CERN-SPS. No performance loss was observed, demonstrating that 50 μm thin sensors constitute a valid baseline assumption for the MVD geometry.

References

[1] S. Amar-Youcef et al., GSI Report 2007-1 18.

R&D for the demonstrator of the CBM-Micro-Vertex Detector (MVD) *

S. Amar-Youcef[1,2], M. Deveaux[1,4], D. Doering[1], J. Heuser[3], I. Fröhlich[1], J. Michel[1], C. Müntz[1], C. Schrader[1], J. Stroth[1], T. Tischler[1], and B. Wiedemann[1]

[1]IKF, University Frankfurt; [2]Helmholtz Research School, Frankfurt; [3]GSI, Darmstadt; [4]IPHC, Strasbourg

Status of the MVD-Demonstrator

The MVD of the future CBM-experiment at FAIR is needed to identify open charm particles by reconstructing their secondary decay vertex (SV). To reach the required SV resolution, the detector will be installed in beam vacuum and its material budget (MB) has to stay below $\sim 0.5\% \ X_0$ per layer. Monolithic Active Pixel Sensors (MAPS) [1] are the currently preferred sensing elements and provide the necessary spatial resolution of few μm.

To study their integration to a detector, a demonstrator is being built in the IKF technology lab of University Frankfurt. This project addresses open questions regarding the design of an ultra thin cooling support for the sensor chips, their handling and their integration into a central data aquisition system. The latter includes the design of particular hardware and algorithms for readout and data sparsification [2]. Our concept for a demonstrator module is depicted in

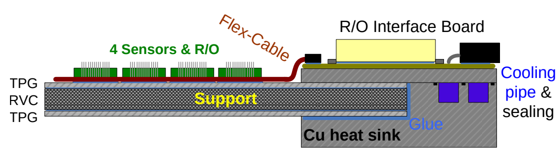

Figure 1: Side view of demonstrator layout: Support sandwich structure applied to a cooling and connecting entity

Figure 1. A cooling support based on the very heat conductive and stiff Thermal Pyrolytic Graphite (TPG) hosts the sensors and evacuates their power (up to ~ 1 W/cm^2). Additional stiffness is reached by adding the very light RVC (Reticulated Vitreous Carbon) between two layers of TPG. "MIMOTEL" MAPS ($\sim 1\ cm^2$, $\sim 1\ ms$ readout time) can be mounted on each side of the support. These sensors, which are provided by IPHC Strasbourg, are biased and read out with flexprint cables connecting them with a small PCB hosting signal buffers.

The trade off between low MB, efficient heat evacuation and mechanical stability is being optimized with thermal and mechanical simulations. We assume today that the thickness of the cooling support will be $\sim 0.2\% \ X_0$. The multilayer flexprint cables required will add $\sim 0.3\% \ X_0$ if being installed on both sides. After mounting sensors being thinned to $\sim 100\ \mu m$ by conventional industrial means, we will reach a MB of $\sim 0.4\% \ X_0$ ($\sim 0.7\% \ X_0$) for a MVD station with a single (a double) layer of MAPS. This value is not yet satisfactory for CBM but the experiences obtained with this demonstrator will guide further optimisation steps. Lower MB may be reached by using thinner sensors [3] with digital output. This output requires fewer pins and allows using lighter flexprint cables.

Radiation Tolerance

A second important issue for the CBM MVD is its radiation tolerance. Intense studies were performed in the context of a common R&D activity of IKF and IPHC. Measurements with ^{55}Fe-photons on neutron irradiated sensors highlighted that the radiation induced drop of the charge collection efficiency (CCE) is substantially reduced for small pixels (see figure 2). As this drop forms the dominant radiation damage, the radiation tolerance of MAPS increases substantially with smaller pixel pitch. This was cross checked and confirmed with beam tests [3]. However, using small pixels comes with draw backs in terms of lower time resolution and higher power dissipation.

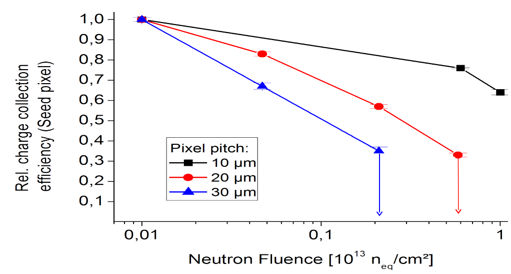

Figure 2: The CCE of pixels as function of the pixel pitch. CCEs below 0.4 are considered as upper limits.

A second potential way of improving the radiation tolerance of MAPS is to operate them at LN$_2$-temperatures. The CERN-RD39 collaboration recently demonstrated that the CCE of heavily irradiated, n-doped silicon detectors is partly restored at this temperature [4]. Substantial improvements in the radiation tolerance might be reached, if those promising results could be reproduced with the p-doped sensors of MAPS. An experiment for testing this approach and to establish the radiation tolerance of cryogenic MAPS is currently under preparation.

References

[1] R. Turchetta et al., NIM **A458**(2001)677-689

[2] C. Schrader et al., 'A Readout System for the CBM-MVD Demonstrator', this report

[3] A. Besson et al., 'Achievements of CMOS Pixel Sensors for the CBM Micro-Vertex Detector', this report

[4] CERN-RD 39, K. Borer et al., NIM **A440**(2000)5-16

* In collaboration with IPHC.

First microstrip detector prototypes for the CBM Silicon Tracking System

J. M. Heuser[1], Chr. J. Schmidt[1], A. Lymanets[2], R. Röder[3], and L. Long[3]

[1]GSI, Darmstadt, Germany; [2]FIAS, J. W. Goethe University, Frankfurt, Germany; [3]CIS, Erfurt, Germany

The first prototypes of a double-sided silicon microstrip detector for the CBM Silicon Tracking System (STS) have been produced in cooperation of GSI and the CIS Institute for Micro Sensors in Erfurt.

Low mass silicon tracking stations

The STS plays a central role in the CBM experiment as it will exclusively perform track and momentum measurements of the charged particles created at the target. One of its key requirements is an especially low-mass construction, essential for achieving momentum resolution down to about 1%. This is particularly challenging because the high charged-particle densities (up to 30 per cm^2) and the high interaction rates (up to 10 MHz) require a large number of detector channels equipped with fast power dissipating front-end electronics. The necessary cooling system introduces an excessive material budget. We have started to explore an STS concept that avoids the readout electronics and its cooling infrastructure in the aperture [1]. The building block of the STS tracking stations is a ladder structure made from double-sided microstrip detectors. It comprises several sectors of different strip lengths, realized with single or multiple chained sensors, that are individually read out at the periphery of the stations through very thin flat cables with high line density.

Microstrip detector prototype CBM01

A double-sided microstrip detector compatible with this STS concept has been designed in 2006 [2]. It addresses specific connectivity issues of the module. The prototype features a 15 degree stereo angle between the p and the n side strips. Their readout is performed in AC mode. Punch-through biasing structures are applied. On both detector sides, 1024 contact pads are arranged near the top and bottom edges. Their pitch of 50.7 μm matches the input of the n-XYTER chip that will be used during the initial prototyping phase. On the stereo (p-implanted) side, unconnected corner regions are avoided by linking the metal of every short strip with its matching partner in the opposite corner through a line on a second metal layer.

Production and first test results

In Summer 2007, a first batch of 24 4-inch wafers has been produced with 285 μm thick polished 5 kΩcm float zone material. The production involved a set of 17 masks. A wafer, seen on the photograph in Fig. 1, fits the 5.5 cm wide CBM01 detector, five test sensors with 256 by 256 orthogonal strips of 50.7 μm and 80 μm pitch, and several other test structures. Current-voltage and capacity-voltage characterizations have been performed. The requested specifications were achieved with high yield. Detailed measurements of other quantities, e.g. inter-strip capacitances, and in-beam tests are being prepared.

Next steps

For the next design iteration, systematic simulations of the detector technology have been performed. A technology wafer with various test structures has been submitted for production, now addressing improved radiation tolerance with poly-silicon bias structures, measures to increase the breakdown voltage, as well as several insolation technologies of n-strips.

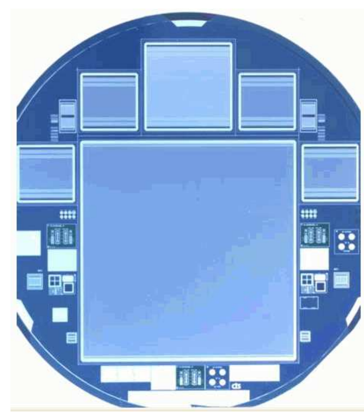

Figure 1: The CBM01 detector (center), five test detectors, and various test structures on a silicon wafer of 4” diameter.

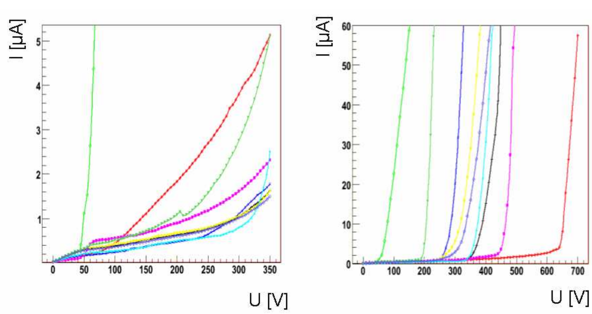

Figure 2: Current-voltage behaviour of 9 CBM01 sensors: Low voltage region (left) and breakthrough region (right).

References

[1] J. M. Heuser, Nucl. Instr. Meth. Res. **A582** (2007) 910-915

[2] J. M. Heuser et al., GSI Report 2007-1 19

Layout studies of the Silicon Tracking System for the CBM experiment

R. Karabowicz and J. M. Heuser
GSI, Darmstadt, Germany

The Silicon Tracking System (STS) serves the CBM experiment as a track reconstruction and momentum measurement detector. It is designed to provide high tracking efficiency and good momentum resolution for the charged particles produced in nuclear interactions in the target. As the multiplicities in central Au + Au collisions at FAIR energies reach 1000 charged particles a high granularity and low mass detector device is required. The major change in the STS layout compared to the previous versions [1] is an increased number of stations fully based on micro-strip detectors. Other changes include segmentation of the stations according to the prototype designs and introduction of passive material.

Detector Layout

The current STS detector concept comprises 8 detector stations schematically shown in Fig. 1. The stations are built of 300μm thick double-sided silicon micro-strip sensors arranged in vertical modules with fixed horizontal size of 6cm. While the vertical size of the sensors varies from 2 to 6cm to ascertain a maximum occupancy of less than 5%, up to 3 sensors may be chained together to minimize the number of channels. For the radiation studies and occupancy results, see [2]. The arrangement of sensors and modules in a single station is presented in Fig. 2.

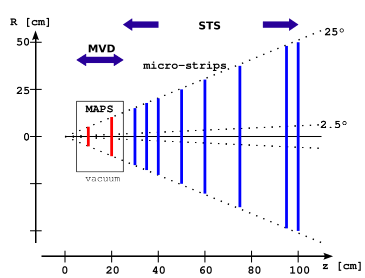

Figure 1: Sketch of the STS + MVD detector systems.

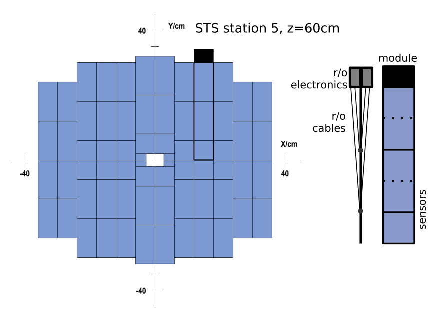

Figure 2: Silicon micro-strip sensors arranged into modules of different lengths building up a tracking station.

In order to achieve a low-mass detector, we have decided to place the read-out electronics at the perimeter of the STS. Signals from the sensors will be read out by thin capton micro-cables. The silicon detector will be mounted on an ultralight carbon fiber skeleton. These additional materials are already present in the GEANT simulations of the CBM experiment as indicated in Fig. 2. The double-sided silicon sensors have active strips with a pitch of 60μm (previously 50μm) on both sides, oriented vertically in the front layer and rotated by a stereo angle of 15° in the back plane. Please refer to [3] for more details on the detector R&D. For high-resolution vertex measurements, e. g. open charm detection, the STS is supported with a Micro-Vertex Detector (MVD) consisting of two very thin and fine-pitch MAPS pixel detector stations close to the target.

Performance studies

The performance of the STS detector was evaluated on various levels. The tracking routines are based on a Cellular Automaton for track finding and a Kalman filter for track fitting [4]. The tracking efficiencies vary from 99.7% for single track events to ca. 95% in central Au + Au events at 25 AGeV (for tracks with momenta exceeding 1 GeV/c). The momentum resolution depends strongly on the detector's material budget and changes from 1.2% in case of standalone silicon sensors to 1.6% for the full STS setup with readout cables and carbon support structure. Although the tracking results depend only weakly and linearly on the strip pitch or the stereo angle, the small deterioration of the track reconstruction performance can have strong impact on the full physics analysis, e. g. of the light vector meson muon decay channel.

Conclusions and plans

A detailed STS detector layout has been implemented in the simulation of the CBM experiment. The dependence of the reconstruction results on several important parameters has been studied. Future plans include the development of realistic detector response functions that include signal sharing between strips and hit clusters. Replacement of the double-sided detectors with single-sided ones as a back-up solution is another topic being studied at the moment.

References

[1] J. M. Heuser et al., *Layout studies and sensor prototypes for the CBM Silicon Tracking System*, GSI Report 2007-1 19

[2] R. Karabowicz et al., *Radiation environment in the CBM experiment*, this report

[3] J. M. Heuser et al., *First microstrip detector prototypes for the CBM Silicon Tracking System*, this report

[4] I. Kisel et al., *Fast SIMDized Kalman filter based track fit*, this report

Development of thin multi-line cables for the STS micro-strip detector modules

V.N. Borshchov, O.M. Listratenko, M.A. Protsenko, I.T. Tymchuk
State Enterprise Scientific Research Technological Institute of Instrumental Engineering (SE SRTIIE), Kharkov, Ukraine

The first pre-prototypes of flexible thin multi-line micro-cables for the STS micro-strip detector modules have been developed and produced in the SE SRTIIE, Kharkov, Ukraine.

Thin micro-strip detector modules for the STS

The Silicon Tracking System (STS) is the central component of the CBM experiment. One of the key requirements of the STS is a low-mass design to achieve momentum measurement with about 1% resolution. Silicon micro-strip detectors are compatible with a low-mass design as the sensors themselves are thin. With an appropriate module structure, active readout electronics with its cooling requirements and material involved may be avoided in the aperture [1].

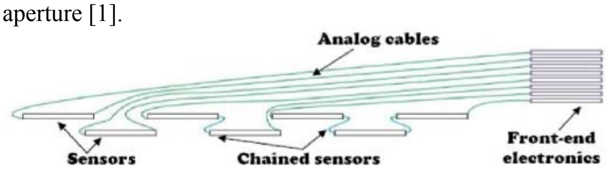

Figure 1: Schematic view of the proposed detector module composition.

Figure 1 shows the concept of such a micro-strip detector module. The module is divided into few sectors of different effective strip lengths, consisting of either single sensors or groups of chained micro-strip sensors. The offered concept of module construction can be realized only by innovative full aluminium "chip on flex" technology with application of flexible cables of two types:

– the analog strip signals of the sectors are individually read out through thin long multi-line cables (so-called analog cable);
– the daisy chain connection of sensors is provided by flexible micro-cables (so-called daisy-chain cable).

Aluminium-polyimide flexible cables

The development of the readout cables, made from aluminum traces on polyimide material for minimum material budget, is a particular important task. This includes the reliable fabrication of fine-pitch traces, matching the strip pitch of the sensors, over lengths up to about 55 cm. The mechanical and electrical connection to both sides of thin double-side sensors must be executed. For the full functionality of the micro-strip detector modules, the total capacitance of sensor and cable at the input of the front-end electronics must be as low as possible in order to achieve a sufficiently large signal-to-noise ratio of the measurements [2].

While selecting a material for fabrication of micro-cables foremost the requirements to minimization of material amount within working volume, as well as requirements to resistance, mutual capacitance of conductors, electric strength and elasticity was reviewed. Comparative calculations for ratio of radiation length versus resistance for copper and aluminium micro-cables have shown that given ratio is as much as 3.8 times better for aluminium micro-cables. Radiation length of aluminium-polyimide micro-cables does not exceed 0.02% of Xo for one layer ($X_{0\,Al} \approx 8.7$ cm, $X_{0\,Pi} \approx 28.4$ cm).

The flexible dielectric substrate of the cable affects the capacitance. The material of choice in high-energy applications is polyimide with a dielectric constant of 3.5 (at a frequency of 1 MHz). This material is radiation-resistant with good mechanical and electrical properties. Other synthesized dielectric materials on the market (such as polyethylene or polypropylenes are used in the flex circuit industry) achieve a lower dielectric constant by adding halogens. They are not radiation-resistant.

As the initial micro-cable construction material has been chosen the serially manufactured FDI-type foiled dielectric. The FDI film is polyimide (10 µm thickness) with (10 ÷ 14) µm aluminium film thickness.

As major technological variant for production of micro-cables has been adopted the micro-electronic technology. Assuming for design features of micro-cables being developed, technology of their manufacturing is based on methods of precision photo-lithography with photo-printing through flexible and rigid photomasks, chemical etching of metal and dielectric layers and plasma-chemical treatment of photo-resist.

Analog cables

Figure 2 shows a schematic view of the arrangement for the sensor and analog cables. Two cables (for each side of sensor) with constant 100 µm pitch are laminated together with a lateral shift of 50 µm (effectively as a cable with 50 µm pitch).

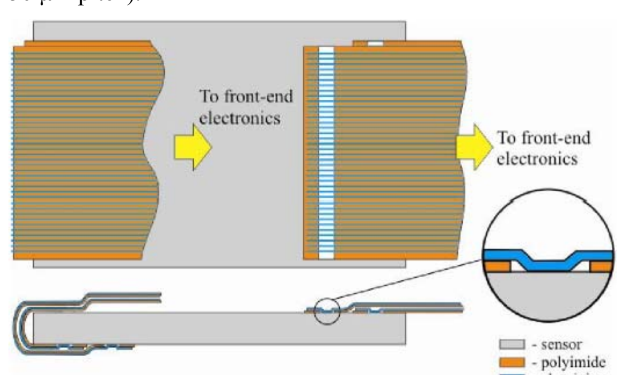

Figure 2: Schematic view of the proposed connections between the sensor and analog cables.

A first iteration of analog cable compatible with this STS detector module concept has been designed and produced at our institute in 2007. Some basic characteristics of such cables are given below:

- material – foiled dielectric FDI-A-24;
- thickness of aluminium layer – (12 ÷ 14) µm;
- thickness of polyimide layer – 10 µm;
- dimension of analog cable is (600×70) mm with technological area and (500×51.5) mm – only work area;
- pitch of traces – 100 µm;
- width of traces – (35 ÷ 45) µm;
- quantity of traces – 512;
- expected resistance Rtr ≈ (5 ÷ 7) Ohm/cm;
- expected capacitance Ctr ≈ (0.3 ÷ 0.33) pF/cm.

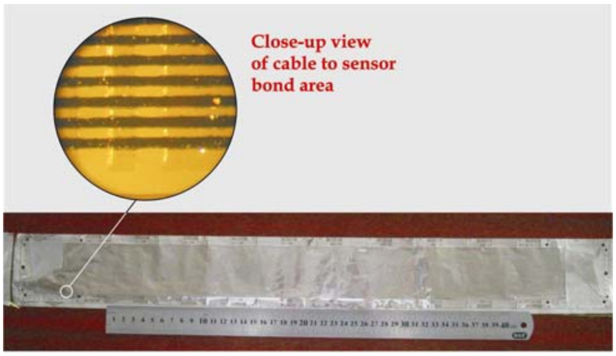

Figure 3: Photo of analog cable first pre-prototype

In order to reduce the capacitance contribution from adjacent cables, a spacer will place between the cables. A candidate for the spacer material is polyimide mesh sheet with dielectric constant 3.5. The effective dielectric constant of the polyimide mesh can reduce by removing more material from a polyimide sheet.

Daisy-chain cable

The application of flexible cables will provide overlapping of sensors (inside the module) for elimination of “dead areas” (including daisy-chained sensors).

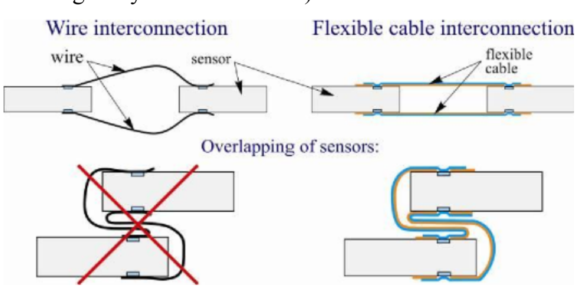

Figure 4: Schematic view of the proposed connections between the sensors.

Figure 4 shows a schematic view of the arrangement for the sensors and daisy-chain cables. A first iteration of daisy-chain cable compatible with this STS detector module concept has been designed and produced at our institute in 2007.Some basic characteristics of such cables are given below:

- material – foiled dielectric FDI-A-20;
- thickness of aluminium layer – (8 ÷ 10) µm;
- thickness of polyimide layer – 10 µm;
- dimension of daisy-chain cable is (71.2×22.9) mm with technological area and (51×12.4) mm – only work area;
- pitch of traces – 50 µm;
- width of traces – (20 ÷ 30) µm;
- quantity of traces – 1024;
- expected resistance Rtr ≈ (9 ÷ 14) Ohm/cm;
- expected capacitance Ctr ≈ (0.36 ÷ 0.45) pF/cm.

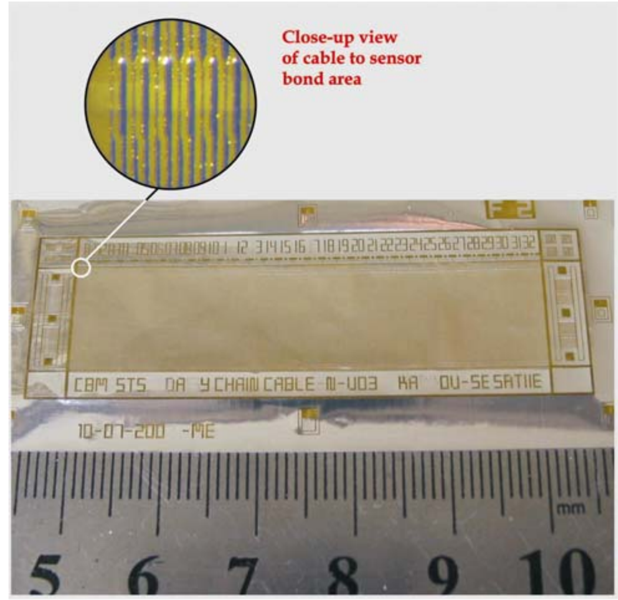

Figure 5: Photo of daisy-chain cable first pre-prototype

Features of assembly

The opportunity of formation of reach-through „windows” in polyimide layers will allow to refuse application of an aluminium wire for connection of sensor contact pad and leads of aluminium-polyimide cables and to carry out connection of leads directly to sensor contact pads by ultrasonic bonding through “windows” in polyimide.

It will allow reducing quantity of bonded connections in detector modules practically twice and will allow considerably simplifying assembly process. Thus during assembly the opportunity of short circuits is completely excluded in the bonding area of sensor contact pads with leads of flexible cables.

The assembly technology of flexible aluminium-polyimide cables with sensor easily adapts for the existing automatic bonders for ultrasonic bonding such as Delvotec. Identical materials application (aluminium sensor contact pads and bonded aluminium cable leads) the high quality and reliability of bonded connections is ensure.

Conclusions and plans

Two types of thin micro-cables were developed and the first samples of long multi-line analog cable (cable length – 500 mm, traces pitch – 100 µm, traces quantity − 512) and daisy-chain cable (cable length – 12.4 mm, traces pitch – 50 µm, traces quantity − 1024) are made.

Future plans must take into account necessity investigations of technological factors influence, construction features of cables and optimal production technological modes selection with the purpose of prototypes and real flexible micro-cables high quality guaranteeing.

References

[1] J.M. Heuser and Chr.J. Schmidt, Development of Microstrip Sensors for the CBM Silicon Tracking System. CBM Progress Report 2006.

[2] J.M. Heuser, Development of a Silicon Tracking and Vertex Detection System for the CBM Experiment at FAIR, Nucl. Instr. Meth. Res. A582 (2007) 910-915

Development of a Microstrip Detector Module Prototype for the Silicon Tracking System of the CBM Experiment at FAIR

M. Borysova[1], J. M. Heuser[2], O. Kovalchuk[1], V. Kyva[1], A. Lymanets[1,3], V. Militsiya[1], O. Okhrimenko[1], V. Pugatch[1], V. Zhora[4], V. Perevertaylo[4], and A. Galinskiy[5]

[1]KINR, Kiev, Ukraine; [2]GSI, Darmstadt, Germany; [3]FIAS, J. W. Goethe University, Frankfurt, Germany; [4]Institute for Microdevices, Kiev, Ukraine; [5]SPA AEROPLAST, Kiev, Ukraine

The development of a low-mass mechanical assembly of single or chained double-sided silicon microstrip sensors and their connection through thin flat low-capacitance analog readout cables to a readout electronics is a goal of the R&D within the Agreement on cooperation between the KINR and GSI. This includes the development and construction of an experimental test stand with cooling infrastructure to characterize the functionality of the device (with focus on sensor-cable-chip interconnection issues, and the signal-to-noise ratio achieved with particle detection), and the elaboration of a quality assurance procedure suitable for a future larger detector module production.

Supporting frame

A low mass STS is one of the key requirements of the experiment to minimize multiple Coulomb-scattering of charged particles in the detector and support materials. In 2007, first double-sided silicon microstrip detector prototypes have become avilable. Few versions of the support frame for the CBM01, CBM01B1, CBM01B2 sensors have been designed and produced by AEROPLAST (Kiev). Construction material is carbon fiber with material budget below 0.3% X_0. The design was focused on low-Z material, minimization of the mass, maximum rigidity, perfect flatness, geometric thickness less than 2.5 mm, stable mechanical properties in the temperature region from -5 °C to 50 °C. This construction material (approximate weight proportions: 65% - carbon, 35% - epoxy resin) has a density 1.5 times less than Al-alloys, elasticity module - at the level of the steel, coefficient of the thermal expansion in the temperature region +/- 60 °C - close to zero. Three-layer frames composed by two flat plates (0.25 mm thick) with foam layer (1 mm thick, density - 0.7 g/cm^3) in between them were produced in three types of geometry shape to match the sizes of prototype silicon sensors.

Cooling

Thermo-mechanical tests with dummy silicon samples glued by silicon glue onto the supporting frames demonstrated perfect mechanical rigidity as well as thermoconductivity (appr. 0.6 W/m°C in the longitudinal direction). A special design has been developed for investigating cooling by circulating a liquid agent in hollow plates. Yet, currently such structure didn't show needed mechanical stability. It might be improved at the price of increasing the transversal size of the frame up to 5 mm (keeping material budget still within a required 0.3% X_0).

Microcables

The readout of the microstrip sensor is planned to be performed through low-mass long readout cables with the same pitch as the sensor strips. A double-layer staggered micro cable with 25 μm wide, 20 μm thick Al strips at 101.4 μm pitch on 24 μm thick polyimide film (thus providing 50.7 μm pitch) is currently under development at the Institute of Microdevices (IMD, Kiev). The pitch of the strips was chosen to match that of the readout chip n-XYTER that will serve for detector prototyping in the CBM experiment. A micro cable must feed signals at distances up to 0.5 m, which creates high input capacitance for readout micro chip. This problem has been simulated using micro cables of similar structure, but with less capacitance. In this approximation pick-up signal was of the order of 1% of the main signal. Currently, three-layer micro cables (with the grounded layer in the middle) are also under design at IMD (Kiev) aimed at the prevention of a pick-up problem.

Tests

The first detector module prototypes equipped with CBM01B1 as well as CBM01B2 sensors have been mounted and connected to a discrete electronics at the readout board.

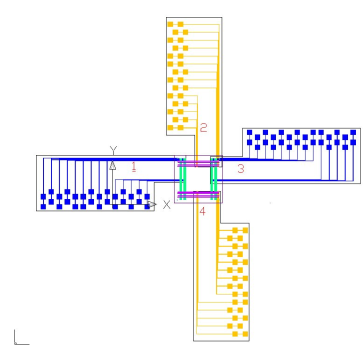

Figure 1: Scheme of the CBM01B2 sensor connection to a readout board.

A scheme of connections is shown in Fig. 1 Tests are performed now at KINR using laser pulses (640 nm) and radioactive sources. The results will be available soon.

Investigations on WLS covered photocathodes for the RICH photodetector

V.V.Brekhovskikh, M.V.Medynsky, V.V.Morozova, V.I.Rykalin, and S.A.Sadovsky*
IHEP, Protvino, Russia

In order to improve the physics performance of the RICH detector an increase of the photodetector sensitivity in the UV region is a promising possibility. As proposed in [1] an effective solution in this direction is based on WLS films covering the PMT glass photo-cathodes. In 2007 we have started R&D on different WLS films aiming at an improvement of the combined efficiency of PMTs with glass photocatode covered with transparent WLS films.

It was shown [2] that the effective quantum yield of photomultipliers (PMTs) with a flat glass photocathode window covered with transparent WLS films can achieve 130% of the maximal value of the quantum yield of the uncovered photocathode. This effect has been obtained experimentally and calculated analytically. It is due to the multiple transition of some of the photons emitted by the WLS through the photocathode because of the total internal reflection.

Spectral dependences of relative quantum yields of a multialkali photocathode with flat glass window with and without WLS coverage and of a bialkali photocathode on a quartz window are shown in Fig.1, see [2]. The short wavelength boundary of the spectral region is restricted by the transparency of the polymethylmetacrylat based WLS film in the ultraviolet region. At the same time, the optical non-transparent (diffuse view) WLS film allows to obtain an excess above the quantum yield of no more than 10%, see [3].

Therefore, for RICH photodetectors an optically transparent WLS film would be needed with a high efficiency in the region of ultraviolet wavelengths. The evaporated paraterphenyl WLS films are not optically transparent (diffuse view), i.e. they have not an optimal structure. For the CBM RICH we have designed a new type of thin WLS film with a monocrystalline paraterthenyl layer of a few μm thickness on a 20 μm teflon substructure. These paraterphenyl films have a high optical transmissivity and have no visible diffuse light scattering. First preliminary measurements show that the efficiency of monocrystalline paraterthenyl films are substantially higher than those of polymethylmetacrylat based and evaporated paraterphenyl films. For tests a MgF_2 crystal excited by a $^{90}_{38}Sr$ radioactive source was used as the light emitting source. The WLS film efficiency was defined as the ratio

$$R = (I(PMT + WLS) - I(PMT))/I(PMT),$$

where $I(PMT+WLS)$ is the photocathode current in the case of using the WLS film and $I(PMT)$ is the photocathode current without the WLS film. Results are shown in Fig.2.

* Serguei.Sadovsky@ihep.ru

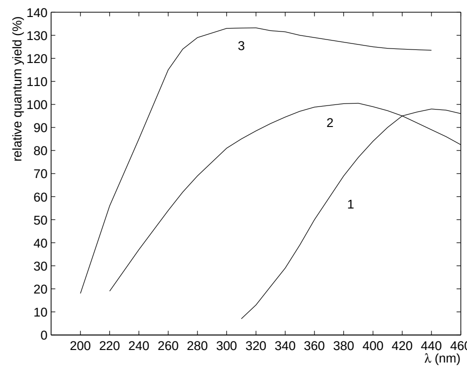

Figure 1: The measured spectral dependences of PMT quantum efficiencies: (1) PMT FEU 110 (glass window), maximum quantum yield $\varepsilon = 24\%$; (2) PMT 56UVP (quartz window), maximum quantum yield $\varepsilon = 24\%$; (3) PMT FEU 110+WLS film (optimal mixture of organic luminophores) normalized for the quantum yield of PMT 56UVP as a typical photomultiplier with the quarz window [2].

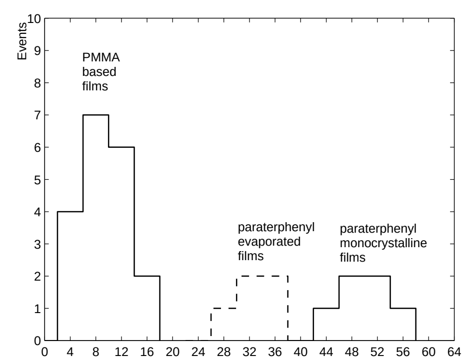

Figure 2: Efficiencies (for definition see text) of different WLS films, along the y-axis the number of tested WLS films is shown.

References

[1] CBM TSR, Darmstadt, Germany, 2005.

[2] A.M. Gorin et al, Nucl. Instr. and Meth.,A251 (1986) 461-468.

[3] G. Eigen and E. Lorenz, Nucl. Instr. and Meth., 166 (1979) 165.

Research and Development of fast readout chamber based on GEM structures

S. Chernenko, S. Razin, Yu. Zanevsky, V. Zryuev,
JINR Dubna, 1419890,Russia

The result of R&D for fast readout chambers based on GEM and thick GEM (THGEM) [1] is presented. The test of the detectors was performed in a laboratory test bench with an X-ray tube with copper cathode and an Fe-55 source. The two-stage GEM detector with sensitive area of 10x10 cm² had a one dimensional readout board with the strips of 0,35 mm, 0,6 mm and 1,0 mm pitch. The drift and induction gaps were 10 mm and 2 mm accordingly [2]. The detector has operated with Ar/CO2 (85/15) gas mixture and an amplification factor of ~ $2x10^3$. A spatial resolution of 90 µm was obtained with strips of 0,6 mm and 60 µm slit collimator (fig.1)

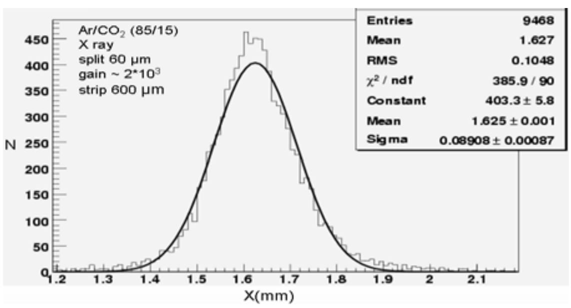

Fig 1. A spatial resolution obtained for GEM detector with a fine collimated X-ray beam.

From the point of view of electronic channel number and spatial resolution this pitch is an optimal one.
The THGEM of 10x10 cm² was manufactured by standard PCB techniques with precise drilling in G-10 of 0,4 mm thickness, hole diameter 0,3 mm, distance between the holes 0,7 mm. and rims 0,1mm (fig2)

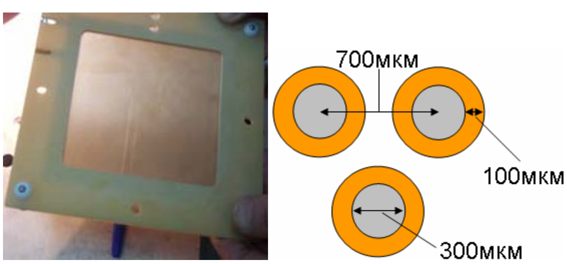

Fig.2 The frame of one stage THGEM detector.

On the base of this structure a one-stage THGEM detector was constructed and tested under the same conditions as the GEM detector. The schematic layout is shown on fig.3. The gas amplification factor was ~ $2x10^3$. The counting plateau obtained with Fe-55 is presented in fig.4, the maximal gas amplification factor was ~ $5x10^3$ (for the end of plateau). On fig.5 is shown the integral nonlinearity for this detector measured with a fine collimated X-ray beam. A spatial resolution of ~ 250 µm. was obtained.

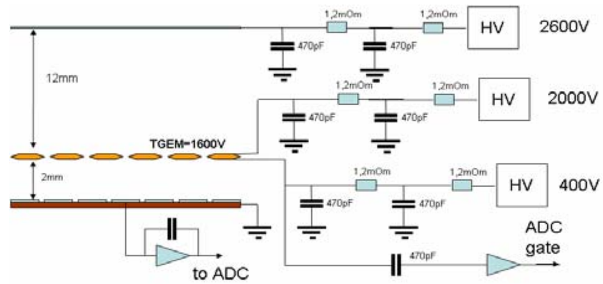

Fig.3. Schematic layout of the one-stage THGEM detector.

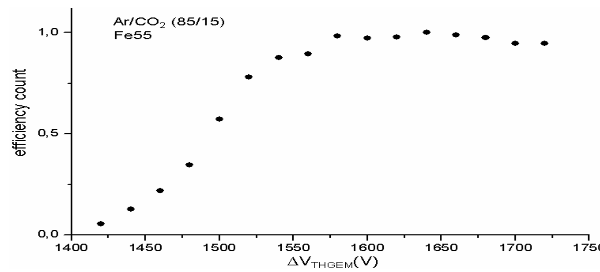

Fig.4. Counting plateau of THGEM detector measured with an Fe-55 source.

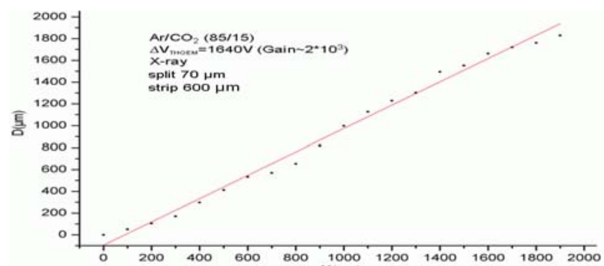

Fig.5. Integral nonlinearity measured for the THGEM detector a with fine collimated X-ray beam.

The study of THGEM detector at JINR is in progress. But we can summarize now that this type of detector permits to get a high gas amplification factor and to work with one stage THGEM. But for a high reliability operation we need to manufacture this THGEM (holes and rims) with an accuracy about 1,5 µm [3].

References:

[1]. C.Shalem et al. “Advances in Thick GEM-like gaseous elec tron multipliers” Nucl. Instr. and Meth. **A 558** (2006)475
[2]. A. Andronic “ Research and Development of fast TRD read out chambers”, CBM Progress Report 2006, 34.
[3] M. Gai for the Yale-Weizmann Collaboration. “Toward Applications of Thick GEM for a Dark Matter Detector” A Progress Report at Big Sky Workshop,,February 14, 2007.

R&D with GEMs and THGEMs towards developing a muon tracker for CBM experiment

A. K. Dubey *[1], S. Chattopadhyay[1], and G. S. N. Murthy[1]
[1]Variable Energy Cyclotron Centre, Kolkata

A large acceptance, high-resolution and high rate muon detection system is being proposed by the Indian collaboration for the CBM experiment for carrying out measurements of charmonium ($J/\psi, \psi'$ ..) and the low mass vector mesons exploiting their decay via muonic channels. These measurements are key probes for the indication of in-medium modification of hadrons, chiral symmetry restoration and deconfinement. Current design of the muon system consists of 16 detector stations with several absorber layers placed in between. For first few stations, it is proposed to implement high rate gas detectors based on Micropattern technology. Gas electron multipliers(GEM) [2] and thick GEM(THGEM) [3] are two such suitable options envisaged for this purpose. GEM is made out of a $50\ \mu m$ thick polymer foil coated with a thin layer of metal on both sides a regular array of holes are chemically pierced which are a fraction of a millimetre across and apart. On applying high voltage ($\Delta V \approx 500$) across the two conducting surfaces, a primary electron produces an avalanche of electrons and ions inside the holes and this signal can be readout using pads or strips. THGEMs are an augmented version of GEMs where holes are mechanically drilled on thick FR4 plates having thickness $500\ \mu m$ or more. The holes are of larger size (about $300\ \mu m$) and operate at higher voltages. While GEMs need to be imported and require delicate handling, THGEMs, inspite of their slightly inferior position resolution, have an advantage that they can be manufactured indegenously in India and are more robust.

As a first step in the direction of searching for an appropriate device for muon detector, we have assembled and successfully tested a mutli-GEM stack with a drift mesh and pad readout. A 10 cm x 10 cm GEM foil was stretched using a double layer perspex jigs which on heating stretched the foil sandwiched between the two layers. Two G10 frames cut to size were glued on the either side of the foil thus producing a framed and stretched GEM mesh ready for testing. Signals have been obtained using radioactive sources with $Ar/CO_2(70/30)$ as the gas mixture. The picture of the detector under test is shown in Fig. 1(a). The pulse height spectra using Fe55 source acquired using an MCA, is shown in Fig. 1(b). Also, we have for the first time, locally fabricated a THGEM element using conventional PCB technology involving mechanical drilling of holes. The hole has a diameter of 0.3 mm while the copper rim around it has a diamter of 0.5 mm. a 10 cm x 10 cm G10 based PCB was used to drill such holes at a pitch of 1.2 mm. Fig. 2 shows a picture of the THGEM as well as the pulse height spectrum from Ru-106 corresponding to a ΔV=1600 using the THGEM.

* anand@veccal.ernet.in

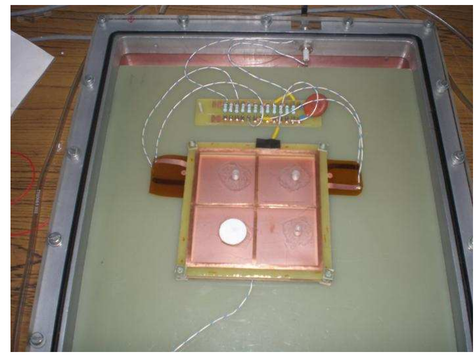

(a) A 2-GEM assembly under test in lab.

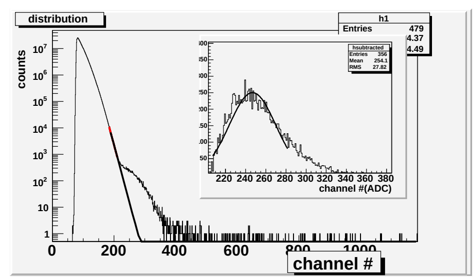

(b) Pulse height spectrum for Fe55-source

Figure 1: R&D with GEM

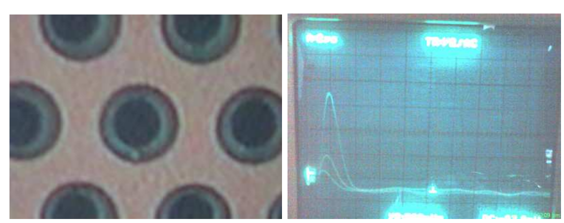

Figure 2: Left: Closeup of a THGEM (10 cm x 10 cm foil) fabricated locally. It shows holes of 0.3 mm with a 0.1 mm rim around it. Right : Pulse height spectrum from a THGEM using Ru-106 source for Δ V=1600 V.

References

[1] Conceptual Design Report for CBM.

[2] F. Sauli, Nucl. Instrum. Methods A386(1997) 531.

[3] R. Chechik, A. Breskin, C. Shalem and D. Mormann, Nucl. Instr. and Meth. A535(2004) 303.

Systematic studies on MWPCs for TR detection at high rates

D. Gonzalez-Diaz[1], A. Andronic[1], C. Garabatos[1], A. Kalweit[1], and F. Uhlig[1]
[1]GSI, Darmstadt, Germany

In a series of measurements conducted at GSI ([1], [2]), the possibility of using MWPCs based on Xe/CO_2 for TR detection at the anticipated CBM fluxes of 100 kHz/cm^2 was explored. Here, the already existing data are enhanced by including additional measurements on Ne mixtures, together with the characteristic 'gain vs voltage' curves for a number of chamber configurations, focusing on the maximum achievable gain. Furthermore, the theoretical formalism of [3] is used in its full extent by resorting to only two free parameters for each noble gas mixture, according to $1/\mu = f/\mu_{Xe(Ar,Ne)} + (1-f)/\mu_{CO_2}$ with f being the fraction of noble gas and μ_i the mobility of the drifting ion on gas i (Blanc's law [4]). Following [3], the functional dependence of the gain vs rate can be readily obtained as:

$$M = M_o \exp(-a^2 \frac{q_e n_o}{2\mu} \frac{sh^2}{C_l} \frac{Mr}{\ln M - b}) \qquad (1)$$

where M stands for the detector gain at a given rate r, M_o is the gain at zero rate, q_e the electron charge, n_o the primary ionization, s the wire pitch, h the gap, C_l the capacity per unit length, and the gain is described by an exponential law such that $\log_{10} M = aV - b$. After numerical evaluation, the transcendental equation 1 can be used for fitting the data for all the mixtures in the spirit of [1], [2], yielding μ_{Xe}, μ_{Ar}, μ_{Ne} and 3 values for μ_{CO_2} (assuming the nature of the drifting ion to be uncertain). By defining the gain drop $F = 1 - M/M_o$, the maximum affordable rate at operating gain M_o if a maximum gain drop F is allowed in the chamber will be given by:

$$r = \frac{\ln[(1-F)M_o] - b}{(1-F)M_o} \frac{1}{a^2} \frac{2\mu}{q_e n_o} \frac{C_l}{sh^2} \ln(1-F) \qquad (2)$$

and it is shown in Fig. 1 for the case where $F = 5\%$ and $M_o = 10^4$ under X-ray illumination at an average energy $E = 6.7$ keV (approximately 2 times more than mips).

The effect of the finite beam size was evaluated from measurements at 10 times bigger illumination area ($A \sim 6$ cm^2) and estimated to be less than a factor 2, nevertheless a more precise determination will be pursued in the future. Fig. 1 indicates that operation of the chamber at $M_o = 10^4$ and fluxes up to 100 kHz/cm^2 is feasible in Xe mixtures and can be pushed higher roughly proportionally to F/M_o.

A very fundamental issue for operation of MWPCs is the maximum achievable gain before photon or ion feedback results in self-sustained currents that make impossible the chamber operation. For $s = 3$ and $s = 4$ mm pitch, Xe/CO_2 based mixtures could be operated up to $M_o = 10^5$, being the maximum gain slightly higher for Ne and Ar based mixtures (Fig. 2). Operation at gains lower than $M_o = 10^4$ ensures therefore a safe margin for dealing with

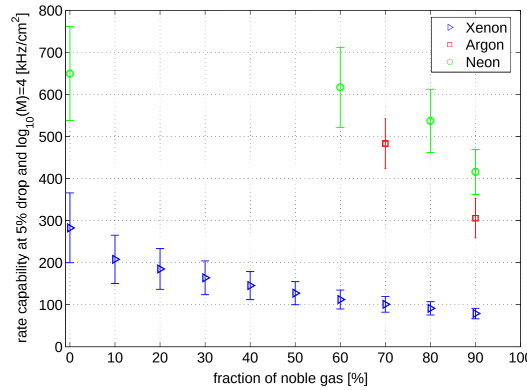

Figure 1: Rate capability at 5% drop and $M = 10^4$ for $s = 4$, $h = 3$ mm chamber.

a wide range of primary ionizations, providing at the same time the rate capability required by CBM.

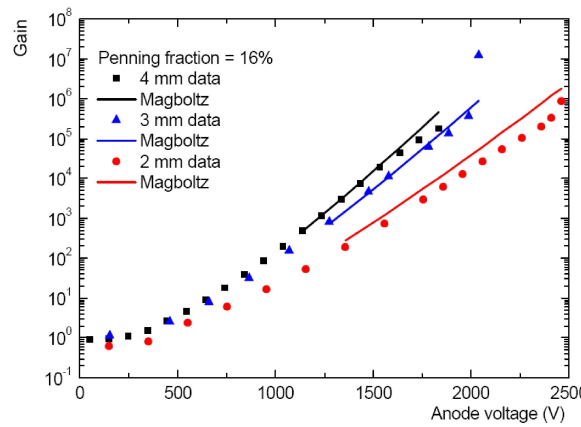

Figure 2: Gain vs voltage curve for $s = 2, 3, 4$ mm chambers, together with a preliminary Magboltz description assuming 16% Penning fraction.

With the still on-going measurements we plan to systematically explore a broad set geometries and gas mixtures that will be of interest for CBM, providing valuable information for making a sound choice of the final detector.

References

[1] A. Kalweit, Bachelorarbeit, Darmstadt TU, May 2006.

[2] C. Garabatos, F. Uhlig, G. Hamar, GSI-report 2006-02-28.

[3] G. C. Smith and E. Mathieson, IEEE Trans. Nucl. Sci. 34(1987)420.

[4] F. Sauli, CERN 77-09, 1977.

High efficiency TRD for CBM in test beam and simulation

M. Klein-Bösing[1], J. P Wessels[1], M. Petriş[2], M. Petrovici[2], V. Simion[2], and F. Uhlig[3]
[1]Institut für Kernphysik, Münster; [2]NIPNE, Bucharest; [3]GSI, Darmstadt

The CBM (Compressed Baryonic Matter) experiment is designed as a fixed target experiment, in which a TRD shall provide tracking of all charged particles, electron identification and discrimination against a large pion background. In order to fulfill these tasks in the context of high count rates of up to 150 kHz/cm^2 and high particle multiplicities, we constructed TRD prototypes based on a symmetric arrangement of two MWPCs with a common, central pad readout electrode. In this way the anode-cathode gap is small enough to reach the required speed and to reduce space charge effects in a high counting rate environment. At the same time a high conversion efficiency of the transition radiation is obtained due to the duplication of gas volume.

The prototypes have been tested in a beam of electrons, pions and protons with p=1.5 GeV/c and they have shown very good discrimination capability of electrons versus pions which meets the requirements of CBM [1]. The deposited charge spectra have been compared to a simulation in CBMRoot considering this new detector geometry.

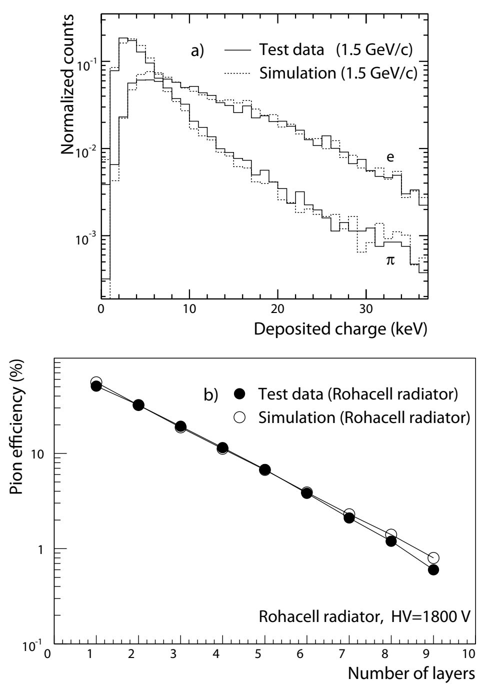

Figure 1: a) Deposited charge for electrons and pions and b) pion efficiency in simulated and test beam data with 5% electron contamination of the pion data sample.

The measured spectra can be described very well by these simulations, see Fig. 1a). With these spectra the misidentification probability for pions can be calculated. This pion efficiency as function of the number of extrapolated detector layers also shows good agreement of simulated and test beam data, see Fig. 1b). In addition, an electron contamination level of 5% of the pion data sample in the test beam could be diagnosed. The pion efficiency of the detector in a pure electron and pion beam is 0.4% for 9 layers TRD.

In the test beam the position resolution of two identical prototypes aligned in a row along the beamline has been determined. The measurement of the coordinate of the avalanche along the wire direction is done by interpolating the pulse height recorded on adjacent readout pads. The intrinsic position resolution of the two prototypes is given by the variance of a Gaussian fitted to the distribution of residuals defined as the distance between the position of the reconstructed clusters in both chambers and a linear fit to the alignment. For the measurement of the rate dependence shown in Fig. 2 a moderate voltage of 1700 V has been chosen, to prevent instabilities of the chambers at high rates. For $\mathrm{Xe}(90\%)\mathrm{CO_2}(10\%)$ the value of the position resolution at moderate intensity is (161 ± 3) μm or 3.2% of the pad width. No significant deterioration of the position resolution is observed up to average particle rates of 200 kHz/cm^2, where it is still much better than the required 200 μm [2].

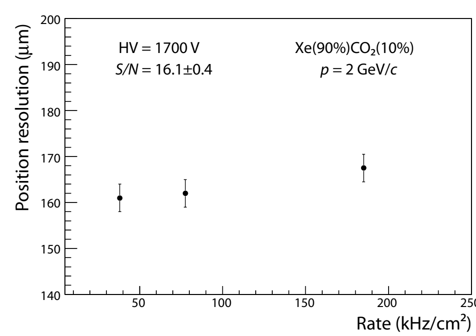

Figure 2: Position resolution as a function of particle rates with HV = 1700 V and $p = 2$ GeV/c, using a $\mathrm{Xe}(90\%)\mathrm{CO_2}(10\%)$ gas mixture.

References

[1] M. Petrovici et al., Nucl. Instr. Meth. Phys. Res. **A 579** (2007) 961.

[2] M. Klein-Bösing et al., Nucl. Instr. Meth. Phys. Res. **A 585** (2008) 83.

Development of large dimension straw tube arrays for high rate capability coordinate detector application

V. Peshekhonov[1], L. Naumann[2], K. Davkov[1], V. Davkov[1], L. Kudin[3], J. Marzec[4], V. Myalkovskiy[1], D. Seliverstov[3], V. Tikhomirov[5], S. Vasiliev[1], P. Wintz[6], and K. Zaremba[4]

[1]JINR Dubna, Russia; [2]FZ Dresden-Rossendorf, Germany; [3]Institut of Nuclear Research, Gatchina, Russia; [4]University of Technology, Warszaw, Poland; [5]Lebedev Institut, Moscow, Russia; [6]FZ Jülich, Germany

A new development of multiple anode assembly technique for straw tube detectors allows to provide the readout of embedded anode wire segments. We assembled up to 10-fold segmented multiple anode drift tubes with a granularity from 1.6 cm^2 to 10 cm^2 and investigated a two-layer prototype consisting of 19 straws to check the feasibility of assembling of multiple segment anodes [1]. The straws are 500 mm long and 4 mm in diameter. The anodes are subdivided in two, three or four parts of different length. containing 57 readout channels. The prototype tests confirmed on the one hand the functionality of the multifold segmented drift tubes and on the other hand the necessity to improve the quality of the detector signal by double sided readout of each anode wire segment of the straw. A main element for multifold straws is a special spacer. The cylindrical spacer unit consists of a plastic tube and a glass capillar to fix the anodes and contact wires (see Fig.1,2,3 in [1]). We investigated long and flat cable connector prototypes (Fig.1). The cables provide the high voltage to the anode wires and connect the anode to the front end electronics. The flat cables are up to 2 m long, to guarantee that the FEE could be located outside the active detector area to minimize its contribution to the radiation thickness. Test prototypes with up to 2 m long flat cables and 1.6 m long segmented straws have been build (Fig.2). For the measurements the signals were generated in a straw tube by irradiation with collimated Gammas (^{55}Fe).

Fig.3 shows that computer simulation and measurement of signal transmission of the flat cables are in a good agreement. The decrease of the signal amplitude shows a linear dependence on the cable length and amounts to $8\%/m$. For the longest cable an increase of the signal rise time from 5 ns to 9 ns and a cross talk of 2.2$\%$ have been measured. The radiation thickness of the prototype flat cable has been estimated and amounts to $0.1\%\mathrm{X}_0$. The design of the cable allows to improve this parameter by a factor 2. Fig.4 shows the measurement of the amplitudes in dependence on the cable length and the straw segment length. This information is important because adjacent signal transmission lines have the same length, but the length of the corresponding anode wires can differ. The signal amplitude variation in dependence on the straw length amounts to 10 $\%$. This value is negligible.

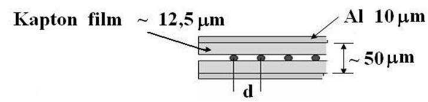

Figure 1: Cross section of the flat flexible cable.

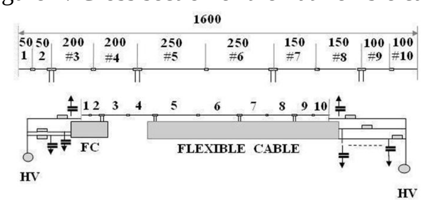

Figure 2: Schematical drawing of the straw segmentation (top) and the readout concept (bottom).

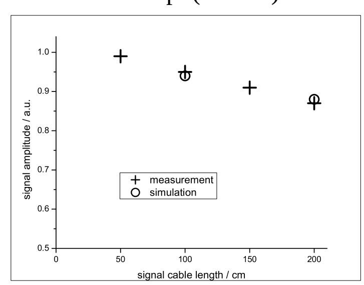

Figure 3: Comparision of measured and simulated anode signal amplitudes in dependence on the signal cable length.

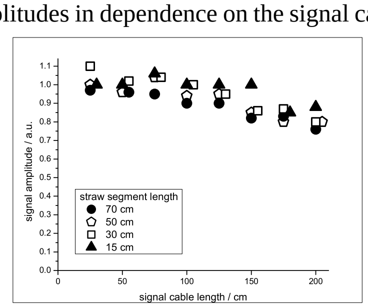

Figure 4: Anode signal amplitude in dependence on the flat cable length for straw segments of different size.

References

[1] K. Davkov et al., Nucl. Instr. and Meth. **A584** (2008) 285.

Progress with semi-conductive glass tRPCs

V. Ammosov[1#], F. Guber[2]
[1]IHEP, Protvino, Russia; [2]INR, Moscow, Russia

The Time-of-Flight (TOF) system of the CBM experiment is proposed to be based on timing Resistive Plate Chambers (tRPC), which have become a reliable and approved tool for timing measurements. The TOF system should have a time resolution of about 80 ps and a counting rate capability up to 20 kHz/cm^2.
The tRPC used for TOF applications are usually multi-gap chambers with glass as resistive plates operated in the saturated avalanche mode. With all the other parameters of tRPC being fixed, the tRPC rate capability is determined by the bulk resistivity of glass. The resistivity of conventional glass (~10^{12} Ω cm) results in a rate capability of RPC as low as several hundred Hz/cm^2, which turns to be the main drawback of such chambers. Usage of semi-conductive glass with a resistivity of 10^8–10^{11} Ω cm is an inspiring way of improving the RPC rate capability, so that it can meet the CBM TOF requirements. Development of semi-conductive glass production to obtain glass samples with a resistivity in the range 10^8 – 10^{11} Ohm·cm for phosphate and silicate compositions was achieved.

The average resistivity of phosphate glass samples was about 10^9 Ω cm. For the silicate glass samples 3 batches of different average resistivity of ~10^8 Ω cm, ~10^9 Ω cm and ~10^{11} Ω cm were produced. The spread of the resistivity within a single batch of the same glass composition is in the range of a factor 4. A typical behavior of resistivity as a function of applied voltage is shown in fig.1 for the silicate glass sample with lowest resistivity.

The bulk resistivity of the silicate glass was measured as a function of temperature and time. An exponential decrease of the resistivity was measured at the level of 5% / deg. A few times a decrease of the resistivity within a few ten minutes was observed, then the behavior became more and more flat.

Intensive R&D work was done for single cell tRPCs as basic element for the TOF system. It included design of tRPCs with adaptation of existing read out electronics, construction of tRPCs with different semi-conductive glasses, tests of tRPCs with cosmic rays, electron and hadron beams at IHEP and Rossendorf [1,2]; tests of tRPCs for long term stability and ageing effects.

A tRPC prototype of a minimal (4 × 0.3 mm gaps) configuration with electrodes made of phosphate glass with a bulk resistivity of the order of 10^9 Ω cm has been tested with beam and shown satisfactory behaviour in terms of efficiency and time resolution (see fig. 2). The rise of rate from 2.25 to 18 kHz/cm2 leads to allowable degradations of efficiency (from 98% to 95%) and time resolution (from 90 ps to 120 ps).

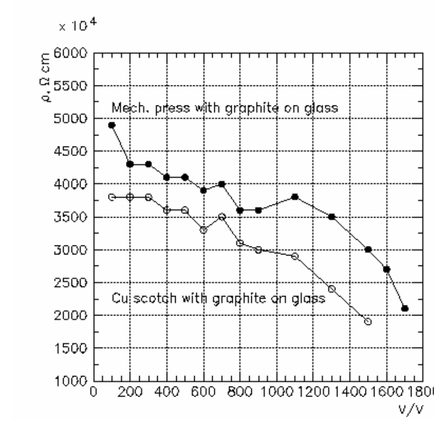

Figure 1: Bulk resistivity as a function of applied voltage for silicate glass sample

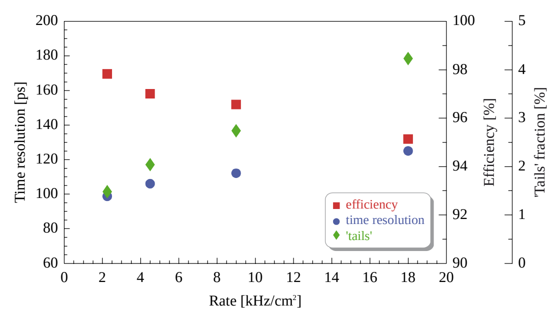

Figure 2: Time resolution (squares), efficiency (circles) and estimated 'tails' fraction in the timing spectrum (diamonds) of RPC as functions of the rate.

. For four-gap RPC prototypes with silicate glass detection efficiencies for minimum ionizing particles (electrons) beyond 95% at a constant time resolution of roughly 100 ps were found at flux densities up to 20 kHz/cm^2. Thus, a figure of merit for high rate capability of tRPCs defined by the experiment has been met. FEE development to improve the time resolution is foreseen.

A multi cell approach for the tRPC shows large value of cross talk between pads. It seems that a system of independent tRPC cells is a feasible solution for the central part of the CBM TOF detector. Such solution comprises of an array of separate single cell tRPCs and makes it possible to keep the cross-talk between neighboring cells at the least possible level.

This work was supported partially by INTAS 06-1000012-8810 project.

References

[1] A.Akindinov et al., Nucl.Instr.Meth. A572(2007)676
[2] V.Ammosov et al., Nucl.Instr.Meth. A576 (2007)331

ammosov@ihep.ru

System studies for the CBM-TOF detector at FAIR

A. Blanco[1], P. Cabanelas[2], M. Ciobanu[3,4], I. Deppner[4], P. Fonte[1,5], J. A. Garzon[2], D. Gonzalez-Diaz[3], N. Herrmann[4], K. D. Hildenbrand[3], T. I Kang[3,6], M. Kiš[3,7], P. Koczon[3], Y. Leifels[3], K. Piasecki[4,8], A. Reichel[4], M. S. Ryu[3,6], A. Schüttauf[3], N. Zernezki[3,4], and the CBM Collaboration

[1]LIP, Coimbra, Portugal; [2]USC, Santiago, Spain; [3]GSI, Darmstadt, Germany; [4]Universität Heidelberg, Germany; [5]ISEC, Coimbra, Portugal; [6]Korea University, Seoul, South Korea; [7]RBI, Zagreb, Croatia; [8]Warsaw University, Poland

The CBM ToF wall will consist of 60.000 independent cells featuring a ToF resolution of $\sigma_{TOF} \leq 80$ ps over 150 m^2 [1]. For this purpose, the Multi-gap Resistive Plate Chamber (MRPC) technology is ideally suited in terms of timing performances, granularity and cost. The specific CBM environment defines 2 differentiated regions both in terms of rate and occupancy: for instance, existing layouts based on pad readout (ALICE-like) could be efficiently used in the more critical inner region while strip readout (FOPI or HADES -like) would be a natural choice for the periphery, where a large area needs to be covered at moderate occupancies/rates. In any case, none of the existing technologies can cope with the maximum expected rates (20 kHz/cm^2) and a substantial effort in material research is being carried out [1]. For the region at more moderate rates, that actually amounts for 75 % of the wall, either FOPI or HADES designs can cope with the anticipated rates. Both systems emphasize, nevertheless, different critical aspects: as shown in this report, while the former features a high azimuthal resolution, the later focuses on minimizing inter-strip cross-talk aiming at a reduced system occupancy.

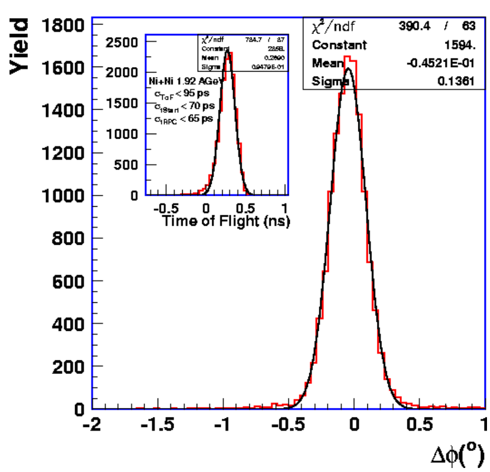

Figure 1: FOPI's $\Delta\phi$ distribution, yielding $\sigma_{\Delta\phi} \leq 0.15\,^o$ for matched tracks between CDC and the new ToF-barrel.

The new FOPI ToF-barrel, covering 5 m^2 with 2400 individual strips, has been commissioned in a first heavy ion production run in 2007 [2]. Combining a Multi-strip MRPC (MMRPC) technology with a custom designed electronics (4800 ch) based on MMIC high bandwidth preamplifiers and a custom designed TAC-ASIC chip [2], a very high azimuthal resolution of $\sigma_{\Delta\phi} \leq 0.15\,^o$ ($\sigma_{pos} \leq$ 2.5 mm) could be achieved, with system-time resolutions well below the design goal (Fig. 1).

One HADES sextant, comprising 200 shielded strips (2-5 x 15-60 cm^2) has been also tested successfully in 2007 [3]. As shown in Fig 2, the fraction of cross-talk events is at a level of 2% for the large majority of strips (the notable exception likely suffers from cross-talk at the FEE). Furthermore, the inset shows the combined time resolution of tracks crossing two overlapping strips when a simultaneous (disturbing) hit is present in any neighbour. Within the usual ± 5 ps experimental uncertainty, no sizeable deterioration is observed in such a case.

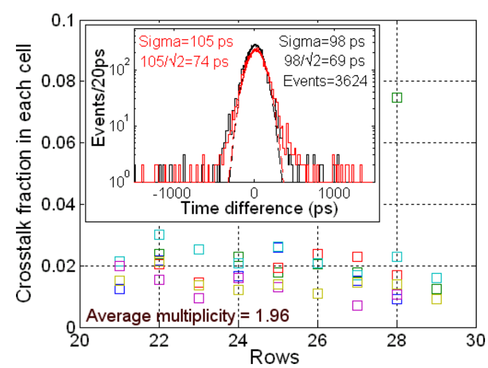

Figure 2: HADES crosstalk performance for different rows of strips at different polar angles.

As a summary, during 2007 HADES and FOPI carried out successful system measurements, showing time resolutions within CBM requirements and bringing important data on heavy ion environments. Such data is being analyzed and is a necessary input for design optimization. Even if for CBM the position resolution is not a critical issue, a multi-strip configuration will largely simplify the overall mechanics provided cross-talk can be kept at moderate levels. Therefore, based on the expertise accumulated so far, we plan to systematically investigate different multi-strip anode structures, focusing on minimizing and understanding strip coupling and charge sharing.

References

[1] D. Gonzalez-Diaz et al, GSI annual report 2007.

[2] M. Kis et al, GSI annual report 2008.

[3] A. Blanco et al, GSI annual report 2008.

RPC performance tests at the electron linac ELBE

F. Dohrmann[1], R. Kotte[1], L. Naumann[1], D. Stach[1], J. Wüstenfeld[1], F. Guber[2], A. Ivashkin[2], V. Ammosov[3], and A. Semak[3]

[1]Institut für Strahlenphysik, Forschungszentrum Dresden-Rossendorf, Dresden, Germany; [2]Institute for Nuclear Research, Moscow, Russia; [3]Institute for High Energy Physics, Protvino, Russia

Resistive plate chambers (RPCs) are considered to be well suited for large area time-of-flight (TOF) arrays as planned for the CBM experiment at FAIR. The possibility of testing the performance of RPCs at the radiation source ELBE has been shown with prototype detectors equipped with standard float-glass electrodes owing bulk resisitivities of about $10^{13}\,\Omega\,\mathrm{cm}$ [1].

Besides investigations of the rate capabilities of RPC detectors made of phosphate glass electrodes with a volume resistivity of about $10^{10}\,\Omega\,\mathrm{cm}$ [2], also detectors have been built and successively tested using silicate glass with resisitivities of $10^8 - 10^9\,\Omega\,\mathrm{cm}$ [3]. It should be stressed that we have measured the volume resistivities of the resp. materials ourselves. Both types of four-gap prototype detectors delivered promising results, i.e. efficiencies above 95 % and time resolutions of about 100 ps up to flux densities of 20 kHz/cm^2 (cf. fig. 1), thus meeting the requirements of CBM-TOF.

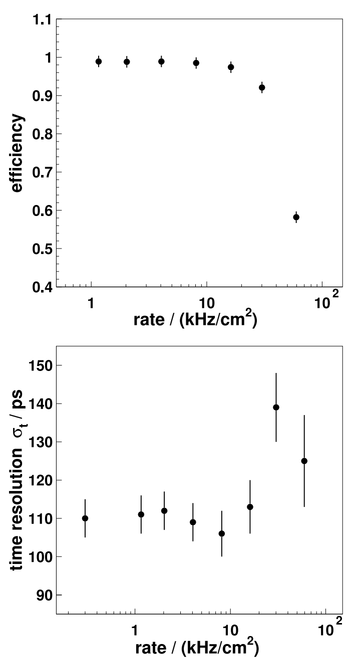

Figure 1: Efficiency (top panel) and time resolution (bottom panel) as a function of flux density for a RPC detector with low-resistivity silicate glass [3].

Furthermore, in FZ Dresden-Rossendorf 4-gap RPCs (six resistive plates of 2 mm thickness, gas gaps of 260 μm, layout similar to that described in ref. [1]) were built with resistive plates made of different plastics materials. One of them is Permastat 100, a special kind of polypropylene with a volume resistivity of $1.5 \cdot 10^{11}\,\Omega\,\mathrm{cm}$, produced by RTP Company, MN, USA. Though the resistivity would meet the requirements of a high-rate RPC for CBM-TOF, the results are not encouraging:

- Already at low detector load, about 30% higher potential voltage than used for similar RPCs with float-glass plates was necessary to get efficiencies of 95 %. (Note that a naive estimate would yield an apparent field strength in the gas gaps above 130 kV/cm!)
- Even at that high potential, the amplitudes did not reach those values found for float-glass RPCs.
- A rapid drop of amplitude, efficiency and time resolution, with increasing detector load was observed, already at rates as low as 100 Hz/cm^2.
- The corresponding detector current was surprisingly low. The maximum current of 20 nA, drawn at rates of 200 Hz/cm^2, would cause a potential across each resistivity plate of a few volts only, hence not distubing the gap fields.

There exists a report [4] on successful operation of RPCs equipped with a commercially available plastics (ENSITAL®SD) with resistivities ranging from 10^8 to $10^{12}\,\Omega\,\mathrm{cm}$ (according to specification by the manufacturer). However, the authors of [4] observed also serious drawbacks of the material like a severe increase of the resistivity with transferred charge. For Permastat 100, we did not find significant changes of the volume resisitive with time or introduced charge. Nevertheless, it is assumed that these materials have an ionic type of conductivity. The ions cannot leave the bulk of the material and transit into the conductive electrodes. Thus, very quickly a space-charge layer builts up and reduces the gap field [5].

The material R&D w.r.t. RPCs suitable for FAIR experiments will be continued, concentrating on low-resistive glasses and ceramics.

References

[1] R. Kotte, F. Dohrmann, J. Hutsch, L. Naumann, D. Stach, Nucl. Instr. Meth. **A 572** (2006) 676.

[2] A. Akindinov et al., Nucl. Instr. Meth. **A 572** (2007) 676.

[3] V. Ammosov et al., Nucl. Instr. Meth. **A 576** (2007) 331.

[4] L. Lopes, R. Ferreira-Marques, P. Fonte, A. Perreira, V. Peskov, A. Policarpo, Nucl. Instr. Meth. **A 533** (2004) 69.

[5] P. Fonte, private communication.

Study of photomultiplier stability for ECAL

V.V.Brekhovskikh, V.A.Dyatchenko, V.G.Lapshin, M.V.Medynsky, and V.I.Rykalin*
IHEP, Protvino, Russia

The CBM experiment will work with a very high interaction rate, up to 10^7 s^{-1}, at which photomultipliers (PMT) of the ECAL detector, especially in its very central region, will experience a high anode current. This operation mode can affect the amplification factor of PMT's and can lead to non-equipotentiality of the photocathode. i.e. to instability of PMT. Therefore, only PMT's which are stable under such conditions can be accepted as ECAL photodetectors.

It is necessary to distinguish between long-time and short-term stability of photomultipliers. While the long-time stability can be controlled with the help of a LED monitoring system, it is impossible to do so in case of short-term stability. The rate-effect (a dependence of amplification on the mean value of the PMT anode current) is the main and likely the most unpleasant source of the short-term instability. To understand the causes of short-term instability we have studied for different types of PMT's the dependence of amplification on the mean anode current in a range up to 10 μA and an amplification of around 10^6. A Booster power supply for the last 3 dynodes was used to keep the distribution of potentials at the last dynodes. Two measurements of the PMT signal have been performed. In one measurement, the PMT amplitude A_1 was induced by LED pulses superimposed over a constant light emitted by another LED. The reference measurement included only LED pulses, the relevant amplitude was A_0. The measured mean values of relative short-term instability $(A_1 - A_0)/A_0$ in the range of $0 - 10$ μA are shown in Table 1.

Type of PMT	Type of dynodes	Relative instability
FEU 110	massive CuAlMg	$+25$ %
FEU 139	massive CuAlMg	$+25$ %
FEU 84	massive AlMg	-8 %
FEU 115M10	massive CuBe	-12 %
FEU 115M10	evaporated	-10 %
FEU 85	evaporated	≤ 10 %
FEU MA	evaporated	-1.8 %
FEU KS	evaporated	-1.3 %
R7899-20	evaporated	-1.5 %

Table 1: Relative short-term instability for different photomultipliers.

Photomultipliers FEU 110, FEU 139, FEU 84, FEU 115M10 are Russian industrial devices, Hamamatsu R7899-20 is a type of PMT which is used in LHCb electromagnetic and hadron calorimeters. FEU MA and FEU KS are experimental PMT's designed and produced at IHEP, Protvino. The basic difference in the dynode construction of FEU MA and FEU KS from dynodes with focusing (FEU 115, FEU 115M10, FEU 85, R7899-20) is essentially another type of support structure for the dynodes which does not permit secondary emission electrons to fly to dielectric plates of the support and to charge them. In the case of industrial PMT's the charge from these electrons can change the electric field inside the dynode gaps and therefore change PMT amplification. This results in the rate-effect which is a characteristic feature for the majority of industrial types of photomultipliers. We don't know precisely why PMT R7899-20 has such a small value of instability, but the new type of support of the dynodes permits to obtain at least the same value of instability and possibly less. PMT's FEU MA and FEU KS have side-on photocathodes with sizes around 10×200 mm^2 and dynodes with a length of 200 mm and therefore cannot be used in calorimeter modules. We have designed another PMT (FEU RDS) with a head-on photocathode and a tube diameter of 30 mm and the new type of the dynode support. Instability of the first samples of these PMT is around 2% and we hope to decrease this value. In addition, we plan to design a two-channel PMT with a diameter of 30 mm and a small value of cross talk between the channels. Prototypes of such a PMT were designed earlier jointly with Moscow Electrolamp Plant on the base of the PMT FEU 115. Such a PMT is intended for two-section modules of electromagnetic calorimeters.

The long-term stability was measured for two PMT's, R7899-20 and FEU RDS. The light source used for these studies was based on a yttrium alimunate crystal, excited by a radiative source $^{241}_{95}Am$. This light source is much more stable than a LED. The measured long-time stability of R7899-20 and FEU RDS are shown on Fig.1

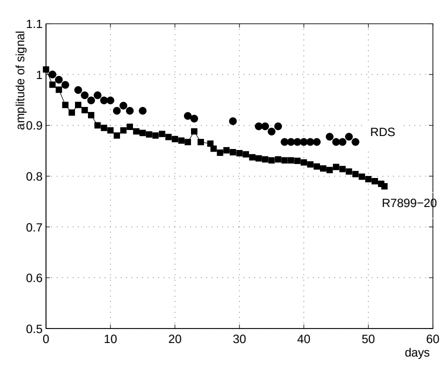

Figure 1: Dependences of output signal amplitude v.s time for PMT R7899-20 (squares) and FEU RDS (bullets).

* Vladimir.Rykalin@ihep.ru

Development of Projectile Spectator Detector

M.Golubeva[1], F.Guber[1], A.Ivashkin[1], A.Kurepin[1], A.Maevskaya[1], V.Marin[1], A.Sadovsky[1], and K.Shileev[1]

[1]INR RAS, Moscow, Russia

The Projectile Spectator Detector (PSD) at CBM has a spectrum of the experimental tasks such as precise determination of the centrality of nuclear collisions and the number of participants, reconstraction of the reaction plane and the beam intensity monitor by detecting the EMD neutrons. The experimental extraction of event-by-event fluctuations requires a very precise control over the fluctuations caused by the variation of the number of interacting nucleons due to event-by-event changes in the collision geometry. Main requirements to the PSD are excellent energy resolution (about $50\%/\sqrt{E(GeV)}$), good transverse uniformity of this resolution and fine granularity. These parameters as well as the linearity in a wide range of detected energies (10-10000 GeV) are critical in the appropriate description and subsequent correction of the physical parameters to the detector response. A full compensating modular lead/scintillator hadron calorimeter meets the above requirements. The calorimeter includes a 12x9 array of individual modules placed at a distance of about 15 m downstream from the target. A single module with dimensions of 10x10x120 cm^3 consists of 60 lead/scintillator layers with 16 mm and 4 mm thickness, respectively. Light readout is provided by WLS-fibers embedded in round grooves in the scintillator plates, ensuring a high efficiency and uniformity of light collection over the scintillator tile within a very few percent. WLS-fibers from each 6 consecutive scintillator tiles are collected together and viewed by a single photodetector at the end of the module. The longitudinal segmentation in 10 sections ensures the uniformity of light collection along the module as well as the rejection of secondary particles from interaction in the target. The use of micropixel avalanche photodiodes, MAPDs, seems to be an optimum choice due to their remarkable properties of high internal gain, compactness, low cost, and immunity to the nuclear counter effect. 10 MAPDs per module are placed at the rear side of the module together with the front-end-electronics. As a photodetector for the PSD, MAPDs with an active area of 3x3 mm^2 and a pixel density 10^4/mm^2 were selected [1].

During 2007 9 PSD modules were assembled at INR, Moscow. In September 2007 a first beam test of the PSD supermodule prototype was performed in a hadron beam at SPS, CERN, see Fig.1.

During the beam test the calibration of each readout channel was done with a muon beam. To obtain the full set of the calibration coefficients a muon beam scan was performed for all 9 modules. After that the central module of the calorimeter was irradiated by a pion beam with 5 energies: 20, 30, 40, 80 and 158 GeV. Fig.2 presents the dependence of the obtained energy resolution on beam energy. A fit results in a stochastic term of about 55% and a constant term of 3.6%. The calorimeter prototype with 30x30 cm^2 front size is too small for full containment of the entire hadron shower and a non-negligible lateral shower leakage might be expected. MC simulation confirms that about 16% of the hadron shower escapes from the PSD supermodule. The influence of shower leakage on energy resolution was considered in [2], where a third term together with stochastic and constant ones in the parameterization of resolution is added. The fit of the experimental points with three terms (Fig.2) results in a stochastic term of 53.5% and a constant term of 1.9% at a fixed leakage term of 16%.

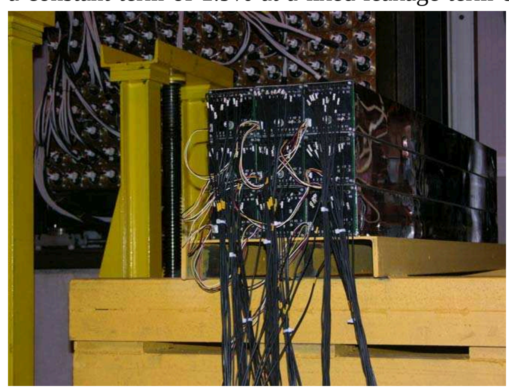

Figure 1: PSD supermodule at CERN beam test.

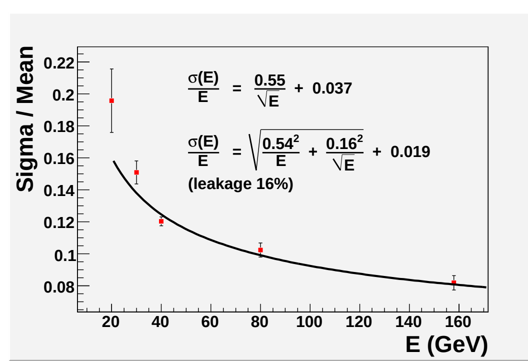

Figure 2: The energy resolution of PSD supermodule.

Longitudinal segmentation of the calorimeters provides a unique opportunity to develop an off-line compensating algorithm, which is a challenging task for an essential improvement of the PSD performance.

References

[1] Z. Sadygov, NIM **A567** (2006) 70-73.

[2] D.Acosta et al., NIM **A308** (1991) 481-508.

CBM-XYTER: towards high count rate, data driven detector readout electronics for CBM and other FAIR experiments

C. J. Schmidt[1] and the CBM collaboration

[1]GSI, Darmstadt, Germany

Technological Challenge

CBM projects a large area multi station Silicon tracking station (STS) as one of its core detector systems. Due to the very high hit rates that these detectors will experience at CBM, no trigger information will be available in time to tag events of interest. In particular, the complex analysis needed to generate a trigger on the open Charm channel does not appear feasible within a latency of just a few microseconds. Further, multi event confluence in time must be considered typical rather than exceptional and event generation may not be assumed synchronous to any global pace giving clock. This harsh environment not only poses tough demands on front-end detector and readout technology in terms of radiation hardness but also sets the stage to a novel, purely data driven readout architecture currently under development through the EU-FP6 project DETNI [1] and further pushed by the GSI detector laboratory for applications in various FAIR experiments.

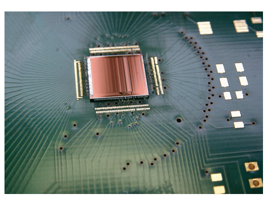

Figure 1: The n-XYTER chip

The XYTER Architecture

n-XYTER is a 128 channel integrated mixed signal front-end ASIC [1, 2]. Every channel is equipped with charge sensitive pre-amplifier and shaper circuitry to asynchronously capture incoming signals of either preset polarity. For every channel, both, analogue pulse height and a digital time stamp are stored in a short fifo, where it will remain until read out. Data is read out of the fifos through a token ring structure, that un-prejudicedly reads out whichever channel has data and skips non-hit channels. The chip is designed to be able to pump out data elements at an average rate of 32 MHz.

The n-XYTER realization shows noise figures of 850 ENC on the fast channel (30 ns peaking time) at 30pF input capacitance, which is perfectly suited for MIP detection at standard silicon thickness. The higher resolution slow channel with a peaking time of 140ṅs shows noise figures of about 600 ENC at 30pF input capacitance.

Project Outline

Such asynchronous, non triggered, high rates and self sparcifying front-end is the option of choice to cope with the projected challenges for CBM. The development efforts go along a two tier project structure, reflecting and supporting system development needs on different time scales:

- Tier one addresses the imminent need for readout electronics as well as a DAQ system for detector prototyping work towards the elaboration of the technical design reports for various FAIR experiments and their subsystems, such as CBM STS and CBM Muon chambers (MUCH) but also the PANDA Multi Vertex Detector (MVD) or the PANDA Central Tracker (in its realization as a GEM based TPC).
  Here the existing n-XYTER ASIC will be integrated into a complete, generic DAQ chain that will serve as supporting infrastructure for the detector prototypes. To this end, CBM and GSI closely cooperate with DETNI. GSI engaged in extensively evaluating the first 128 channel prototype n-XYTER at the GSI detector laboratory. Currently, a second submission of the n-XYTER as an engineering run is in preparation and will provide the number of chips needed for extensive detector as well as detector-system prototyping.

- As a tier two development thread on a longer time scale and as a development target for the technical design report in its own, the dedicated CBM-XYTER engineering work was started in 2007. Here, a second evolutional iteration of the n-XYTER architecture will be realized addresses the particular needs for FAIR applications. These are among others the radiation hardness ($\approx$ 10 MRad), power minimization, noise criteriy, the on chip integration depth, timing as well as energy resolution, dynamic range and finally also variable bandwidth or daisy-chaining data transfer strategies.

References

[1] NIM A, 568 (2006) 301-308

[2] CBM-Progress Report 2006 p. 49

[1] DETNI is a JRA of NMI-3 focussed upon neutron detector development, targeting thermal neutron scattering applications

Front End Electronic Building Blocks for CBM

T. Armbruster[1], P. Fischer*[1], C. Kreidl[1], and I. Perič[1]
[1]University of Heidelberg, Germany

Abstract

The project aims mainly at the development, in collaboration with other groups, of a self-triggered multi channel charge amplifier chip with integrated time stamping capability. This *CBMXYTER* chip will be used in the CBM silicon tracker and possibly in other detector subsystems as well.

Introduction

The CBM FEE development is concentrating on a self-triggered multi channel charge amplifier with integrated time stamping which is targeted mainly for the silicon tracker, but which could be used as well for other CBM detector subsystems, like for instance the muon detector. Low power operation is crucial for strip readout chips, as usual, to keep the amount of material small which is required to bring power in and heat out. Due to the simpler shape of signal pulses from a semiconductor detector (as compared to gaseous detectors with significant ion tails), the previously planned power hungry immediate digitization has been abandoned and a simpler peak sensing scheme is pursued. Signals without significant ion tails can be processed as well. The anticipated timing resolution is in the range of $1\,\mathrm{ns}$. A very similar chip, the *NXYTER*, which has been developed for neutron detection with double sided detectors, is taken as a guideline. Its power dissipation is much too high, however, and the $0.35\,\mu\mathrm{m}$ technology used is not expected to have sufficient radiation tolerance. A new design in the UMC $0.18\ \mu\mathrm{m}$ technology with lower power and a CBM compatible readout is therefore developed. The partitioning of the various building blocks has been organized in 2007. Our group in Heidelberg (formerly Mannheim) takes care of overall integration and simulation and will also contribute building blocks like charge injection circuitry, slow control and readout. A prototype of a charge sensitive preamplifier with various input device geometries has been submitted. Some other small blocks have been designed. As a part of the *CBMXYTER* project, the group is providing assistance to the collaboration for radiation tolerant design.

Charge Amplifier Test Chip

A test chip (fig. 1) with several charge amplifiers, injection circuitry and a circuit to achieve absolute calibration of the injected charge has been designed and submitted. The amplifiers have different transistor sizing and variable bandwidth, so that the measured noise for a wide range of conditions can be compared to simulations. All bias currents are generated on chip with high resolution DACs. A USB based compact test setup and a software test environment have been prepared for testing, which has just started. This design, in conjunction with measurements from other groups, will help to find an optimized input stage (trading power, speed and noise) once the detector parameters are frozen.

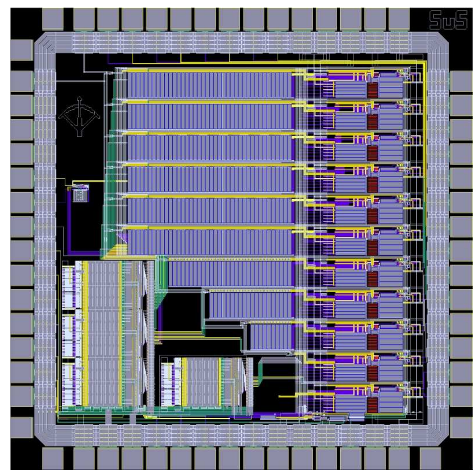

Figure 1: Layout of the Charge Amplifier Test Chip

Design Flow for Radiation Tolerance

The modifications to the device extraction tool 'ASSURA' required to correctly recognize enclosed NMOS gates of various types and geometries, as they are required for radiation hard design, have been implemented and optimized. A library containing the most important digital cells has been layed out and the views required for automatic synthesis have been generated. The initial design has been optimized for better manual and automated routing.

CBMXYTER Design Flow, Others

We have started to set up a simulation environment for the *CBMXYTER* chip. Verilog-AMS descriptions of all cells will be used to check the correct interfacing between blocks. The initial distribution of building blocks among the participating groups, first thoughts on global floor planning and power distribution, pinout and control have been presented. A possible bump connection of the chip (replacing wire bonding) is being studied.

* peter.fischer@ziti.uni-heidelberg.de

Low Power Pipelined ADC IP-blocks

E. Atkin[1], Yu. Bocharov[1], A. Gumenyuk[1], D. Osipov[1], A. Polyakov[1], A. Simakov[1], M. Simakov[1], V. Shunkov[1], and A. Voronin[2]

[1]MEPhI, Moscow, Russia; [2]SINP MSU, Moscow, Russia

Two variants of low power 20 MSPS pipelined ADC have been designed for CBM STS. Prototype blocks of the first version of ADC have been tested. Tests for radiation hardness demonstrated the advantage of ELT MOS devices over the conventional NMOS transistors.

In 2007 our team focused on the design of analog and mixed signal IP-blocks for the STS readout chip, including ADC design and prototyping, as well as the radiation tolerant devices design and testing.

A 7-bit 20 MSPS pipelined ADC has been designed using UMC mixed signal 0.18 μm CMOS 1P6M technology with metal-insulator-metal (MIM) capacitors. ADC is based on the well known pipelined 1.5-bit per stage architecture. It consists of a wideband sample-hold amplifier (SHA), a low noise 1.5-bit input stage, five identical 1.5-bit intermediate stages and a 2-bit flash ADC for the least bits. The differential switched capacitor architecture is used.

The precision analog switches were designed using a bootstrapping technique. The sub-ADC and MDAC, contained in a pipeline stage, are based on fully differential operational amplifiers with a common-mode switched capacitors feedback.

All amplifiers have p-channel MOSFET transistors in the input stages to provide a common-mode input range from the ground level up to 1V. They have the following parameters: differential gain 62 dB, bandwidth 190 MHz, current consumption 780 μA.

Front-end SHA uses a charge redistribution architecture and provides also a single-ended to differential signal conversion. The micropower bandgap voltage reference is based on a Brokaw cell followed by buffer stages. An internal synch generator provides a multiphase clock from a sine input and low jitter pulse input. The ADC also incorporates a pipelined error correction circuitry, based on an original successive carry fast adder, output registers and buffers. Chip area is 0.4 mm^2 (Fig. 2).

ADC has been simulated on the component level with post-layout extracted parameters. Modeling has demonstrated a full functionality at sampling frequencies up to 20 MHz, as well as a high linearity and a lack of missing codes. ADC featured a power dissipation of 26 mW at a 1.8 V supply, at 20 MSPS in an active mode. The test chips of ADC main blocks were fabricated at the UMC facility. The static and dynamic parameters of OpAmp and SHA circuits were measured using an especially developed test board and confirmed the simulation results.

An updated version of ADC had a resolution of 9 bit and a power consumption of 10 mW. It has the following features:

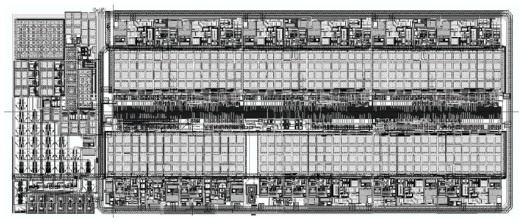

Figure 1: Pipelined ADC layout.

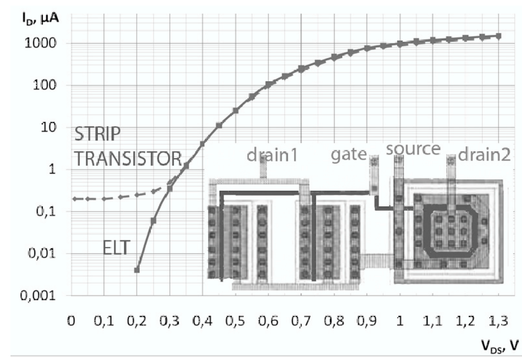

Figure 2: I-V curves of the irradiated (3 Mrad) strip transistor and ELT.

- optimized circuitry with shared opamps and comparators in adjacent stages;
- conversion latency reduced to 6 CLK;
- area reduced by capacitors scaling;
- supply current reduced by using the dynamic comparators;
- dc accuracy increased by OpAmps offset compensation in the first three stages.

Table. Summary of both ADC versions.

	ADC-I	ADC-II
Resolution	7 b	9 b
Sample rate	20 MSps	
Input voltage range	1 Vpp differential	
Supply voltage	1.8 V	
Total power	26 mW	10 mW

In order to study the radiation hardness of the UMC 0.18 μm process several test transistor structures (Fig. 2) have been irradiated and evaluated. ELT devices demonstrated a 3 Mrad total dose tolerance in comparison with the conventional strip transistors, which demonstrated a larger leakage current at the same conditions.

Perfomance tests with the PADI-ASIC chip for the CBM-ToF-wall

M.Ciobanu[1,2], M.Kiš[1,4], A.Schüttauf[1], I.Deppner[2], N.Herrmann[2], K.D.Hildenbrand[1], T.I Kang[1,3], P.Koczon[1], Y.Leifels[1], M.Marquardt[1], A.Reichl[2], M.S.Ryu[1,3], K.Piasecki[2], J.Weinert[1], and N.Zernezki[1,2]

[1]GSI, Darmstadt, Germany; [2]Universität Heidelberg, Germany; [3]Korea University, Seoul, South Korea; [4]Rudjer Boskovic Institut, Zagreb , Croatia

We started to investigate the new ASIC based preamplifier and discriminator chip (PADI 3 channels) for the CBM-ToF project in an experimental enviroment. To test the experimental performance for this first iteration of the chip we used a 4 pixel Diamond detector in a direct beam test. The main goal of this test-experiment was to verify the channel-to-channel variations for high rates and the stability of the chip, before submitting the next iteration. For this purpose we designed a new PCB for the PADI chip and connected 3 out of 4 pixels of the Diamond detector. The experiment took place at the SIS accelerator at GSI using a Carbon beam of 356 AMeV with a 2 s spill structure and 1.5×10^8 particles. By comparing the time dependence within spill and the integral rate for the 3 channels of PADI, we found an excellent uniformity within 0.02 % for all channels. With an independent measurement, using an ionisation chamber, we monitored the carbon beam position and intensity.

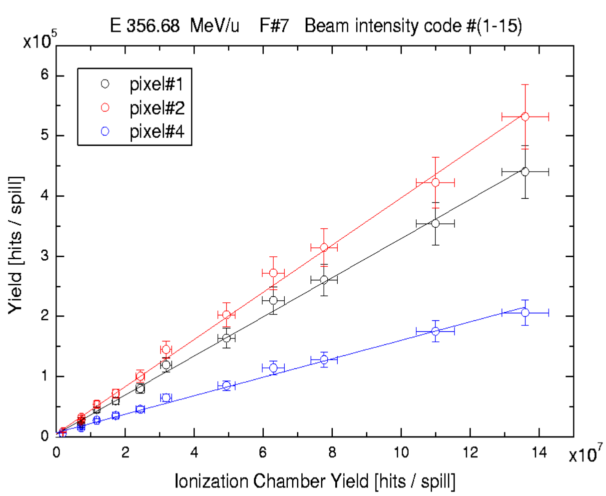

Figure 1: Correlation between the 3 pixels of the diamond detector, which are read out by PADI, and the total integrated yield of the primary Carbon beam, measured with an ionisation chamber.

By correlating the intensity measurements of both detectors, we saw a linear relation between the ionisation chamber and all 3 diamond pixels (see Fig. 1), which indicates an excellent stability and linearity of the PADI chip up to high rates (75 MHz).

To determine the timing performance of PADI we used a pulser with a small timing jitter to generate an input signal and measured with an active probe and a digital oscilloscope (3.5 GHz, 20 MS) at the output stage of PADI. These measurements are shown in Fig. 2 as a function of the primarary signal size and the discriminator threshold. This first timing measurement confirm that PADI can reach a time resolution blow $\sigma_t \leq$20 ps for signals above Q $\geq$ 50 fC.

As a last step we will use PADI with an existing MRPC to test his timing performance. In parallel we will finish simulations and layout for the next iteration of PADI (4 channels). Due to the very successful performance during all laboratory and experimental test we will submit the second iteration of PADI in 2008.

We would like to thank M.Rebisz and B.Voss from the GSI detector laboratory for their support and the possibility to use the diamond detector during the beam time.

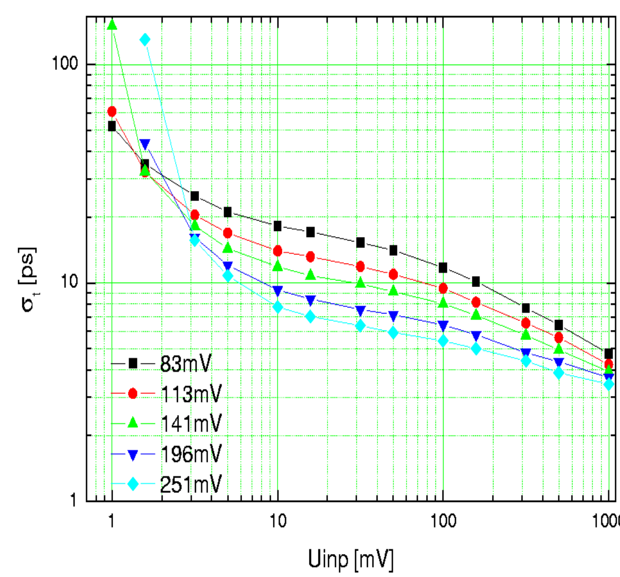

Figure 2: This figure shows the measured timing performance of PADI, as a function of the input signal and discriminator threshold.

References

[1] M.Ciobanu et.al.,IEEE Trans. on Nucl. Sci. 54 (2007) 1201

Development of High Resolution TDC ASICs for CBM-ToF

H. Deppe[1] and H. Flemming[1]
[1]GSI, Darmstadt, Germany

Introduction

The ASIC design group of GSI has evaluated two approaches for an optimal fitting new TDC ASIC for the CBM ToF-detector. The first one is a new implementation of a Time to Amplitude Converter (TAC) core developed at GSI [1] in a current CMOS technology. The other one is using a Delay Locked Loop (DLL) to get a very fine time binning for direct time digitisation. Even though the TAC core based TDC achieves a better time resolution, the DLL based approach fits better in other requirements so in end of 2007 it was decided to use a DLL based TDC for CBM-ToF.

Table 1: Requirements for the ToF readout electronics

Requirements
time resolution (for digitization) $\leq$ 25 ps
event driven architecture
event rate per channel $\approx$ 50 kHz
time over threshold measurement for walk compensation
$\approx$ 65 000 channels

A Delay Locked Loop based TDC

The principle of a Delay Locked Loop based TDC (Fig. 1) is well known and successfully implemented in many experiments. In a regulated delay line a set of clock signals with constant phase shifts is generated. These clock signals are used to clock a hit register to sample the input signal. This way an image of the input signal time structure is latched in the hit register. One can get the digital timing information by encoding this image. This architecture is called clock driven.

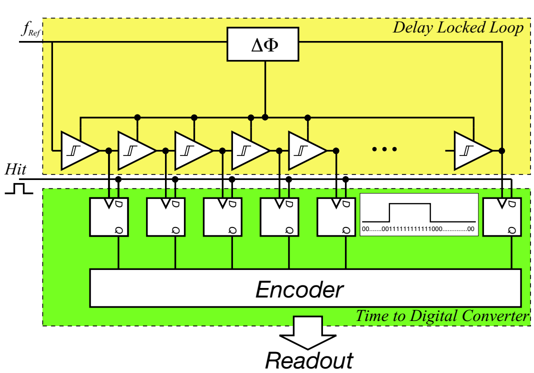

Figure 1: Block diagram of a DLL based TDC

After a first DLL testchip submitted already in 2005 a second chip called *DANTE* was submitted in 2007. Based on the promising results of the first DLL chip *DANTE* was designed to increase the timing resolution by using inverting delay cells with a delay of 50 ps in comparison to 100 ps delay cells in the first chip. For the design of this DLL structure the different charge carrier mobilities of pmos and nmos transistors had to be compensated very carefully to prevent an odd even structure of the bin sizes. This was very successful which is reflected in good DNL and INL values below $\pm$ 0.5 LSB (DNL) and $\pm$ 0.75 LSB (INL).

The time resolution of the *DANTE* chip in comparison to the first DLL chip is plotted in Fig. 2. The correlated time resolution of $\sigma_{2Ch} = 28.67$ ps leads to an uncorrelated time resolution for the *DANTE* chip of

$$\boxed{\sigma_{1Ch} = \frac{1}{\sqrt{2}}\sigma_{2Ch} = 20.27 \text{ ps}} \qquad (1)$$

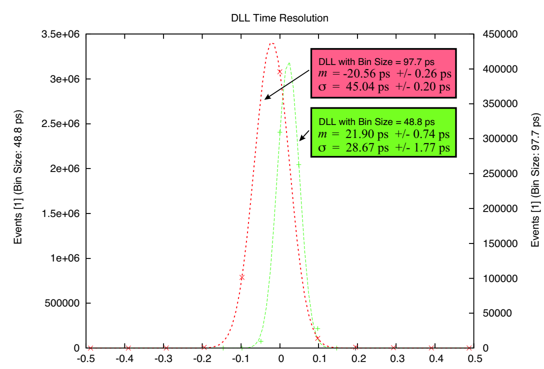

Figure 2: Time Resolution of DLL based TDCs

During 2008 it is planed to design a first prototype of a complete DLL based TDC chip. The aim is to get a multi channel TDC with at least four channels with time over threshold measurement capability and a double hit resolution below 3.5 ns. For readout a simple daq interface with serial communication will be implemented.

References

[1] K. Koch et.al.: A New Multi Channel Front-End Board for TOF Experiments with Excellent Timing Resolution, GSI Scientific Report 2004, p. 339

Development of the Read Out Controller for the nXYTER Front End Board

N. Abel[1], N. Schroer[1], B. Stopfkuchen[1], M. Block[1], and U. Kebschull[1]
[1]KIP, Heidelberg, Germany

Introduction

In 2007 our contribution focused the FEE (Front End Electronic), consisting of the nXYTER, an ADC (Analog Digital Converter) and the ROC (Read Out Controller). The nXYTER is recieving analogue data directly from the sensors and detects the value and the exact time of a signal peak. It provides the time stamp digitally and the peak value analog. For further processing the analog data has to be converted by an ADC into digital data. Since the conversion needs time, the correlation between time stamp and signal value is lost. The correlation needs to be recombined. This, the transfer of the measured data and the controlling of the functional behavior of the nXYTER and the ADC is done by the ROC Board we developed.

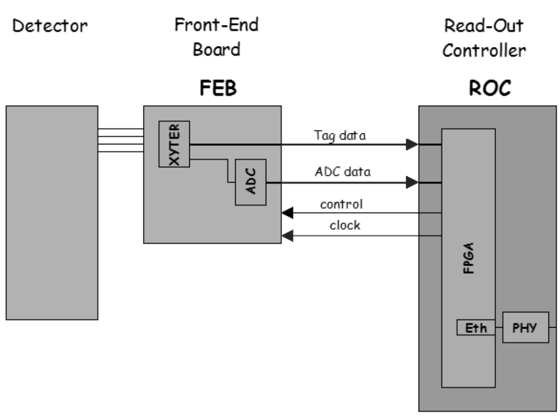

Figure 1: The FEE with ROC Version 1.0

Data Synchronisation

One major task of the ROC is the preparation of clock signals for the nXYTER and the ADC with well defined frequencies and phase relations to each other. This is a very sensitive point, since the ADC converts the data exactly at the rising edge of its clock and the time slot for the conversion is just about 3 ns. At the moment it is possible to change the delay at runtime from 0 ns to 31 ns (full clock cycle is 32 ns) in steps of 1 ns manually. In future we want to implement an auto calibration beeing able to determine the right delay automatically. After the conversion the ROC recombines the timestamp and the digitalized peak value.

Linux

The nXYTER and the ADC have user settable parameters which can be changed using serial busses. Using our ROC, one can access these busses over Ethernet. For this Linux is running on the ROC making it possible to use all operating system standard functions. Special modules make it possible to control the nXYTER and the ADC registers like files. Hence, one can use ordinary scipt files for slow control. Linux is beeing loaded automatically by a boot loader from a connected SD card. The content of the SD card can be changed at runtime. Hence, the software functionality of the ROC can be changed or updated remotely. In future we want to use the possibility of reading back the configuration of an FPGA to perform a so called ”fast boot” making it possible to leap the boot process at startup. [2]

Radiation Tolerance

Most of the functionality of the ROC is realized in a Virtex4 FX20. Former measurements with FPGAs in a test beam showed that the configuration of the FPGA can change due to the beam. Hence, we developed a method to undo these unwanted changes: a radiation hard Actel CPLD takes the original bit file stored in flash memorys and refreshes the configuration of the FPGA permanently. In future we want to be able to change the bit file over network making it possible to change or update the hardware functionality of the ROC remotely.

MGTs

In our first test setup the FEE Board transmits the measured data via Ethernet. At the next step, we will replace this Ethernet transmission by an optical transmission using SFPs and MGTs. Furthermore, the central FPGA clock will be recovered from the optical input signals. Our tests showed that we are able to recover the clock with a jitter of less than 100 ps. [1]

References

[1] N. Schroer, “Clock Distribution / Synchronization for the Readout-Chain of the CBM experiment at GSI Darmstadt using Xilinx FPGAs”, KIP Heidelberg 2007

[2] B. Stopfkuchen, “Workflow zur automatisierten Konfiguration und Generierung eines Linux-Systems für eingebettete Hardware auf FPGAs”, Uni Leipzig (in preparation)

A Readout System for the CBM-MVD Demonstrator*

C. Schrader[1], S. Amar-Youcef[1], N. Bialas[1], M. Deveaux[1], D. Doering[1], J. Heuser[2],
I. Fröhlich[1], J. Michel[1], C. Müntz[1], S. Schreiber[1], J. Stroth[1], T. Tischler[1], B. Wiedemann[1]

[1]IKF, University Frankfurt, Germany, [2]GSI, Darmstadt, Germany

A micro-vertex detector for track reconstruction, consisting of two layers of monolithic active pixel sensors (MAPS [1]) is planned for the CBM experiment. Here, the readout of the MAPS detector stations, which will deliver a raw data rate of up to ~100 Gbit/s/cm² [2], is challenging.

To study the electronic and mechanical integration of these sensors into a detector system, a so-called "demonstrator" is being constructed at the IKF Technology Lab.

The sensor planned to be used in the demonstrator (MIMOTEL, with 4 matrices of 64 x 256 pixel array, 30 µm pixel pitches and a readout speed of ~1 ms/frame) delivers a data rate up to 100 MB/s, which places high demands on the readout electronics. A fast readout add-on board for the TRBv2 [2] standard was developed with on-board functionality for data reduction in order to replace an existing USB board as provided by IPHC, Strasbourg.

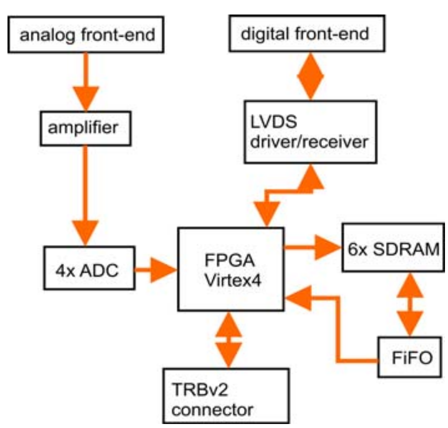

Figure 1: Components of the MAPS readout board.

The new board comprises 4 analog input signal channels which receive the analog signals from the 4 matrices of each MAPS chip via an RJ45 connector. A differential-to-differential amplifier helps to balance the input for the differential ADCs, so that the 4 ADCs provide maximum performance.

The ADCs with sampling frequences of up to 50 MHz, convert the analog signals to 12-bit digital signals. The digital front-end with low voltage differential drivers and receivers (LVDS) is mainly used to control the sensor.

The data is further processed online using a VIRTEX IV LX40 FPGA with internal FIFO and 512 MB external SDRAM organized in 6 memory banks.

To process the MAPS data on-line the system has to work with pipelined algorithms for correlated double sampling (CDS) and hit discrimination until the identified hits are transmitted externally via the optical link (2Gbit/s) of the TRBv2. Since the data is continuously delivered by every MIMOTEL chip the algorithms have to work in real-time.

The interface between the TRBv2 board and the add-on board is established with two high-speed LVDS connectors (15Gbit/s), which also provide power for the add-on board (+5V, 10A), converted on the add-on board to supply the voltages for the individual units (between ±12V). The digital and analog components have separate power supplies and ground planes to reduce electrical cross talk.

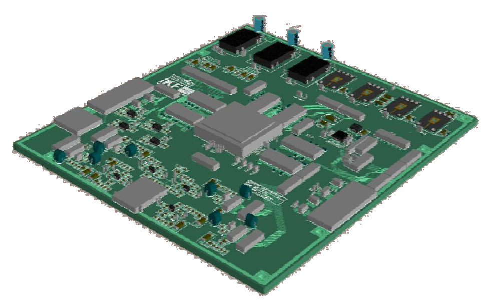

Figure 2: Layout of the MAPS add-on prototype board.

The schematics and the layouts of the 12 layer board were designed in collaboration with the electronic workshop of IKF, using the design software Altium©. The board was submitted for production and will be assembled and tested. In parallel to the hardware developments, data acquisition algorithms for the FPGA (including CDS, bit reduction and hit finding) were developed and successfully simulated in VHDL.

REFERENCES

[1] R. Turchetta et al., NIM **A458** (2001)677-689.
[2] S. Amar-Youcef, Diploma Thesis (2007).
[3] I. Fröhlich et al., A General Purpose Trigger and Readout Board (TRB), IEEE Trans. Nucl. Sci, in print

Data Communication Tests on Active Buffer Board

J. Adamczewski[2], W. Gao*[1], A. Kugel[1], R. Männer[1], G. Marcus[1], and A. Wurz[1]
[1]Informatik V, University of Mannheim, Germany; [2]GSI, Darmstadt, Germany

Abstract: The Active Buffer Board (ABB) was redesigned and equipped with a larger FPGA, Virtex-4FX60. A test infrastructure, based on the embedded PowerPC processor, was developed and applied to verify memory controllers and high-speed serial links. A protoype integration into a PCIe based DAQ system was started, employing partial reconfiguration, interrupt handling and dual-channel DMA.

ABB hardware

In order to test the re-designed ABB cards and to test memory and interconnection modules a number of IP-cores have been developed.

Test Infrastructure

The infrastructure module is based on the embedded PowerPC processor in the Virtex-4 FPGA. Specialised IP-cores to access the serial links and memory interface via the processor bus (PLB) enable to build a complete system using the XILINX EDK software, together with the default modules, like timer and UART.

Serial Link (MGT) Test

This module consists of a pseudo random number generator to generate the bits pattern and the corresponding comparison logic for the error rate statistics. Test patterns and run paramters are software programmable via the PLB interface, which attaches to the infrastructure module. MGT paramters can be controlled likewise, using the MGT ICAP interface. The serial links have been successfully tested with data-rates of 5 Gbps over coaxial cable and PCB traces. 2.5 Gbps have been tested with optical transceiver modules and differential flat cables. Multiple MGTs can be tested simultaneously.

Memory Controller

High-speed dual-ported memory controller are required for a data-acquisition purpose of the ABB. With today's high capacity SRAMs and DRAMs this can become a non-trivial task, due to the asymetric read/write behaviour of DDR-2 SRAMs and the inherent complexity of dynamic memory (page structure, refresh, precharge times etc.). The ABB memory controller provides independent, FIFO buffered fast read and write paths with data transfer on every clock edge. In addition, a PLB interface is available to exercise the memory under software control. Memory interfaces are available for DDR-2 SRAM and DDR-1 DRAM. DDR-2 DRAM has been tested as well but becomes very inefficient on random access.

PCIe DMA Project

PCI Express DMA Engine Improvement

Two DMA channels, upstream and downstream, are built to transfer data between the Active Buffer Board and the host through the PCI Express bus. External memory is currently emulated using internal block RAM (BRAM). FIFOs are used to emulate external I/O to/from DCB/BNet via MGTs. The two channels can run simultaneously. The maximum transfer per DMA command size is 4GB. DMA descriptors for scatter-gather DMA reside in host memory. The DMA DONE status is acknowledged through interrupt messages. The driver and the test programs have been well improved and modified both in Mannheim and GSI targeting Intel and AMD machines. For large transfersize, we achieve around 700MB/s downstream (to peripheral) and 800 MB/s upstream (to host) with a 4-lane PCIe interface.

Partial Reconfiguration Experiment

In order to resolve licensing issues an attempt was made to employ the partial reconfiguration technique to combine developments from different project partners (PCIe core and user logic respectively) into a single FPGA device. Unfortuately the XILINX software tools are not fully mature in this respect and several work-arounds have been neccessary. A stable design, however only with 1 PCIe lane, was successfully generated finally.

PCI Express Interrupt Generator

A programmable interrupt generator was developed and used to measure the latency of the driver and the system. Basic tests show that the system we are using can stand an interrupts arrival rate of 60 000 Hz.

References

[1] W. Gao, A. Kugel, R. Männer and G. Marcus, "PCI Express DMA Engine Design", CBM Progress Report 2006, February 2007.

* wgao@rumms.uni-mannheim.de

Data Acquisition Backbone Core DABC

J. Adamczewski[1], H.G. Essel[1], N. Kurz[1], and S. Linev[1]
[1]GSI, Darmstadt, Germany

DABC design

The DABC [1] addresses requirements of FAIR experiments like CBM [2] for detector and data acquisition test beds as well as the need for a general purpose DAQ backbone for experiments in production. The backbone is able to handle any kind of front-end systems and provides event building over fast networks using commodity hard- and software. Especially a mixture of commonly used MBS (daq.gsi.de) based front-ends and others will be needed. Event building based on time stamped data streams gets more common and must be supported.

The DABC software written in C++ runs on standard Linux PCs. A schematic view is shown in Figure 1. Arbitray front-end systems (FES) can be connected to standard Linux PCs (by hardware or network). Application plug-ins for handling the front-ends must be written by the application programmers. More plug-ins may process the data streams. To combine two data input streams on one PC a specific plug-in knowing the data formats is needed. Senders/receivers provided by DABC do the event building over networks like Ethernet or InfiniBand. Behind the receivers the event processing is done by other plug-ins.
The DABC core design has been revised for a better separation from the XDAQ environment [3]. This environment could now be easily replaced by other libraries providing state machines, task controls, and setup/configure mechanisms. The plug-in APIs also have been redesigned to be optimal for general purpose data acquisition applications.

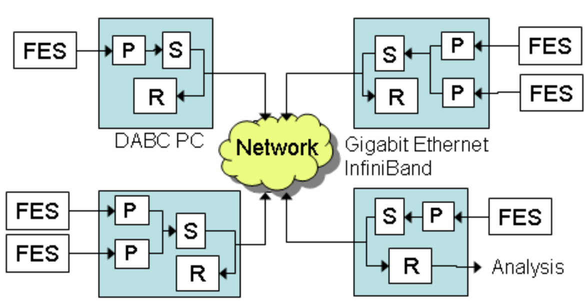

Figure 1: Front-end systems (FES) connected to DABC by application plug-ins (P). Data flow from senders (S) over event building network to receivers (R).

MBS integration

The general purpose DAQ system MBS had to be upgraded to connect MBS front-end systems via TCP to DABC nodes for event building. A new list mode data file format allowing for large files (> 2 GB) and direct event access has been designed and an API library implemented. DIM servers (dim.web.cern.ch) running on the MBS nodes provide control and monitoring by the DABC standard Java GUI. In DABC, MBS plug-ins have been implemented.

Controls and Monitoring

The standard control access to DABC is via DIM. Parameters and commands can be specified in the application plug-ins. A naming convention provides the locations. A generic Java GUI displays all parameters and commands provided by the DIM servers. Special parameters like rates, status, and histograms are visualized as shown in Figure 2.

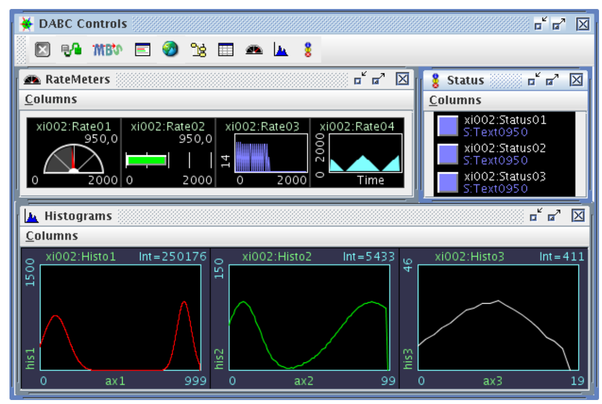

Figure 2: Rate meters, status displays and histograms.

Status and outlook

The new plug-in API description will be published soon. The modifications due to the design review have to be implemented. The MBS plug-ins will be adjusted. The MBS control by DABC GUI must be completed (support for all MBS commands, running standard MBS without DABC). In 2008 DABC will be ready for the test beds as well as for the event building of MBS based DAQ systems. Latest news on wiki.gsi.de/DABC

References

[1] J. Adamczewski, H.G. Essel, N. Kurz, S. Linev, "DataAcquisition Backbone Core DABC", IEEE Trans.on Nucl. Science, Vol.55, No.1, February 2008, to be printed.

[2] "CBM technical status report", GSI, January 2006

[3] J. Adamczewski, H.G. Essel, N. Kurz, S. Linev, "Developments for future DAQ framework DABC", GSI report 2006

Infiniband performance for Future DAQ

J. Adamczewski[1], H.G. Essel[1], and S. Linev[1]
[1]GSI, Darmstadt, Germany

Event building performance

High performance DAQ systems are required by the next generation experiments at FAIR like CBM [1] [2]. After combining data from several input channels in the front-end systems the event building is done through standard networks. A bidirectional data rate per node of 1 GByte/s is needed. Several hundred nodes might be necessary to achieve the required total bandwidth. One of the fastest network available today is InfiniBand (IB). Therefore we started, after detailed simulations, investigations in IB performance for event building. First measurement have been done at GSI on a small IB cluster with four nodes [3]. All available software packages for IB have been evaluated. Finally, we selected the **verbs** API of the OpenFabrics Alliance [4]. We measured a single data rate per node of 950 MByte/s in all to all scheme.

Performance scaling

The open question how this scales to over hundred nodes could not be answered at GSI. Therefore we established cooperations with the Forschungszentrum Karlsruhe (FKZ, http://www.campusgrid.de) and the University of Mainz (UM, http://www.zdv.uni-mainz.de/3401.php). In Karsruhe, 23 machines were available, in Mainz 110, all double dual-core Opterons. Karlsruhe has IB switches from QLogic, Mainz from Flextronics. Measurements have been performed with stand alone test programs emulating event building traffic. All nodes work as data sources and data collectors. In round robin mode senders distribute buffers circular to the receivers without synchronization. In synchronized mode the senders follow a time schedule trying to avoid congestions at the receivers. Figure 1 shows the results.

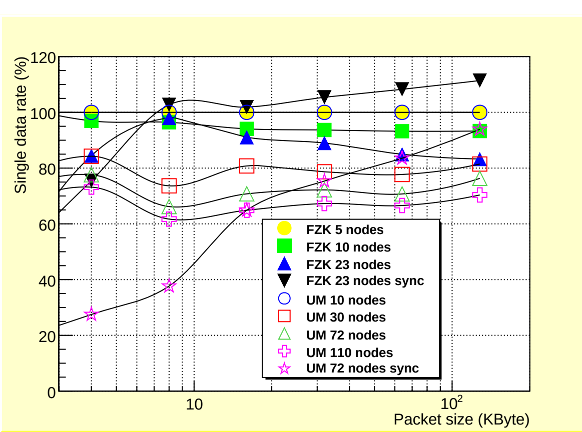

Figure 1: Normalized single data rates.

To see the scaling effects, the transfer rates have been normalized to the ones for 5 nodes (FZK) and 10 nodes (UM), respectively. All shown measurements are done with the round robin scheme, FZK 23 and UM 72 also with the synchronization scheme. Below 16K packet size the synchronized mode is rather worse the round robin. With larger packets synchronization gives significant better results. Synchronizing the 23 FZK nodes and the 72 UM nodes gives about 700 MBytes/s. With 110 nodes and packet sizes above 16K the single data rate per node is 500 MByte/s. This is about 50% of the rate measured at the four nodes at GSI. With high number of nodes synchronization gets much more complicated because the switch topology must be taken into account. This works up to 72 nodes, but gets more difficult up to now for 110 nodes. Besides that the 50% are surprisingly good!

Event building with DABC

Network event building tests have also performed in a more realistic environment, the data acquisition backbone core DABC [5][6]. On the four GSI machines four threads on each machine generate data wich are combined in another thread, sent over IB to the other nodes for event building. With packet sizes above 32K the single data rate per node is more than 800 MBytes/s.

Summary

More detailed studies are necessary to optimize the traffic on large clusters, because the switch topology becomes the critical issue. The data rate achieved up to now with more than hundred nodes is at least 50% of what is required in some years from now. The concept of network event building with very high data rates seems to be feasable.

References

[1] "CBM technical status report", GSI, January 2006

[2] H.G.Essel, "FutureDAQ for CBM: On-line event selection", IEEE TNS Vol.53, No.3, June 2006, pp 677-681

[3] J. Adamczewski, H.G. Essel, S. Linev, "InfiniBand cluster for Future DAQ", GSI report 2006

[4] OpenFabrics Alliance website, http://www.openfabrics.org

[5] J. Adamczewski, H.G. Essel, N. Kurz, S. Linev, "Data Acquisition Backbone Core DABC", IEEE Trans.on Nucl. Science, Vol.55, No.1, February 2008, to be printed.

[6] J. Adamczewski, H.G. Essel, N. Kurz, S. Linev, "Data Acquisition Backbone Core DABC", GSI report 2007

CBM publications 2007

- A. Akindinov *et al.*
  RPC with low-resistive phosphate glass electrodes as a candidate for the CBM TOF
  Nucl. Instr. Meth. Phys. Res. A **572** (2007) 676
- P. Senger
  Strange particles and neutron stars - experiments at GSI
  Int. J. Mod. Phys. E **16** (2007) 1135
- C. Höhne
  The CBM experiment at FAIR exploring the QCD phase diagram at high net baryon densities
  Int. J. Mod. Phys. E **16** (2007) 2419
- A. László, Z. Fodor and G. Vesztergombi
  New results and perspectives on R_{AA} measurements below 20 GeV CM-energy at fixed target machines
  Int. J. Mod. Phys. E **16** (2007) 2516
- V. Ammosov *et al.*
  Performance of RPC with low-resistive silicate glass electrodes exposed to an intense continuous electron beam
  Nucl. Instr. Meth. Phys. Res. A **576** (2007) 331
- M. Petrovici *et al.*
  A high-efficiency Transition Radiation Detector for high-counting-rate environments
  Nucl. Instr. Meth. Phys. Res. A **579** (2007) 961
- M. Petris *et al.*
  High counting rate transition radiation detector
  Nucl. Instr. Meth. Phys. Res. A **581** (2007) 406
- J. M. Heuser
  Development of a silicon tracking and vertex detection system for the CBM experiment at FAIR
  Nucl. Instr. Meth. Phys. Res. A **582** (2007) 910
- M. Deveaux *et al.*
  Charge collection properties of Monolithic Active Pixel Sensors (MAPS) irradiated with non-ionising radiation
  Nucl. Instr. Meth. Phys. Res. A **583** (2007) 134

In press

- J. Adamczewski *et al.*
  Data acquisition backbone core DABC
  to appear in J. Phys. Conf. Ser.
- V. Friese
  The CBM Experiment at FAIR
  to appear in PoS
- S. Gorbunov *et al.*
  Fast SIMDized Kalman filter based track fit
  to appear in Comp. Phys. Comm.
- J. M. Heuser
  The Compressed Baryonic Matter experiment at FAIR
  to appear in J. Phys. G.
- C. Höhne *et al.*
  Development of a RICH detector for electron identification in CBM
  to appear in Nucl. Instr. Meth. Phys. Res. A
- M. Klein-Bösing *et al.*
  Position resolution of a high efficiency transition radiation detector for high counting rate environments
  to appear in Nucl. Instr. Meth. Phys. Res. A

- K. Davkov *et al.*
  Development of segmented straws for very high-rate capability coordinate detector
  to appear in Nucl. Instr. Meth. Phys. Res. A

CBM Notes 2007

Public notes

- S. Gorbunov *et al.*
  Fast SIMDized Kalman Filter based track fit
  CBM-SOFT-note-2007-001
- P. Akishin *et al.*
  Methods for event reconstruction in the CBM experiment
  CBM-SOFT-note-2007-002
- S. Gorbunov and I. Kisel
  Reconstruction of decayed particles based on the Kalman Filter
  CBM-SOFT-note-2007-003
- A. B. Kurepin *et al.*,
  Charmonium detection in the CBM experiment
  CBM-PHYS-note-2007-001

Internal notes

- V. Ammosov and F. Fuber
  Development of the high rate multigap RPC prototype for the central part of the CBM TOF detector. Final report
  CBM-TOF-note-internal-2007-001

CBM Meetings, Workshops, Conferences

- What do we learn from dilepton measurements in heavy-ion collisions?
  Forum, GSI Darmstadt, 27 February 2007
- 9th CBM Collaboration Meeting
  GSI Darmstadt, 28 February - 2 March 2007
- Silicon Detector Systems for the CBM Experiment
  Workshop, GSI Darmstadt, 18 - 20 April 2007
- Critical Point and Onset of Deconfinement (CPOD07)
  International workshop, GSI Darmstadt, 9 - 13 July 2007
- 2nd CBM Indian Collaboration Meeting
  VECC Colcata, 30 - 31 July 2007
- The Physics of Compressed Baryonic Matter
  Symposium, Dresden, 25 September 2007
- 10th CBM Collaboration Meeting
  Dresden, 26 - 28 September 2007

List of CBM member institutions

- **Aligarh**, India, **Department of Physics, Aligarh Muslim University**
- **Bergen**, Norway, **Department of Physics, University of Bergen**
- **Bhubaneswar**, India, **Institute of Physics**
- **Bucharest**, Romania, **National Institute for Physics and Nuclear Engineering**
- **Budapest**, Hungary, **Eötvös University**
- **Budapest**, Hungary, **KFKI**
- **Chandigarh**, India, **Department of Physics, Panjab University**
- **Coimbra**, Portugal, **LIP**
- **Darmstadt**, Germany, **GSI**
- **Dresden**, Germany, **FZD, Institut für Strahlenphysik**
- **Dubna**, Russia, **JINR-LHE**
- **Dubna**, Russia, **JINR-LPP**
- **Dubna**, Russia **JINR-LIT**
- **Frankfurt**, Germany, **Institut für Kernphysik, Universität Frankfurt**
- **Gatchina**, Russia, **PNPI**
- **Hefei**, China, **Department of Modern Physics, University of Science & Technology of China**
- **Heidelberg**, Germany, **Kirchhoff-Institut für Physik, Universität Heidelberg**
- **Heidelberg**, Germany, **Physikalisches Institut, Universität Heidelberg**
- **Heidelberg**, Germany, **Zentrales Institut für Technische Informatik, Universität Heidelberg**
- **Jaipur**, India, **Physics Department, University of Rajasthan**
- **Jammu**, India, **Department of Physics, University of Jammu**
- **Katowice**, Poland, **University of Silesia**
- **Kharagpur**, India, **Department of Physics and Meteorology, Indian Institute of Technology**
- **Kolkata**, India, **High Energy Physics Division, Saha Institute of Nuclear Physics**
- **Kolkata**, India, **Variable Energy Cyclotron Centre**
- **Kraków**, Poland, **AGH University of Science and Technology**
- **Kraków**, Poland, **Jagiellonian University**
- **Kyiv**, Ukraine, **Taras Shevchenko National University of Kyiv**
- **Moscow**, Russia, **Institute for Nuclear Research**
- **Moscow**, Russia, **ITEP**
- **Moscow**, Russia, **SINP, Moscow State University**
- **Moscow**, Russia, **Kurchatov Institute**
- **Moscow**, Russia, **MEPhi**
- **Münster**, Germany, **Institut für Kernphysik, Universität Münster**
- **Nikosia**, Cyprus, **Cyprus University**
- **Obninsk**, Russia, **Obninsk State University of Atomic Energy**
- **Prag**, Czech Republic, **Technical University**
- **Protvino**, Russia, **IHEP**
- **Pusan**, Korea, **Pusan National University**
- **Rez**, Czech Republic, **Czech Academy of Sciences**
- **Seoul**, Korea, **Korea University**
- **Split**, Croatia, **University of Split**
- **Srinagar**, India, **Department of Physics, University of Kashmir**
- **St. Petersburg**, Russia, **Khlopin Radium Institute (KRI)**
- **St. Petersburg**, Russia, **St. Petersburg State Polytechnic University**
- **Strasbourg**, France, **Institut Pluridisciplinaire Hubert Curien IN2P3-CNRS/ULP (IPHC)**
- **Varanasi**, India, **Department of Physics, Banaras Hindu University**
- **Warszawa**, Poland, **University, Nuclear Physics Division**
- **Wuhan**, China, **Institute of Particle Physics, Hua-zhong Normal University**
- **Zagreb**, Croatia, **Ruđjer Bošković Institute**

Contacts

Spokesman
Peter Senger (p.senger@gsi.de)

Technical Coordinator
Walter Müller (w.f.j.mueller@gsi.de)

Physics Coordinator
Volker Friese (v.friese@gsi.de)

Chairman of the Collaboration Board
Mihai Petrovici (mpetro@ifin.nipe.ro)

Management Board

A. Golutvin, N. Herrmann, F. Rami, D. Röhrich, J. Stroth, J. Wessels

http://www.gsi.de/fair/experiments/CBM

ISSN: 0171-4546
ISBN: 978-3-9811298-5-4
GSI Report 2008-4
Hrsg: Peter Senger
Druck: GSI

D-64291 Darmstadt, Germany
http://www.gsi.de